University of Alberta

A Feasibility Study of U-Pb Ilmenite Geochronology, Monastery Kimberlite, South Africa

by

Andrea K. Noyes

A thesis submitted to the Faculty of Graduate Studies and Research in partial fulfillment of the requirements for the degree of Master of Science

Department of Earth and Atmospheric Sciences

Edmonton, Alberta

Spring, 2000

National Library of Canada
Acquisitions and Bibliographic Services
395 Wellington Street
Ottawa ON K1A 0N4
Canada

Bibliothèque nationale du Canada
Acquisitions et services bibliographiques
395, rue Wellington
Ottawa ON K1A 0N4
Canada

Your file Votre référence

Our file Notre référence

The author has granted a non-exclusive licence allowing the National Library of Canada to reproduce, loan, distribute or sell copies of this thesis in microform, paper or electronic formats.

L'auteur a accordé une licence non exclusive permettant à la Bibliothèque nationale du Canada de reproduire, prêter, distribuer ou vendre des copies de cette thèse sous la forme de microfiche/film, de reproduction sur papier ou sur format électronique.

The author retains ownership of the copyright in this thesis. Neither the thesis nor substantial extracts from it may be printed or otherwise reproduced without the author's permission.

L'auteur conserve la propriété du droit d'auteur qui protège cette thèse. Ni la thèse ni des extraits substantiels de celle-ci ne doivent être imprimés ou autrement reproduits sans son autorisation.

0-612-60161-7

Canada

University of Alberta

Library Release Form

Name of Author: Andrea K. Noyes

Title of Thesis: A Feasibility Study of U-Pb Ilmenite Geochronology, Monastery Kimberlite, South Africa

Degree: Master of Science

Year this Degree Granted: 2000

Permission is hereby granted to the University of Alberta Library to reproduce single copies of this thesis and to lend or sell such copies for private, scholarly or scientific research purposes only.

The author reserves all other publication and other rights in association with the copyright in the thesis, and except as herein before provided, neither the thesis nor any substantial portion thereof may be printed or otherwise reproduced in any material form whatever without the author's prior written permission.

Andrea Noyes

#901, 11135-83rd Ave
Edmonton, AB
T6G 2C6

Date: April 14, 2000

University of Alberta

Faculty of Graduate Studies and Research

The undersigned certify that they have read, and recommend to the Faculty of Graduate Studies and Research for acceptance, a thesis entitled **A Feasibility study of U-Pb Ilmenite Geochronology, Monastery Kimberlite, South Africa** submitted by Andrea Noyes in partial fulfillment of the requirements for the degree of Master of Science.

Dr. L. M. Heaman

Dr. R. W. Luth

Dr. R. A. Creaser

Dr. A. Meldrum

Date April 12, 2000

Abstract

The Monastery kimberlite, South Africa, is considered to be a Group 1 kimberlite with an emplacement age of 90 Ma. This study demonstrates that multiple isotopic techniques can be applied to a single kimberlite and yield precise and consistent emplacement ages: Rb-Sr phlogopite age of 89.9 ± 3.1 Ma, U-Pb perovskite age of 91.0 ± 1.0 Ma, U-Pb mantle zircon age of 89.9 ± 3.5 Ma.

The results of a U-Pb ilmenite geochronology study are highly encouraging. There is a considerable variation in parent/daughter ratios (39.8-311.4) between ilmenite megacrysts and macrocrysts and even within a single megacryst (39.8-115.5). These variations are interpreted to be of primary origin. The U-Pb ilmenite age obtained for the Monastery kimberlite in this study is 95 ± 14 Ma, in good agreement with the age of kimberlite emplacement determined by other radiometric techniques both in this study and in previous studies. Although further refinement of the technique is needed, this study demonstrates for the first time the feasibility of U-Pb geochronology of kimberlitic ilmenite.

Dedication

To: Helen Mary Smelko-Lainson

who is my strength and guiding light

Acknowledgements

I would like to begin by thanking my supervisor Dr. Larry Heaman, for helping me develop an innovative thesis topic and introducing me to the world of radiogenic geochronology. I would like to extend my gratitude to Larry for the time and patience he has devoted to editing my thesis and also for the funding enabling me to attend the 7th International Kimberlite Conference in Cape Town, South Africa. The experience is unforgettable. I would like to thank my co-supervisors, Dr. Bob Luth for helping me get on the right track of scientific writing and Dr. Rob Creaser for suggesting the Rb-Sr isotopic technique that became an integral part of my project. Their advice and suggestions were a valuable asset to this project.

It would be impossible to begin a project without the support of technical staff. I would like to thank Mark Labbe and Don Resultay in the rock cutting and thin section lab for their efforts in getting samples done under time constraints; Barbara Böhm for showing me the rock crushing and mineral separation procedures; Lang Shi for help on the microprobe; George Braybrook for SEM analyses of some 'unknown' minerals; Stacey Hagen for her tutorials and patience in the mass spectrometry lab and Randy Pakan for scanning diagrams and preparing slides for talks when time had run out.

Becoming a graduate student at the University of Alberta has been a rewarding experience both academically and socially. I have had the great opportunity of meeting many wonderful people who have become life long friends. I would like to thank Dave for all his help when he found me in a panic, spending many hours getting diagrams 'just right' for presentations, for taking the time out to edit portions of my thesis and for hours of entertainment of 'pictionary fun' at the Next Act. I would like to thank Candice, Nancy and Steph for all the hours of gab sessions, for being there when 'you just needed to talk' and for all the laughs at silly things I don't think anyone else would have found funny. I also want to thank Al, Cathy, Mike H., Rajeev, Karen and Elspeth, who have listened to me during tough times and have never doubted my abilities as 'it's normal to feel like that'.

When I arrived, there were a group of people that took me under their wing and made the transition of living in a new city more comfortable. I thank Betsy, Kim, Leslie, Devon, George, Skids and Joe for all the fun times on hiking and back-country skiing trips in the mountains and party nights (Halloween-flower power, malt whiskey parties at

George's, dancing at the Commercial and Next Act nachos on cold winter nights). I would also like to thank the 'Monopros Gang' who are real troopers and who do things 'for the team'. Deirdre, Jason, Aaron, Cody, Siobhan and Claudine have all made work experience 'interesting'. I value the time and the experiences with them in the 'land of the midnight sun'.

Lastly but certainly not least, I thank my parents and my brother, Stephen, for their unending support and confidence in my endeavors. They have provided advice and encouraging words when things felt grim, have always had the utmost belief in me and taught me that perseverance is the key to every trial in life. Keep on keepin' on.

I cherish all the memories gained and the ones to come.

Table of Contents

Introduction 1

Geology of the Monastery Mine

Regional setting 4

Geology of the Monastery kimberlite 12

Previous Work

Historical 15

Background on ilmenite mineral chemistry 15

Summary of previous geochronology for the Monastery kimberlite 19

Petrography 20

Mineral chemistry of some Monastery megacrysts 25

Ilmenite Discrete Nodules 28

Groundmass Ilmenite 32

Comparison with ilmenite from other kimberlite studies 34

Phlogopite 35

Perovskite 38

Isotope Geochemistry

Analytical Techniques

Rb-Sr 39

U-Pb (perovskite, zircon and ilmenite) 42

Results

Rb-Sr Phlogopite 47

U-Pb Perovskite 50

U-Pb Mantle Zircon 52

U-Pb Ilmenite 55

Discussion

Geochronology of kimberlite - traditional techniques

Rb-Sr Phlogopite 60

U-Pb Perovskite 61

U-Pb Mantle Zircon 62

Geochronology of kimberlite - new technique

U-Pb Ilmenite

i) Geochemistry 66

ii) Geochronology 67

Summary of Age Determinations 68

Nature of kimberlite source regions

i) Lead 70

ii) Strontium 71

Conclusions 72

References 73

Appendix A 80

Ilmenite macrocrysts 81

Ilmenite megacrysts 84

Groundmass Ilmenite 85

Phlogopite 86

Perovskite 88

List of Figures

Figure 1 Map of South Africa 5

Figure 2 Orogenic events of Africa 7

Figure 3 Timeline of events for the African continent 9

Figure 4 Karoo Sedimentary system of South Africa 10

Figure 5 Monastery kimberlite pipe 13

Figure 6 Ilmenite trends and compositions 18

Figure 7 Published ages for Monastery 18

Figure 8

A Cr_2O_3 vs MgO - Core and rim ilmenites 29

B Cr_2O_3 vs MgO - Groundmass ilmenite

C Ilmenite nodules and groundmass ilmenite comparison 33

D Ternary plot - Monastery ilmenite (this study)

E Cr_2O_3 vs TiO_2 - Phlogopite classification 37

D Ternary plot - Monastery ilmenite (this study)
E Cr_2O_3 vs TiO_2 - Phlogopite classification 37
F TiO_2 vs CaO - Perovskite
Figure 9
A Isochron plot - Phlogopite 48
B $^{84}Sr/^{86}Sr$ vs 1/Sr - Phlogopite spike 48
C Isochron plot - Non-leached phlogopite 49
D Isochron plot - Leached phlogopite 49
Figure 10 51
A Isochron plot - Perovskite
B Weighted Mean $^{206}Pb/^{238}U$ Age for Perovskite
Figure 11 Weighted Mean $^{206}Pb/^{238}U$ Age for Zircon 54
Figure 12 Th vs U - Zircons 54
Figure 13 57
A Isochron plot - Ilmenite (all analyses)
B Isochron plot - East End Type kimberlite ilmenite
C Isochron plot - Ilmenite megacrysts
Figure 14 Th vs U - Ilmenite and Zircon 59
Figure 15 Summary of Monastery ages (this study) 69
Figure 16 $^{207}Pb/^{204}Pb$ vs $^{206}Pb/^{204}Pb$ - Mantle components 69

List of Plates

Plate 1 6
A&B Recent photos of the Monastery quarry and the surrounding area
Plate 2 **Hand sample photographs** 14
A East End Type kimberlite
B Quarry Type kimberlite
C Breccia Type kimberlite
Plate 3 **Thin section photographs** 21
A Quarry Type kimberlite

B East End Type kimberlite
C Breccia Type kimberlite
Plate 4 **Thin section photographs** 23-24
A Kinked phlogopite phenocryst
B Garnet with kelyphite rim
C Sulfides on ilmenite
D Altered Olivine (cross nicols)
E Phlogopite with reaction rim (cross nicols)
F Polycrystalline Ilmenite
G Ilmenite with Mg-rich reaction rim
H Pitted Ilmenite
I Zoned perovskite
Plate 5 **Electron Microprobe images**
A Deformed and highly fragmented ilmenite 30
B Large homogeneous ilmenite 30
C Ilmenite core with reaction rim 30
D Rim with Fe-Ilm and perovskite association 30
E Groundmass ilmenite with sulfides 30
F Phlogopite with ilmenite on rim 36
G Zoned perovskite 36
H MgO and CaO variation diagram for Perovskite 36
Plate 6
A Phlogopite megacryst in Breccia Type kimberlite matrix 40
B Phlogopite megacryst #3 40
C BSE image of phlogopite megacryst #3 40
D Perovskite grain variations 43
E Picked mantle zircon fraction 43
F Ilmenite megacryst in kimberlite matrix 43
G Picked ilmenite fraction 43

List of Tables

Table 1	Karoo Sedimentary formations	11
Table 2	Mineral abundances	15
Table 3	Summary of ilmenite classifications	16
Table 4	Representative analyses of ilmenite, phlogopite, perovskite and oxide ranges - mineral chemistry	26-27
Table 5	Rb-Sr results for phlogopite	41
Table 6	Blank data for ilmenite	46
Table 7	U-Pb results for perovskite	46
Table 8	U-Pb results for zircon	53
Table 9	U-Pb results for ilmenite	56

Introduction

The recent discovery of diamond-bearing kimberlite in Canada (e.g. in Ontario and the Northwest Territories) and the discoveries of new kimberlite fields (e.g. northern Alberta) have initiated a boom in diamond exploration within North America. As a result, there is a restored interest in understanding the formation and origin of kimberlites in North America, especially in Canada. Many North American kimberlites do not contain primary minerals such as phlogopite, perovskite, and mantle zircon commonly used to determine pipe emplacement ages. In addition, kimberlites are notorious for being mineralogically and lithologically heterogeneous. The ubiquitous presence of xenocrysts in many kimberlites makes identification of primary minerals difficult. For this reason, it is preferable to apply more than one isotopic technique, when possible, to determine the emplacement age of a single kimberlite pipe. One dating technique alone may yield geologically meaningless ages, depending on factors such as alteration and/or the presence of xenocrysts.

Radiogenic isotopic methods can be implemented to obtain a more comprehensive understanding of both the origin and timing of kimberlite magmatism world-wide. Kimberlite emplacement ages provide important information on the timing of local and regional tectonic controls associated with kimberlite formation. Mitchell (1986) identified two controls that affect the distribution and mode of kimberlite emplacement. The first involves near-surface structural features such as local and regional fracture patterns. The second control is highly debatable involving deep-seated mechanisms that control magma ascent. The latter control has generated wide-spread research for determining why kimberlites occur and why they occur in the regions in which they are found (Helmstaedt and Gurney, 1984). Mitchell (1986) has summarized the research of the various proposed mechanisms for kimberlite emplacement which include, transform fault extensions, continental rifting, mantle hot spots as well as subduction zones. However, it appears that a single mechanism cannot be applied to all kimberlite provinces world-wide (Helmstaedt and Gurney, 1984; Mitchell, 1986). For example, one mechanism may explain kimberlite occurrences in the eastern North American provinces (e.g. mantle plume hotspot-related magmatism; Heaman and Kjarsgaard, 2000), but cannot be responsible for Type III (as defined by Mitchell, 1986) multiple-age provinces such as the Lac de Gras field, N.W.T. Also, as Mitchell (1986)

noted, many of the mechanisms are not supported petrologically, geochemically or geochronologically. As an example, geochronology can be used to support or dispute the mantle hot spot hypothesis. If kimberlite magmatism is related to mantle plume activity as proposed by Greenwood et al. (1998), then an age progression of kimberlite emplacement should be evident. Many kimberlites in South Africa have been dated by Rb-Sr and U-Pb isotopic techniques and it has been established that these kimberlites were emplaced in restricted time periods (e.g. 80-114 Ma and 114-150 Ma; Smith, 1983) and do not display an age progression of kimberlite emplacement that would be evident with a mantle hotspot origin for the kimberlitic magma.

Many kimberlites are associated with fault zones, however, it is not known why kimberlites concentrate on some faults but not others (Mitchell, 1986). With the combined use of petrology, structural geology, geochemistry and geochronology, the mechanisms that cause kimberlite emplacement can be further constrained. Many questions still remain regarding the genetic relationship between kimberlite and other magmas of deep-seated origin such as alnöite, lamproite and melilitites as well as why repeated kimberlite intrusions are restricted to a particular region (Michell, 1986). In addition, absolute formation ages, the definition of kimberlite (i.e. mis-identification of kimberlite), tectonic environments, as well as theories of diamond formation still require further investigation (Helmstaedt and Gurney, 1984).

A new isotopic technique is necessary in order to determine the emplacement ages of numerous North American kimberlites that currently cannot be dated. Ilmenite is widely used as an exploration tool for kimberlites because of its presence in almost all kimberlites world-wide, its chemical and physical resilience, and its diagnostic Mg-rich character that distinguishes kimberlitic ilmenite from ilmenite in other igneous bodies. Extant research regarding mineral chemistry and petrology have concluded that ilmenite is genetically linked to crystallization in kimberlitic or proto-kimberlitic magmas (Mitchell, 1973; Schulze et al., 1995). Ilmenite was chosen for preliminary U-Pb analyses because it is known to contain uranium (Kresten, 1974). For example, ilmenite from South African kimberlites (Kao, Lemphane and Sekameng/Kolo kimberlites) yielded a range of uranium concentrations for six ilmenite nodules of approximately 0.1-0.2 ppm and analyses of whole rock kimberlite from Monastery yielded uranium concentration of 4.1 ppm (Kresten, 1974). The presence of small amounts of uranium in ilmenite

suggests that this mineral has the potential to yield geologically meaningful U-Pb age information that may help to constrain the emplacement age of kimberlites.

The Monastery kimberlite was chosen because it contains an abundance of ilmenite megacrysts and macrocrysts as well as minerals typically used to determine kimberlite emplacement ages such as phlogopite, perovskite and minor mantle zircon. The Monastery kimberlite is an extensively studied kimberlite intrusion, with numerous previous studies of mineral chemistry (Boyd and Nixon, 1975; Haggerty et al., 1979; and Gurney et al., 1979, 1998), major- and trace-element geochemistry (Moore et al., 1992) and geochronology (Allsopp and Barrett, 1975; Davis et al., 1976; McIntyre and Dawson, 1976; Kramers and Smith, 1983; Smith and Barton, 1996; and Zartman et al., 1998). Of particular importance to this study, the paragenesis of kimberlitic ilmenite has been extensively studied at Monastery (Boyd and Nixon, 1975; Mitchell, 1977, 1986; Haggerty et al., 1979; Gurney et al., 1979, 1998; Moore et al., 1992; and Griffin et al., 1997). Therefore, the Monastery kimberlite represents an ideal natural example for testing new radiometric dating techniques using ilmenite. In addition, the initial Pb isotopic compositions of ilmenite may also provide important constraints regarding the poorly-understood origin of this mineral.

For this study, it is important to completely characterize the mineral chemistry of ilmenite, perovskite and phlogopite and compare with the published data. It is also essential to determine if the ilmenite megacrysts and macrocrysts are compositionally heterogeneous, because such heterogeneity may complicate the interpretation of the isotopic results. Furthermore, it is of interest to identify reaction rims, altered material, and inclusions within the megacrysts as these factors could potentially affect the isotopic results. Minerals that possess complex growth histories could have important ramifications for isotopic results and therefore, should be identified prior to isotopic analyses if possible.

The objectives of this research are two-fold. The first is to provide a comprehensive study of the currently used radiometric techniques on the Monastery kimberlite (e.g. Rb-Sr phlogopite, U-Pb mantle zircon and perovskite) to provide a robust chronology of kimberlite emplacement history. The second is to the feasibility of U-Pb ilmenite geochronology as a new tool in determining the age of kimberlite emplacement.

Geology of the Monastery Mine

Regional Setting

The Monastery kimberlite is located in the Eastern Free State of South Africa, close to the border of Lesotho (Figure 1). After its initial discovery in 1876, mining operations did not begin until 1886, when 150 000 tonnes of Quarry Type kimberlite was mined specifically for diamonds and ilmenite (Whitelock, 1973). Early mining operations (1886-1899) ceased due to the onset of the Anglo-Boer War in 1899 and mining did not resume until 1965 (Whitelock, 1973). Plate 1 A&B are recent photos of the Monastery quarry and the surrounding area, respectively.

Geologically, the Monastery kimberlite is situated within the Kaapvaal craton along with numerous other diamond-bearing kimberlite fields (e.g. Kimberley field; Figure 1). The Kaapvaal craton extends from the Lebombo Mountains to the Orange River at Prieska in an east-west direction, and from the Limpopo Belt to Lesotho in a north-south direction (Figure 1) (Cahen et al., 1984). The Kaapvaal craton is composed primarily of Archean granite-greenstone belts and of sediments and volcanics of Archean and Proterozoic age. Greenstone belts commonly crop out in the northern parts of the craton and include the Barberton Mountainland, the Murchison Range, the Pietersburg schist belt and the Sutherland Range (Figure 1). An approximate age of these greenstone belts is 3300 Ma (Cahen et al. 1984). The Kaapvaal craton is bounded on the south by the Namaqua-Natal Mobile Belt (~1.4 Ga), which is obscured by sediments from the Karoo System (Late Carboniferous to Jurassic) (Nixon, 1987). The Archean Limpopo Mobile Belt bounds the Kaapvaal craton to the north (Figure 1).

There have been six major events that have affected the African continent since the formation of the Kaapvaal craton in the Archean. Regions of the African continent that have been affected by these events are shown in Figure 2. The Shamvaian Orogeny (2800-2500 Ma) and the Eburnian and Huabian Orogenies (1850 ± 250 Ma). The Kibaran Orogeny (1100 ± 200 Ma) responsible for fusing the Kaapvaal craton with the Namaqua-Natal fold belt, the Damaran-Katangan orogeny (550 ± 100 Ma) and the Middle Paleozoic-Early Mesozoic orogeny responsible for the formation of fold belts in north-west Africa and the Cape Fold Belt. Finally, the Alpine Orogeny formed the Atlas mountains in northern Africa (Clifford, 1970).

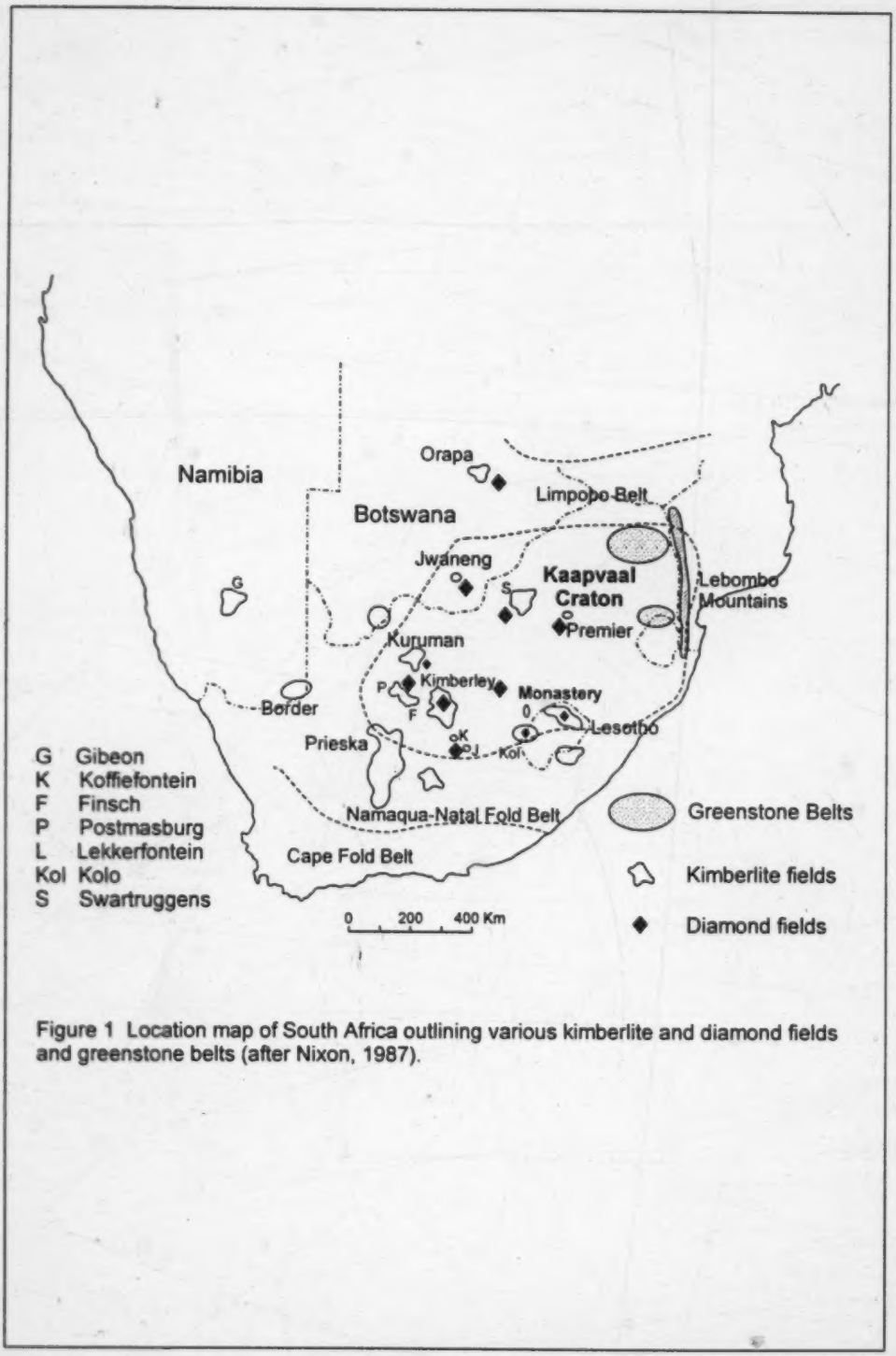

Figure 1 Location map of South Africa outlining various kimberlite and diamond fields and greenstone belts (after Nixon, 1987).

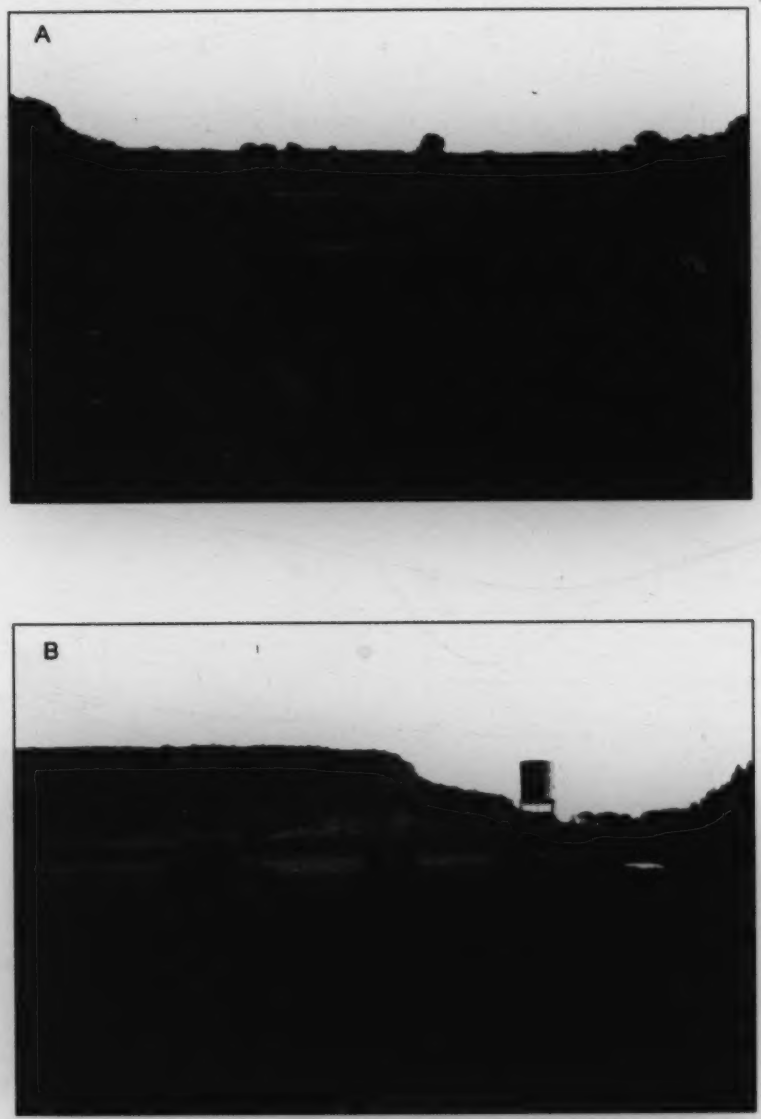

Plate 1 **A:** A view of the Monastery mine in 1998. The circular pit of the kimberlite can be seen in the background. **B:** A view of the area surrounding the Monastery mine with exposed cliffs of the Jurassic Stormberg sediments in the background.

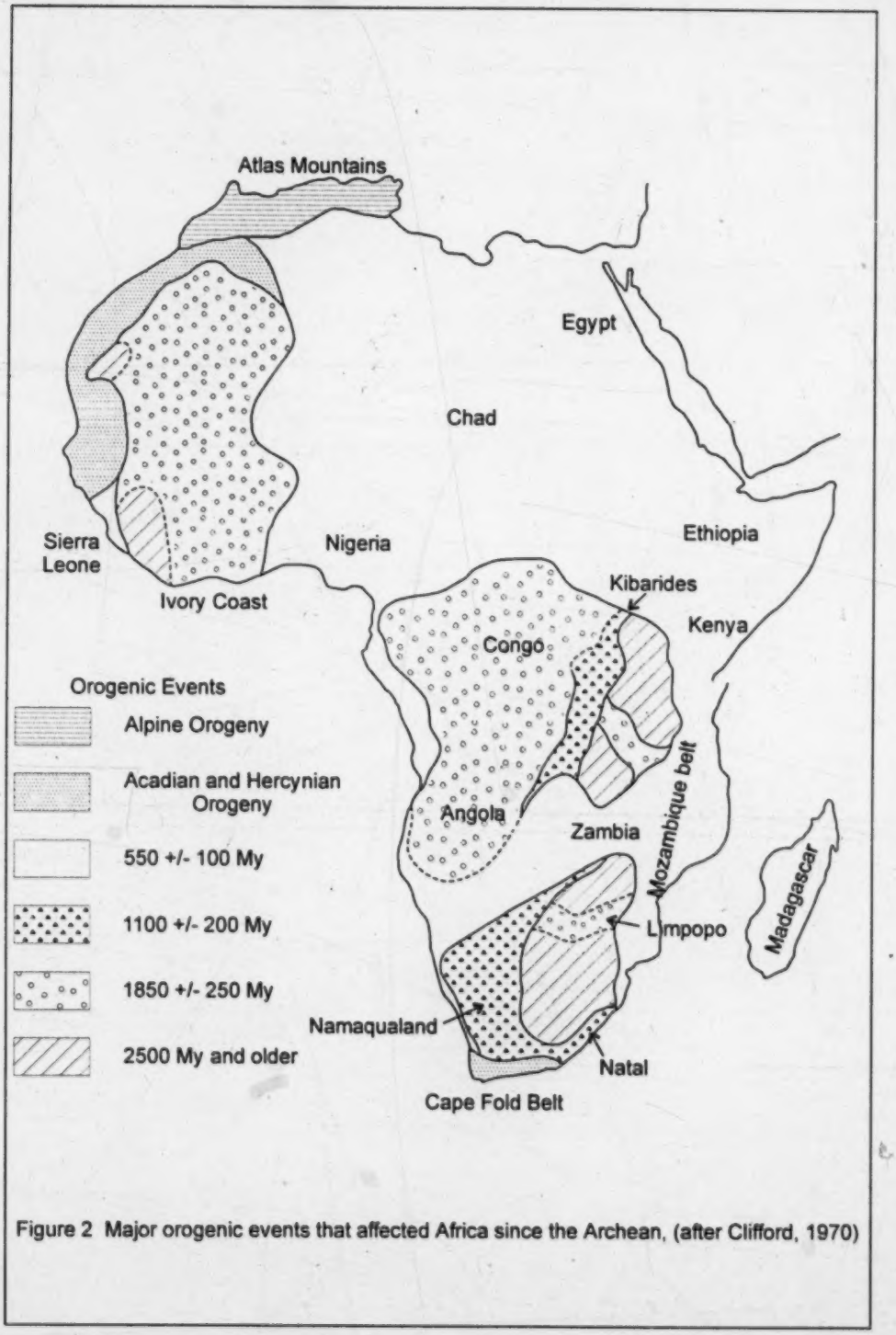

Figure 2 Major orogenic events that affected Africa since the Archean, (after Clifford, 1970)

Clifford (1970) noted that diamond-bearing kimberlites are typically located in cratonic areas in Africa that have not been affected tectonically since the 1850 Ma orogenies (Eburnian and Huabian). Except for the northern region, most of the African continent has been stable since the Damaran-Katangan Orogeny at 550 Ma (Truswell, 1977). Figure 3 is a timeline outlining the events affecting the African continent.

The majority of South Africa is covered by the Karoo sediments that range in age from 300 to 160 Ma (Truswell, 1977). The Karoo sediments have been divided into three groups (Figure 4). The Ecca Group is comprised of shales, sandstones, conglomerates and coal deposits. The Beaufort Group is comprised of a sequence of shales and mudstones with argillaceous units that are typically red, green and purple in colour. The third group is the Stormberg Group which forms the top-most unit in the Karoo sediments. Shale, sandstone (usually massive but sometimes cross-bedded), siltstone, pebbly conglomerate and red mudstone are the rock types found in the Stormberg Group. The Monastery kimberlite intrudes the Red Bed or Elliot Formation of the Stormberg Group (Whitelock, 1973). A table of the Karoo sedimentary formations is shown in Table 1.

The end of the Karoo sedimentation period (190 to 160 Ma) was marked by a spectacular volcanic event in South Africa producing extensive lava flows and dolerite dikes and sills of the Drakensberg volcanics. The Drakensberg lava flows found in northern Lesotho reach a maximum thickness of 1400 m (Truswell, 1977). Associated with the Drakensberg volcanics are the hypabyssal Karoo dolerite dikes and sills. The Drakensberg volcanism spanned a period ranging from 184-179 Ma with the majority of volcanics (lava flows, dolerite dikes and sills) occurring at 183 ± 1 Ma (Duncan et al., 1997). The Karoo dolerites and Drakensberg volcanics appear to be limited to the Karoo basin as they are not found within the Cape Fold Belt (south of Kaapvaal craton) (Truswell, 1977). Cox (1970) estimates the area affected by the volcanism to be ~ 2 000 000 km^2 with ~ 140 000 km^2 of outcrop remaining after erosion and post-Karoo sedimentation.

The kimberlites in South Africa were emplaced post-Karoo sedimentation and volcanism as they intrude these units and many kimberlites contain xenoliths of basement gneiss, sandstone, siltstone, dolerite, gabbro and Drakensberg volcanics (Allsopp and Barrett, 1975; Truswell, 1977; Allsopp and Roddick, 1984).

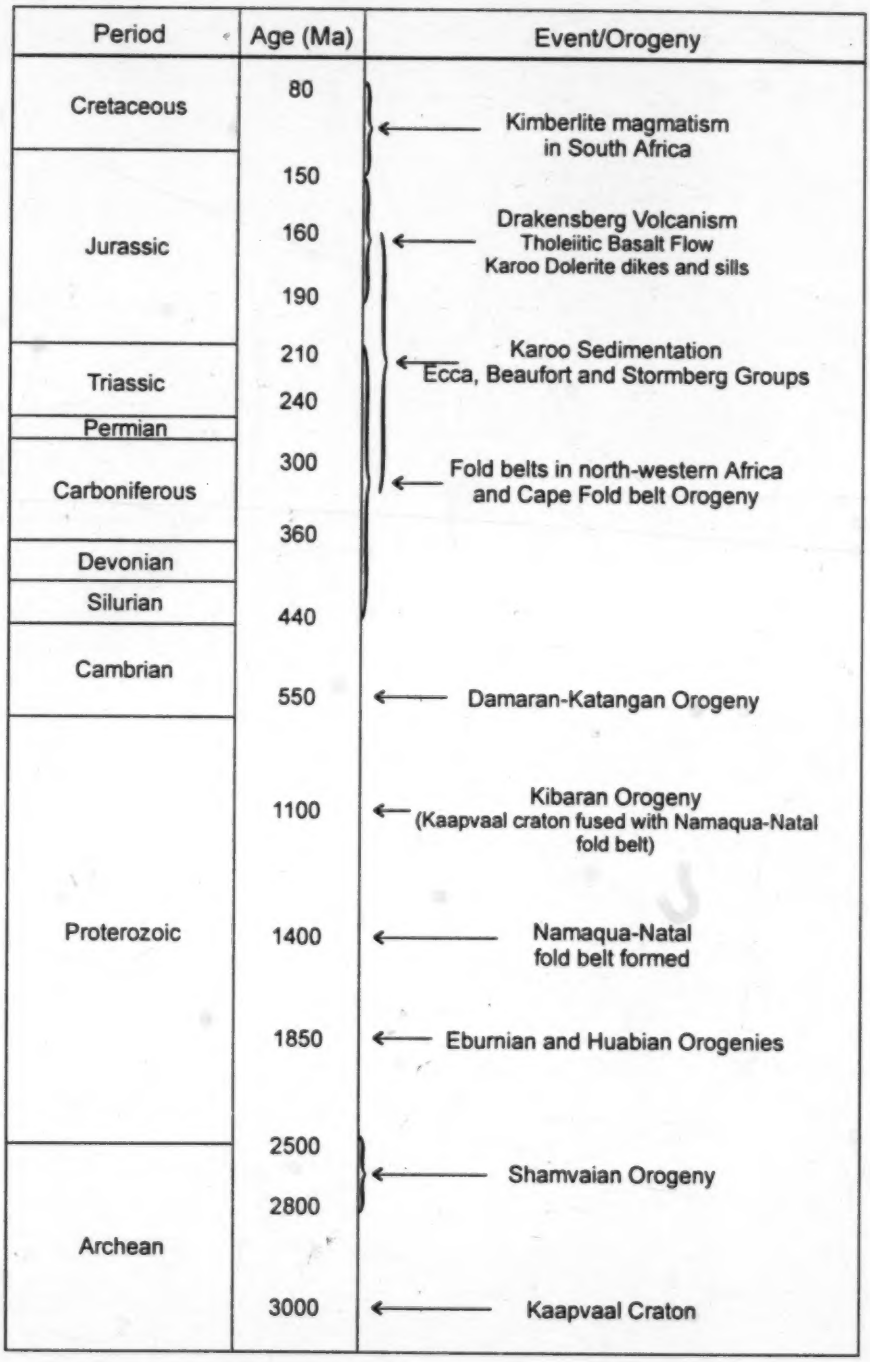

Figure 3 Timeline of events for Africa.

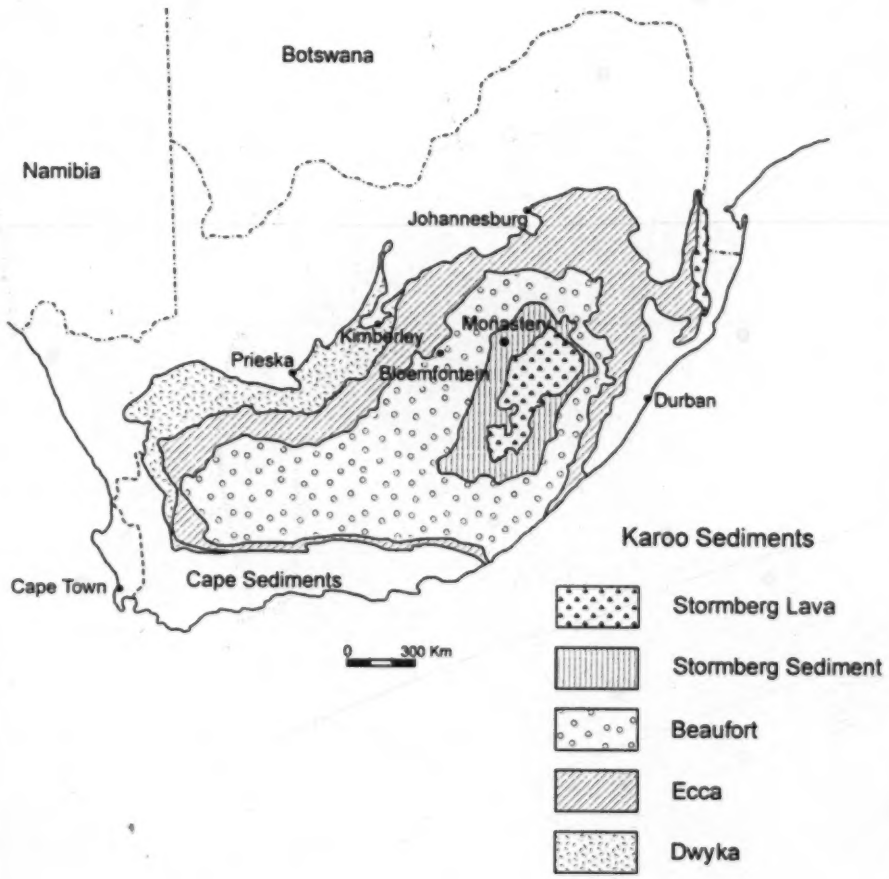

Figure 4 Map of the Karoo sediments of South Africa, (after Truswell, 1977).

Karoo Sediments

Jurassic	Karoo System	Stormberg Group	Drakensberg Volcanics Clarens Formation Elliot Formation Molteno Beds Formation
Triassic		Beaufort Group	Upper Middle Lower
Permian		Ecca Group	Southern Western Northern

Table 1 Sequence of formations of sediments found in the Karoo basin. After Williams (1932).

Geology of the Monastery kimberlite

Figure 5 is a map of the Monastery kimberlite with schematic representation of intrusion shape at various levels. The kimberlite intrusion is irregular in shape with dimensions approximating 180m in length by 70m in width (Figure 5) (Whitelock, 1973). Whitelock (1973) describes four kimberlite types at the Monastery mine: the East End Type, Quarry Type, Breccia Type and Fine-Grained Type. Large blocks of the first three types from the mine dumps, are shown in Plate 2. The East End Type kimberlite is located at the eastern-most tip of the intrusion and was termed the "eastern blow" by Whitelock (1973). This kimberlite type narrows to a dike-like structure, inclining at shallow depths. The Quarry Type kimberlite is the most abundant and most diamondiferous rock type at the Monastery mine (Whitelock, 1973). Dolerite is found at surface exposures along the southern rim of the Quarry Type kimberlite and also occurs as xenoliths scattered throughout the intrusion (Figure 5A). The Breccia Type kimberlite forms a column in the central region of the intrusion and has been noted by Whitelock (1973) to have a westerly dip of 70°. A subsurface "South Vent" (Figure 5B&C) was discovered through a series of bore-holes and it is suggested by Whitelock (1973) that it may be connected to the main body of the kimberlite.

The first estimate of the relative abundance of megacrysts present at Monastery (Gurney et al., 1979) in decreasing order is as follows: ilmenite, diopside-ilmenite, garnet, diopside, olivine, mica, orthopyroxene, garnet-ilmenite, orthopyroxene-ilmenite, orthopyroxene-diopside, and rare garnet-diopside and olivine-ilmenite. Subsequent to further prospecting and mining, the relative megacryst abundance has been revised by Gurney et al. (1998) to: ilmenite, olivine, diopside-ilmenite, garnet, phlogopite, diopside, enstatite, enstatite-ilmenite, garnet-ilmenite, diopside-enstatite and rare occurrences of garnet-diopside, olivine-ilmenite, olivine-garnet, olivine-enstatite, olivine-diopside, phlogopite-ilmenite, zircon, zircon-ilmenite, zircon-olivine, and zircon-phlogopite. In both estimates, ilmenite is clearly the most abundant megacryst. Nixon and Boyd (1973) estimated relative abundances of deep-seated nodules based on a 12 kg kimberlite sample with the results shown in Table 2:

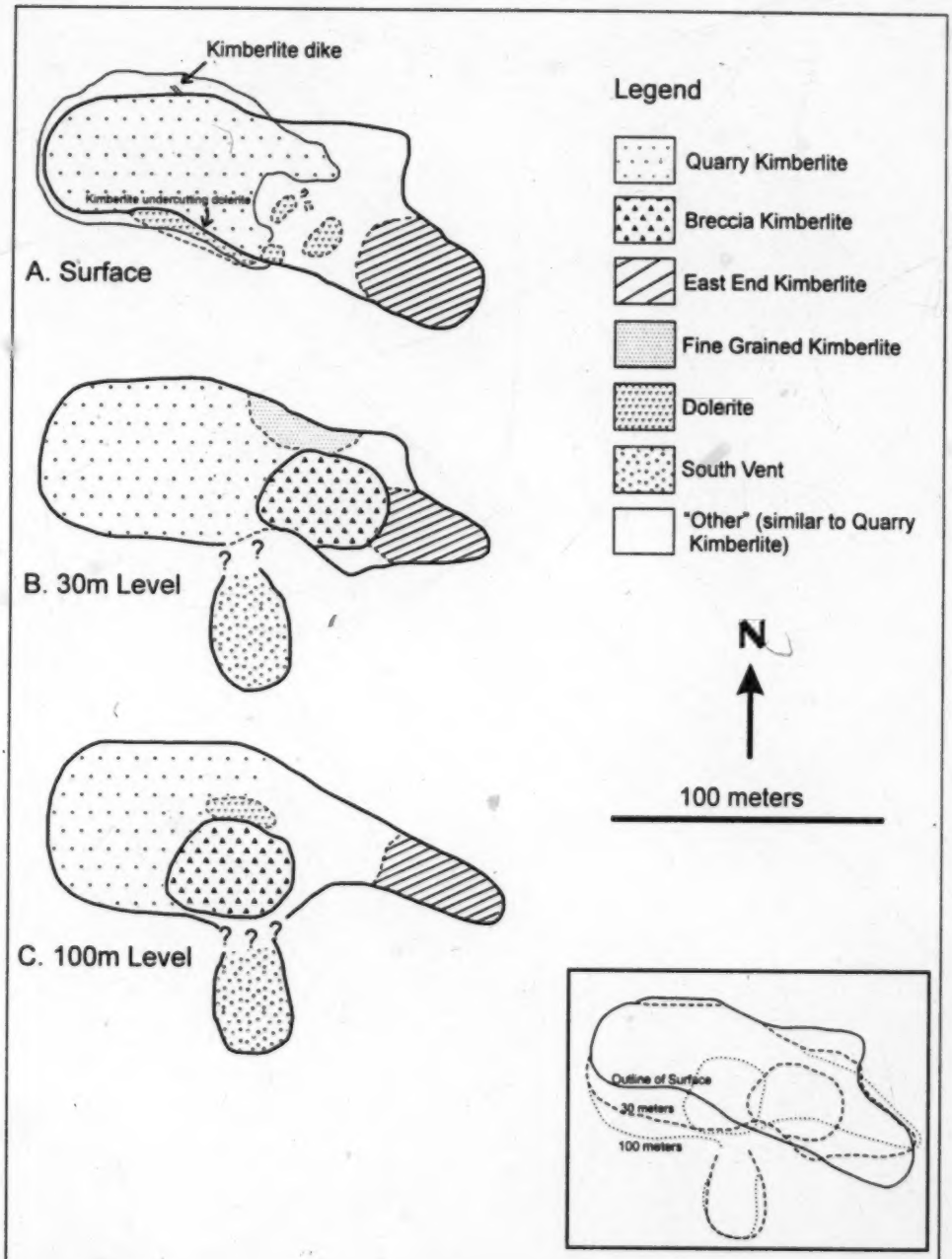

Figure 5 Schematic diagram of the Monastery kimberlite pipe at various mine levels, (after Whitelock, 1973).

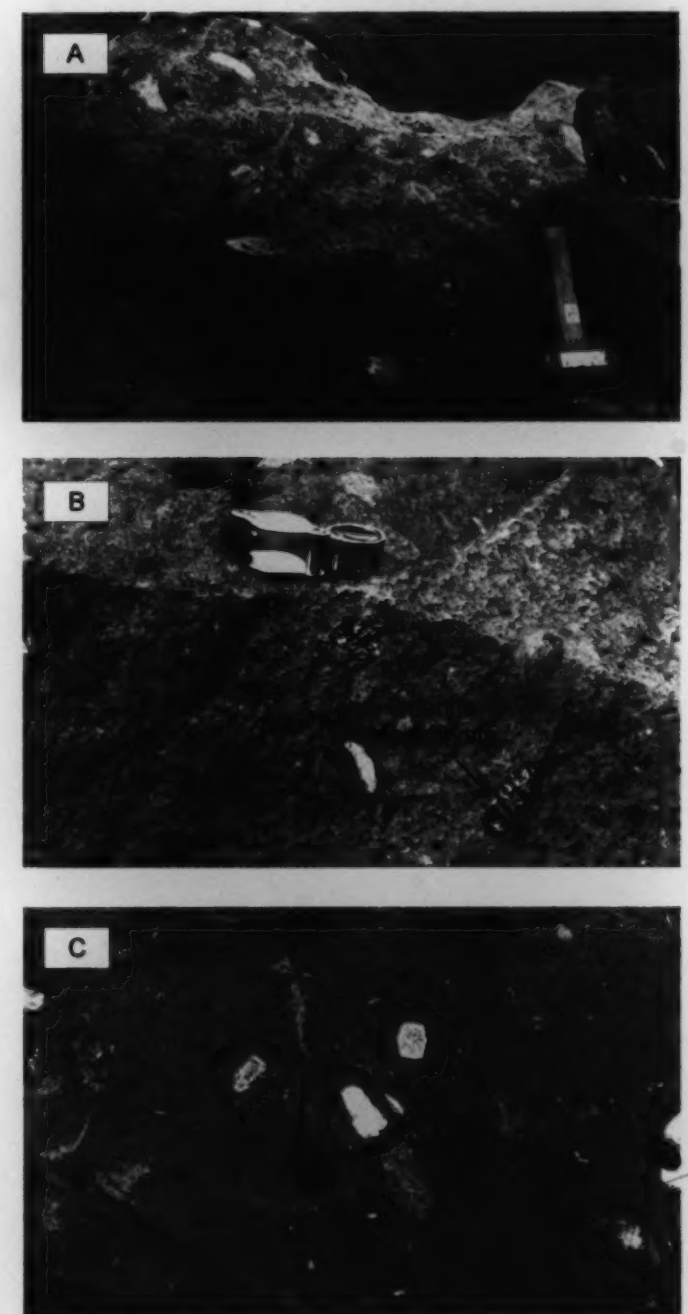

Plate 2 Hand sample photographs of the three main types of Monastery kimberlite. **A** East End Type kimberlite, **B** Quarry Type kimberlite, and **C** Breccia Type kimberlite.

Table 2 Mineral abundances - Monastery	
Mineral	wt%
Ilmenite nodules	47
Ultrabasic nodules	17
Ilmenite-diopside intergrowths	13
Garnet nodules	10
Dunite nodules	7
Garnet-diopside, diopside	4
Bronzite, phlogopite etc	
Basement gneiss	2

Nixon and Boyd (1973)

Previous Work on Ilmenite

Historical

The major- and trace-element geochemistry of ilmenite from Monastery has been studied since the early 1900's. Monastery is known for its ilmenite-pyroxene intergrowths and it is this aspect that has generated much research on this kimberlite, starting with Williams (1932). It was found that the chemistry of ilmenite nodules differs from the ilmenite within ilmenite-pyroxene intergrowths even though it was interpreted that they originate from the same source in the upper mantle (Dawson and Reid, 1970). Various ilmenite associations are documented in the literature and are classified in an attempt to find similarities in ilmenite for all kimberlites. The conditions (temperature: ~ 1200°C and pressure: 50-60 Kb) under which crystallization of ilmenite occurred and therefore the depth of crystallization (150-190 km), have been determined by Gurney et al. (1973) and Boyd and Nixon (1973) through studies of the mineral chemistry of coexisting enstatite, diopside, garnet and ilmenite.

Background on ilmenite chemistry

In an attempt to understand the paragenesis of ilmenite and define the processes responsible for the formation of megacrysts, numerous authors have grouped ilmenite based on mineral associations and chemical compositions (Haggerty et al., 1979; Moore et al., 1992; and Gurney et al., 1998). These classification schemes are outlined in Table 3 and as a comparison, ilmenite data from this study are included.

Table 3 Summary of Monastery Ilmenite Classifications

Reference	Classification
Haggerty et al. (1979) (1040 analyses)	1a Discrete Nodules $Geik_{20}Ilm_{43}Hem_{23}$ b Polycrystalline Nodules $Geik_{45}Ilm_{40}Hem_{13}$ 2 Ilmenite-Pyroxene Intergrowths $Geik_{35}Ilm_{45}Hem_{20}$ Conclusions: Two distinct compositional populations, however, fields do overlap, therefore must be derived from same ilmenite saturated region in mantle.
Moore et al. (1992) (120 Ilmenite analyses)	**Group 1** - Cr-poor (< 0.4 wt% Cr_2O_3) - higher Nb and Zr - associated with minerals from the Main Silicate Trend **Group 2** - moderate Cr (0.5-1.2 wt% Cr_2O_3) - high Nb, intermediate Zr - more evolved compositions (low MgO) - associated with zircon, Fe-rich olivine and phlogopite **Group 3** - high Cr (> 1.2 wt% Cr_2O_3), Ni, Mg and low Fe and Zn (more primitive) - intermediate Nb, low Zr - associated with phlogopite and Ca-clinopyroxene
Gurney et al. (1998)	**Group 1** - Cr-poor - low Nb, high Zr/Nb - Moore et al. (1992) Group 1 **Group 2** - Cr-rich - high Nb, low Zr/Nb - associated with zircon, phlogopite, Fe-olivine, and Ca-clinopyroxene - Moore et al. (1992) Groups 2 and 3
This Study (12 core analyses)	**Discrete Nodules $Geik_{20}Ilm_{43}Hem_{18}$** Conclusions: Combination of discrete nodule, polycrystalline and ilmenite-pyroxene intergrowths. **Cr_2O_3 0-0.9 wt%** Conclusions: falls between Gurney et al. (1998) Group 1 and 2. With more analyses, the distinction may be more clear.

Mitchell (1973) first recognized through the chemistry of ilmenites that the MgO compositions could vary as much as 13 wt% within an individual kimberlite pipe (e.g. Wesselton kimberlite) and as much as 8 wt% MgO variation can be found between homogeneous ilmenite grains within a single hand sample of kimberlite. Mitchell (1973) concluded that these variations resulted from mixing of a hetergeneous cumulate body of ilmenite, during transport of kimberlite magma.

Haggerty et al. (1979) outlined the chemical differences in the two major ilmenite suites found at Monastery: a discrete nodule suite and a pyroxene symplectite suite. In the discrete nodule suite, Haggerty et al. (1979) found that polycrystalline megacrysts ($Geik_{30}$ Ilm_{45} Hem_{25}) of ilmenite plot separately from discrete nodules ($Geik_{45}$ Ilm_{40} Hem_{15}) on a ternary plot of ilmenite-geikielite-hematite (Figure 6). The ilmenite-pyroxene intergrowths have compositions $Geik_{35}$ Ilm_{45} Hem_{20}. The ilmenite-pyroxene intergrowth field overlaps the discrete nodule suite and polycrystalline nodule fields, therefore, Haggerty et al. (1979) concluded that both suites must be derived from the same ilmenite saturated region in the mantle. Haggerty et al. (1979) also identified four distinctive compositional trends for ilmenite. The first is the "Magmatic Reaction Trend" (zoning towards $MgTiO_3$), followed by the Ilmenite-Pyroxene Trend, the "Kimberlite Reaction Trend" (zoning towards $FeTiO_3$) and finally a trend resulting from exsolution and subsolidus reduction (Figure 6). Analyses of the mineral chemistry of ilmenite from Monastery conducted in this study are compared to the ternary classification outlined by Haggerty et al. (1979).

Moore et al. (1992) outlined three distinct ilmenite groups based on trace element geochemistry and mineral associations. Group 1 ilmenites are defined as being associated with the Main Silicate Trend (garnet, clinopyroxene and enstatite) and are typically Cr-poor (<0.4 wt% Cr_2O_3). Group 2 ilmenites are associated with zircon, phlogopite and Fe-rich olivine and are characterized by moderate Cr contents (0.5-1.2 wt% Cr_2O_3). Group 3 ilmenites are typically associated with phlogopite and clinopyroxene and have a high Cr content (> 1.2 wt%) (Moore et al., 1992).

There are two distinct megacryst populations based on Cr, Nb and Zr contents. Gurney et al. (1998) further refined these populations, which are parallel to the grouping based on trace element geochemistry of Moore et al. (1992). The first population is Cr-poor and is characterized by low Nb and high Zr/Nb. Cr-poor ilmenite is often found intergrown with clinopyroxene, garnet or enstatite from the main silicate

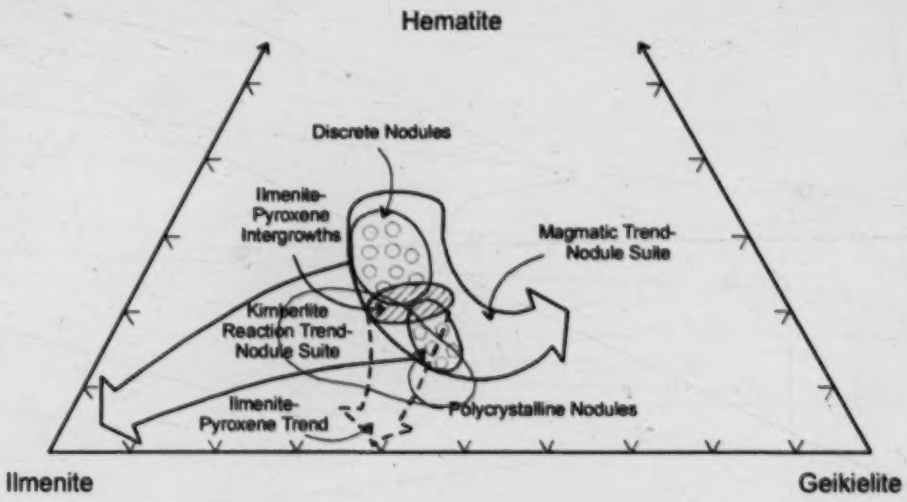

Figure 6 Ternary plot displaying the various trends outlined by Haggerty et al. (1979). Outline in red represents Monastery data from this study.

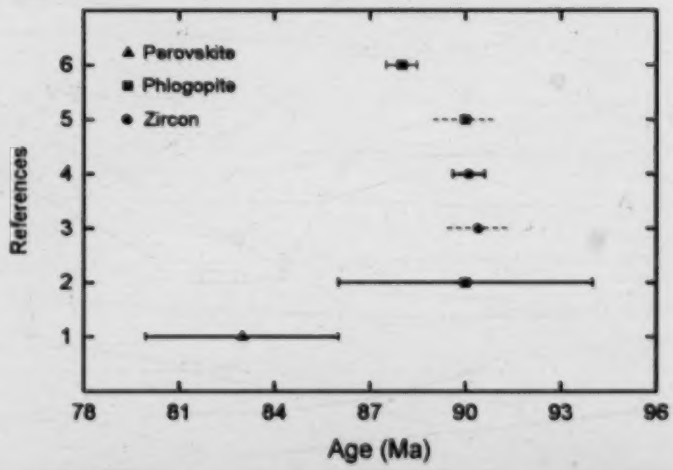

Figure 7 Summary of previous ages for the Monastery kimberlite. References: 1. Kramers and Smith (1983) U-Pb on perovskite (83±3 Ma); 2. Allsopp and Barrett (1975) Rb-Sr on phlogopite (90±4 Ma); 3. Davis et al., (1976) U-Pb on zircon (90.4 Ma); 4. Zartman et al., (1998) U-Pb on zircon (90.1±0.5 Ma); 5. McIntyre and Dawson (1976) K-Ar on phlogopite (90 Ma); 6. Smith and Barton (1996) Rb-Sr on phlogopite (88.1 ± 0.6 Ma). Samples with dashed errors bars are given an estimated ± 1Ma error.

trend (Gurney et al., 1998). This population corresponds to Moore et al. (1992) Group 1. The second population is Cr-rich and is characterized by high Nb and low Zr/Nb. The Cr-rich ilmenite population is often associated with zircon, phlogopite, Fe-rich olivine or clinopyroxene (metasomatic trend) (Gurney et al., 1998). This population corresponds to Groups 2 and 3 of Moore et al. (1992).

With all the research on ilmenite mineral chemistry and its role in crystallizing sequences within kimberlitic magmas, there still appears to be a division into two separate schools of thought. Mitchell (1973, 1977 and 1986) and Pasteris (1980) advocate the hypothesis that ilmenite is a phenocryst phase in kimberlites, whereas Gurney et al. (1979), Moore et al. (1992) and Griffin et al. (1997) support the hypothesis that ilmenite is a xenocryst phase within kimberlites. U-Pb ilmenite geochronology could potentially resolve this problem depending on the closure temperature of uranium and lead in ilmenite. If the U-Pb ilmenite ages are older than kimberlite emplacement age, then this would signify that ilmenite is a xenocryst. However, if the ages are the same as those of the kimberlites, ilmenite would be a phenocryst mineral crystallizing from the kimberlite magma.

Summary of previous geochronology for the Monastery kimberlite

Perovskite, mantle zircon and phlogopite can be used to determine emplacement ages of kimberlites. Previous emplacement ages for the Monastery kimberlite range from 83 ± 3 Ma to 90 ± 4 Ma and are summarized in Figure 7. The U-Pb perovskite age of 83 ± 3 Ma was obtained on a sample of slightly serpentinised, macroporphyritic kimberlite by Kramers and Smith (1983). Due to the small grain size of perovskite, whole rock powders were partially dissolved in an attempt to isolate a perovskite-rich concentrate or minerals with high U/Pb ratios from those which were poor in these elements (Kramers and Smith, 1983). During this leaching step, carbonate material was removed and residual material was significantly reduced in volume facilitating perovskite concentration. In this case, the residue fraction was analysed without further mineral separation. The isochron age of 83 ± 3 Ma was obtained by analysing leach/residue pairs of concentrated perovskite. In contrast, Zartman et al. (1998) obtained a weighted mean $^{206}Pb/^{238}U$ age of 90.1 ± 0.5 Ma from ten crystal fragments of a single mantle zircon megacryst ranging in colour from colourless to medium amber yellow.

Allsopp and Barrett (1975) obtained an age of 90 ± 4 Ma based on an Rb-Sr isochron age derived from nine out of ten analyses of fresh, unaltered phlogopite isolated from five separate kimberlite samples. Smith and Barton (1996) obtained an age of 88.1 ± 0.6 Ma from a single phlogopite megacryst. Smith and Barton (1996) analysed a number of phlogopite pieces from a single 4 cm diameter megacryst and selected portions of the megacryst to specifically identify isotopic and age variations from core to rim; none were found.

South African kimberlites have been divided into two groups based on their emplacement ages and mineralogical components. The Group 1 kimberlites contain little to no late crystallizing groundmass mica and typically have emplacement ages ranging from 80-114 Ma (Smith, 1983). Group 2 kimberlites are mica-rich and have emplacement ages ranging 114-150 Ma (Smith, 1983). The accepted age for the Monastery kimberlite is approximately 90 Ma (Allsopp and Barrett, 1975; Davis et al., 1976 and 1977) and is slightly older than the accepted age for the Kimberley and Jagersfontein area (Group 1) kimberlites (86 to 87 Ma; Smith and Barton 1996).

Petrography

For this study samples of three of the main kimberlite types are described. Samples of the fourth type (Fine-Grained Type) were not collected. Only one thin section was prepared from the Quarry Type and East End Type kimberlites and three thin sections were prepared from the Breccia Type kimberlite. The three main kimberlite types found at Monastery possess minor differences in mineral content and abundance.

Photographs of large blocks of each kimberlite type are shown in Plate 2 A-C and thin section photos are shown in Plate 3 A-C. The Quarry Type kimberlite (M1) is dark-blue in colour and contains visible ilmenite megacrysts and macrocrysts. Rounded, olivine macrocrysts range in size from 0.5 cm to 1mm and are noticeably altered to serpentine. The East End Type kimberlite (M2) is characterized by a pale bluish-grey colour and by an abundance of carbonate flakes in the groundmass. Altered olivine grains possess kelyphite rims, range in size from 0.4 cm to 2 cm in diameter and are reddish-brown in colour. Ilmenite megacrysts and macrocrysts are also abundant.

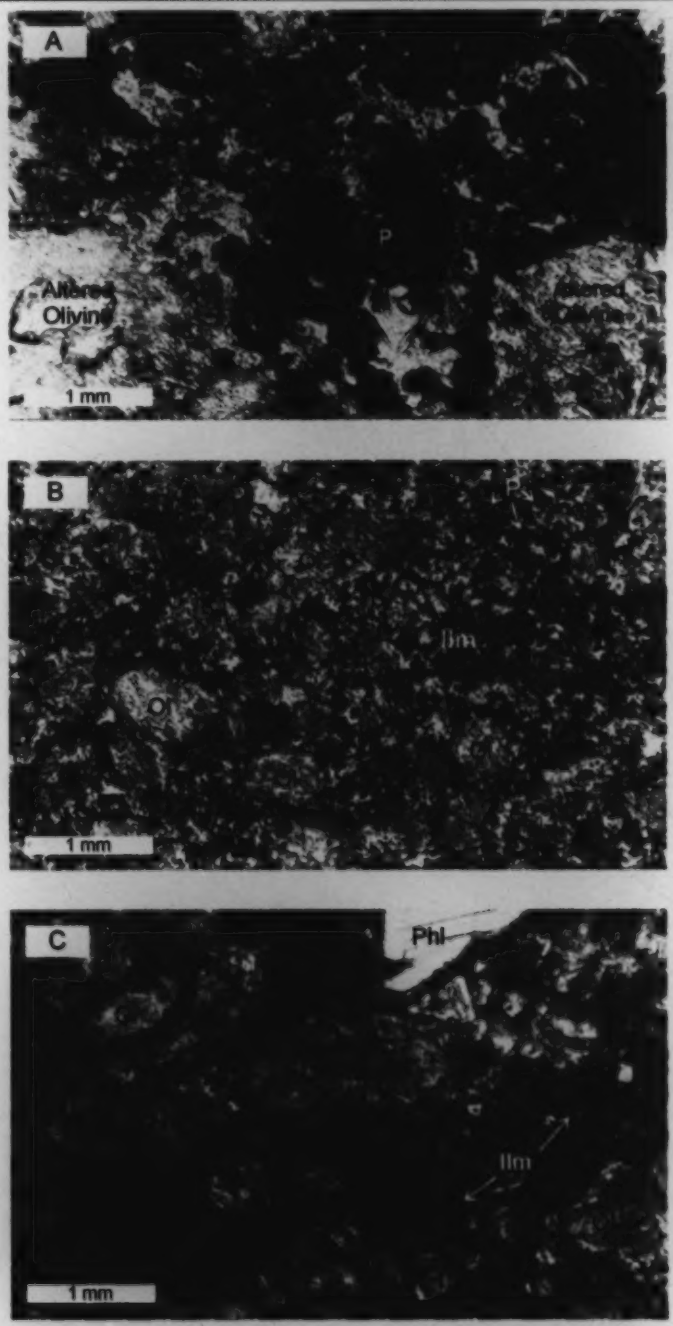

Plate 3 Thinsection photographs of A: Quarry Type kimberlite; B: East-End Type kimberlite and C: Breccia Type kimberlite. Symbols: P-perovskite; Ilm-ilmenite; Ol-olivine; Phl-phlogopite.

The Breccia Type kimberlite (M3) is typically weathered brown in colour and contains a higher abundance of megacrysts. Garnet and phlogopite megacrysts can be as large as 12 cm in diameter, often with kelyphite rims. Ilmenite is present as megacrysts and macrocrysts. In thin section, the megacrysts in the Breccia Type kimberlite are somewhat different than the megacrysts seen in the East End Type and Quarry Type kimberlites. In comparison, phlogopite is more abundant and is unaltered. Some laths contain kink banding (Plate 4A) or ilmenite inclusions; this latter observation has been reported previously to be rare (Mitchell, 1986). Perovskite is less abundant in the groundmass and is smaller in size compared to samples M1 and M2. Garnet macrocrysts possessing kelyphite rims (intergrown pyroxene and phlogopite) (Plate 4B) are more evident in sample M3 than the other two samples. Lastly, small inclusions of chalcopyrite are found in the reaction rims of some groundmass ilmenite (Plate 4C) and euhedral pyrite cubes occur in the groundmass of sample M3.

In thin section, all three samples are similar. The olivine macrocrysts (0.5 mm to 12 mm; modal abundance 35-40%) are completely altered to serpentine (Plate 4D). Similarly, phlogopite macrocrysts (~ 30%) are highly altered to serpentine and calcite. Within the rims of some phlogopite macrocrysts there are ilmenite fragments and perovskite crystals, visible in thin section (Plate 4E). Ilmenite macrocrysts (<1 mm; ~ 20-25%) are typically subhedral to anhedral in shape. A variety of textures are seen in the ilmenite macrocrysts, including polycrystalline grains (Plate 4F), crystals with Mg-rich reaction rims (Plate 4G), pitted crystals (Plate 4H) and single homogeneous crystals. The groundmass is comprised of subhedral olivine grains that are typically <0.5mm in diameter, rounded phlogopite grains (<1 mm), perovskite crystals with a cubic habit (0.2 mm) and anhedral ilmenite fragments (0.1mm to 0.3 mm). Perovskites are tan in colour and are typically zoned (Plate 4I). The alternating light and dark bands correspond to differing chemical and isotopic compositions, which will be discussed later.

There is no published whole rock geochemistry, either for 'average' Monastery kimberlite, or for the various kimberlite types (East End, Quarry or Breccia Type).

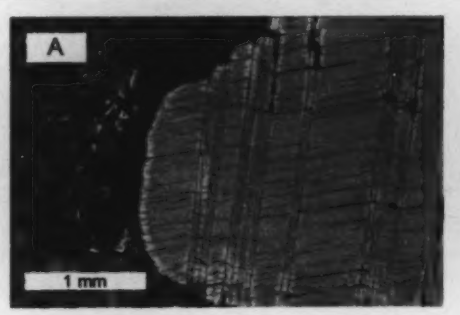

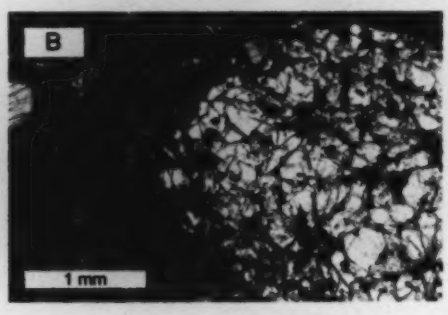

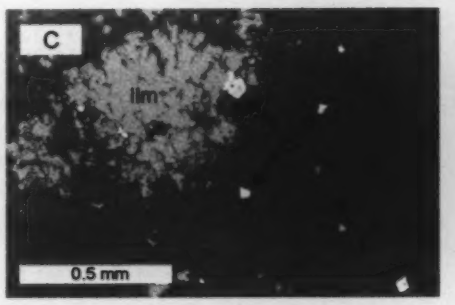

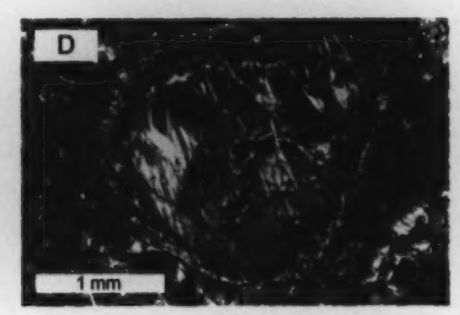

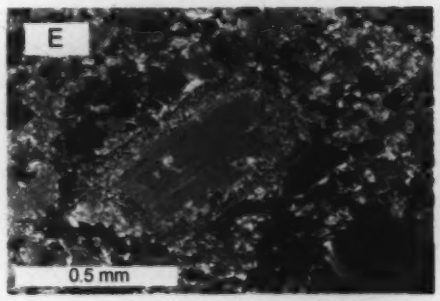

Plate 4 **A:** Sample M3 - Kinked phlogopite macrocryst. **B:** Sample M3 - Garnet with kelyphite rim. **C:** Sample M3 - Sulfides (S) on rim of ilmenite (Ilm) and within kimberlite groundmass (Gm). **D:** Sample M1 - Serpentinized olivine with a slight alteration rim (cross nicols). **E:** Sample M3 - Phlogopite macrocryst with reaction rim (cross nicols).

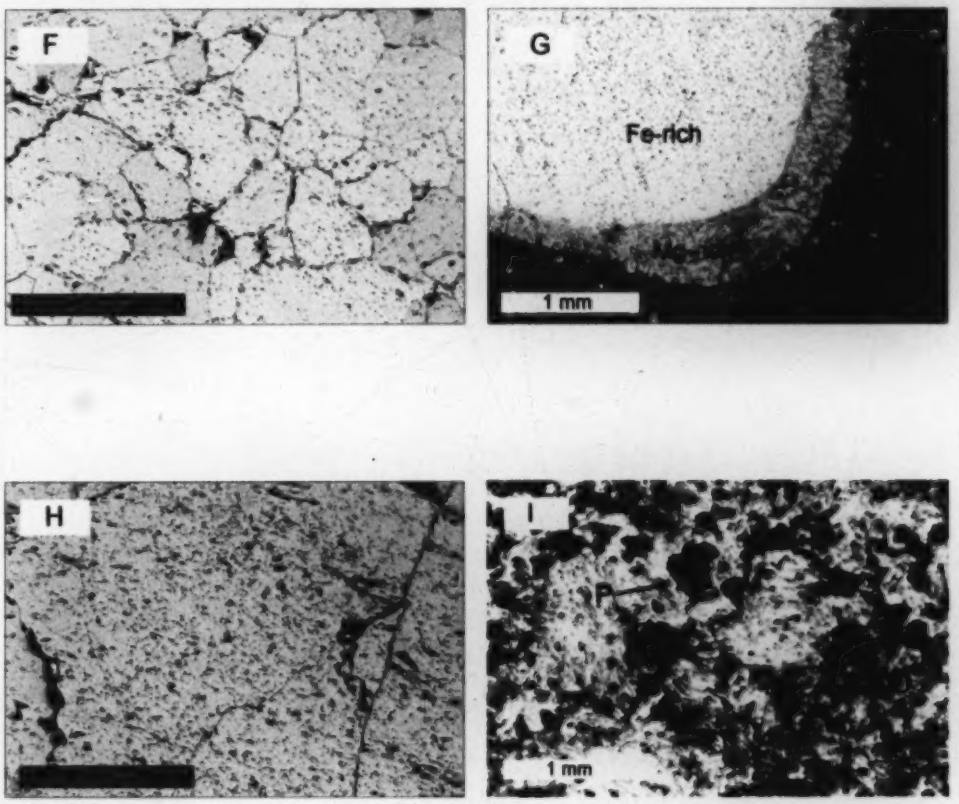

Plate 4 cont'd **F:** Sample M1 - Polygranular ilmenite macrocryst. **G:** Sample M2 - Ilmenite macrocryst (light) with reaction rim (dark; higher Mg content). **H:** Sample M1 - Pitted ilmenite. **I:** Sample M2 - Zoned perovskite (P) in groundmass kimberlite.

Mineral chemistry of some Monastery megacrysts

Ilmenite was chosen specifically for this study because it is abundant in kimberlites world-wide and it is a chemically and physically resistant mineral. For the same reasons, it is used as an indicator mineral in diamond exploration. Ilmenite is also important because it is present in the crystallizing phases throughout the late stages of crystallization in the 'proto-kimberlitic' magma, and could provide information on the timing of crystallization of megacrysts (Moore et al., 1992). As a result, there are numerous published papers that document in detail the mineral chemistry of both megacryst and groundmass ilmenite.

The mineral chemistry of ilmenite has been studied in this research to characterize the nature of ilmenite in the samples used in this study and to provide a comparison with Monastery ilmenite data reported previously. Mitchell (1986) has outlined nine paragenetic types of ilmenite commonly found within kimberlites. This study is restricted to megacryst (>1 cm), macrocryst (<1 cm but >2 mm) and groundmass ilmenite from the Monastery kimberlite. All ilmenite textures described here are representative of ilmenite typically found within our samples of the Monastery kimberlite and are also representative of the ilmenite selected for U-Pb isotope analyses in this study. Mineral chemistry of perovskite and phlogopite has also been included to provide a complete geochemical documentation of the minerals used in the isotopic study.

All mineral chemical analyses were obtained using the JEOL JXS 8900 electron microprobe at the University of Alberta. Operating conditions were 15.0 kV acceleration voltage, 1-2 μm beam diameter, 15 nA probe current, and 20 sec count time on peaks and 10 seconds on background, per element. Raw data were corrected using the ZAF correction scheme. Selected data as well as mineral oxide ranges are presented in Table 4 and all analyses are summarized in Appendix A.

Table 4 Representative ilmenite, phlogopite and perovskite analyses and oxide ranges from the Monastery kimberlite, South Africa (this study).

	1 M-1-2 (C)	2 M-1-2 (R)	3 M-1-2 (R)	4 M-2-2 (C)	5 M-2-2 (bR)	6 M-2-2 (bR)	7 M-3c-2 (C)	8 M-3c-2 (R)	9 M-1b	10 M-1-1	11 M-3a-2 (C)	12 M-3c-2 (C)	13 M-3c-2 (R)	14 M-2-2
F	N/A	N/A	N/A	N/A	N/A	N/A	N/A	N/A	N/A	N/A	N/A	0.49	0.34	N/A
Na2O	N/A	N/A	N/A	N/A	N/A	N/A	N/A	N/A	N/A	N/A	N/A	0.18	0.28	N/A
Cl	N/A	N/A	N/A	N/A	N/A	N/A	N/A	N/A	N/A	N/A	N/A	0.05	0.03	N/A
BaO	N/A	N/A	N/A	N/A	N/A	N/A	N/A	N/A	N/A	N/A	N/A	0.04	0.12	N/A
K2O	N/A	N/A	N/A	N/A	N/A	N/A	N/A	N/A	N/A	N/A	N/A	10.23	10.01	N/A
MgO	12.39	18.10	18.43	10.20	4.91	2.39	8.23	10.98	7.92	18.21	9.94	24.50	21.52	0.05
V2O3	0.19	0.12	0.03	0.18	0.00	0.00	0.10	0.18	0.12	0.08	0.20	N/A	N/A	0.00
CaO	0.00	0.36	0.32	0.02	0.17	0.70	0.00	0.07	0.01	0.19	0.05	0.22	0.01	39.77
MnO	0.29	0.75	0.81	0.30	11.70	12.99	0.29	0.41	0.21	0.72	0.26	0.01	0.01	0.01
Al2O3	0.29	4.35	3.45	0.15	0.18	0.11	0.17	0.23	0.60	4.08	0.71	11.46	14.35	0.18
ZnO	0.00	0.00	0.00	0.00	0.00	0.00	0.06	0.07	0.09	0.05	0.00	N/A	N/A	0.18
TiO2	53.24	17.61	19.41	47.74	33.39	41.16	48.41	49.96	47.32	17.79	48.24	0.97	3.99	56.33
FeO_T	31.93	53.92	52.12	39.06	45.42	37.96	39.48	35.44	41.80	51.41	38.45	6.50	6.30	1.05
SiO2	0.01	0.03	0.01	0.02	0.17	0.24	0.00	0.00	0.02	0.05	0.02	42.34	40.04	0.00
Cr2O3	0.93	1.46	2.06	0.63	0.62	0.51	0.84	0.94	0.02	2.95	0.00	0.10	0.27	0.04
Total	99.28	96.72	96.65	98.29	96.56	96.04	97.58	98.28	98.09	95.54	97.87	96.86	97.14	97.61
Recalculated Analyses														
FeO	25.52	0.00	0.00	24.44	9.40	18.99	28.52	24.80	28.16	0.00	25.37			
Fe2O3	7.13	59.92	57.92	16.25	40.03	21.08	12.19	11.82	15.15	57.13	14.53			
New Total	99.99	102.73	102.45	99.92	100.56	98.15	98.80	99.46	99.61	101.26	99.32			
%ILM	50.23%	0.00%	0.00%	48.93%	26.00%	58.04%	58.59%	49.92%	57.36%	0.00%	51.13%			
%HEM	6.31%	45.53%	44.24%	14.65%	49.79%	28.98%	11.27%	10.70%	13.88%	44.19%	13.18%			
%GEIK	43.45%	54.47%	55.76%	36.42%	24.21%	12.99%	30.14%	39.38%	28.76%	55.81%	35.69%			

N/A = not analysed., ILM = ilmenite, HEM = hematite, GEIK = geikielite endmembers, respectively.

1-3 Core/rim analyses of a macrocryst from Quarry Type kimberlite (M1)

4-6 Core/rim analyses of a macrocryst from East End Type kimberlite (M2)

7-8 Core/rim analyses of a macrocryst from Breccia Type kimberlite (M3)

9 Homogeneous megacryst

10-11 Groundmass ilmenite from M1 and M3 respectively

12-13 Core/rim analyses of phlogopite from Breccia Type kimberlite

14 Perovskite analysis from East End Type kimberlite

Table 4 cont'd

	Ilmenite Macrocryst Cores 12 analyses	Ilmenite Macrocryst Rims 13 analyses	Ilmenite Macrocryst Bright Rims 11 analyses	Ilmenite Groundmass (M1) 8 analyses	Ilmenite Groundmass (M3) 8 analyses	Phlogopite 25 analyses	Perovskite 8 analyses
F	N/A	N/A	N/A	N/A	N/A	0.1-0.8	N/A
Na2O	N/A	N/A	N/A	N/A	N/A	0.1-0.3	N/A
Cl	N/A	N/A	N/A	N/A	N/A	0.0-0.1	N/A
BaO	N/A	N/A	N/A	N/A	N/A	0.0-1.1	N/A
K2O	N/A	N/A	N/A	N/A	N/A	9.2-10.8	N/A
MgO	6.2-12.4	8.5-19.2	0.2-5.2	17.7-19.4	0.2-12.8	21.4-26.1	0.1
V2O3	0.0-0.3	0.0-0.3	0.0-0.1	0.1-0.2	0.0-0.2	N/A	0.0-0.1
CaO	0.0-0.1	0.1-0.4	0.2-12.4	0.1-0.2	0.1-1.3	0.0-0.2	37.2-39.8
MnO	0.2-0.3	0.3-1.2	0.7-13.0	0.7-0.9	0.3-2.2	0.0-0.1	0.0-0.1
Al2O3	0.1-0.9	0.1-4.4	0.0-0.2	3.7-4.5	0.0-3.9	10.7-14.4	0.1-0.2
ZnO	0.0-0.2	0.0-0.3	0.0-0.2	0.0-0.2	0.0-0.2	N/A	0.0-0.2
TiO2	43.4-53.2	15.3-51.8	33.4-53.0	17.5-22.3	20.4-52.8	0.1-4.1	55.5-56.3
FeO_T	31.1-46.1	32.7-57.4	33.6-47.8	46.6-54.4	31.8-57.0	2.4-8.0	1.0-1.4
SiO2	0.0	0.0-0.9	0.0-1.6	0.0-0.1	0.0-0.4	38.9-42.5	0.0
Cr2O3	0.0-0.9	0.0-2.2	0.0-1.2	0.7-3.3	0.0-2.2	0.0-0.8	0.0-0.2
Recalculated Analyses							
FeO	24.4-28.9	0.0-24.9	6.5-43.4	0.0	0.0-44.1		
Fe2O3	7.1-20.3	9.9-63.8	0.0-40.0	54.6-60.5	0.0-63.3		
New Total	-	-	-	-	-	-	-
%Ilm	48.9-59.4	0.0-49.9	22.3-99.4	0.0	0.0-97.3		
%Hem	6.3-19.1	8.8-56.6	0.0-49.8	40.3-46.4	0.0-57.7		
%Geik	23.0-44.4	31.0-58.2	0.6-31.6	53.6-59.7	0.7-45.1		

N/A = Not Analysed

Ilm = ilmenite; Hem = hematite; Geik = geikielite endmembers

Data ranges from Appendix A

Ilmenite - Discrete Nodules

Ilmenite macrocrysts from the three major types of kimberlite; Quarry Type (M1), East End Type (M2), and the Breccia Type (M3) found at Monastery were analysed. Discrete nodules (single crystals), polygranular ilmenite macrocrysts and groundmass ilmenite are present within the Monastery kimberlite.

Ilmenite macrocrysts (discrete nodules and polygranular) from the various types of Monastery kimberlite exhibit narrow ranges in MgO (6.2-12.4 wt%), TiO_2 (43.4-53.2 wt%), Cr_2O_3 (0.0-0.9 wt%) and Al_2O_3 (0.1-0.9 wt%) (Appendix A). These values agree with compositions obtained for ilmenites in the Monastery kimberlite previously reported by Mitchell (1977). Figure 8A is a Cr_2O_3 vs MgO plot showing the distribution of the core and rim compositions for the ilmenite macrocrysts. The majority of ilmenite core compositions vary between 7-12 wt% MgO but M3 cores have a trend to lower MgO contents (c.5 wt%).

Only two grains were analysed from M2 (the East End Type kimberlite) because the majority were too pitted to obtain reliable analyses. Surface pitting within ilmenite nodules is a distinctive optical feature and is quite common within kimberlites (Pasteris et al., 1979). Electron microprobe analyses by Pasteris et al. (1979), on pitted and non-pitted grains did not reveal any chemical heterogeneities, however, the pitting may be the result of alteration. The ilmenite selected for isotopic analyses may all be of this quality, however, only one thin section was made from this kimberlite type. The few M2 ilmenite data are compositionally similar to the majority of ilmenite core analyses in this study.

Plate 5A is an example of a highly deformed and pitted ilmenite macrocryst from the East-End Type kimberlite (M2). The central core of the ilmenite is homogeneous and has compositions similar to other homogeneous ilmenite macrocrysts. The bright area around the ilmenite core has 'bright rim' compositions but noticeably higher MnO (10.3-13.0 wt%) content than found in samples M1 and M3 (Appendix A). The brighter rim is enriched in the ilmenite/hematite component (~ 40 mol % each) compared to the core, which is more ilmenite/geikielite in composition. The high MnO composition of ilmenite corresponds to the kimberlite reaction trend (Haggerty et al., 1979) or the manganese-enrichment trend (Mitchell, 1986). However, the MnO composition seen here, is significantly higher than reported for carbonatitic ilmenite (1-5 wt%) (Haggerty et al., 1979).

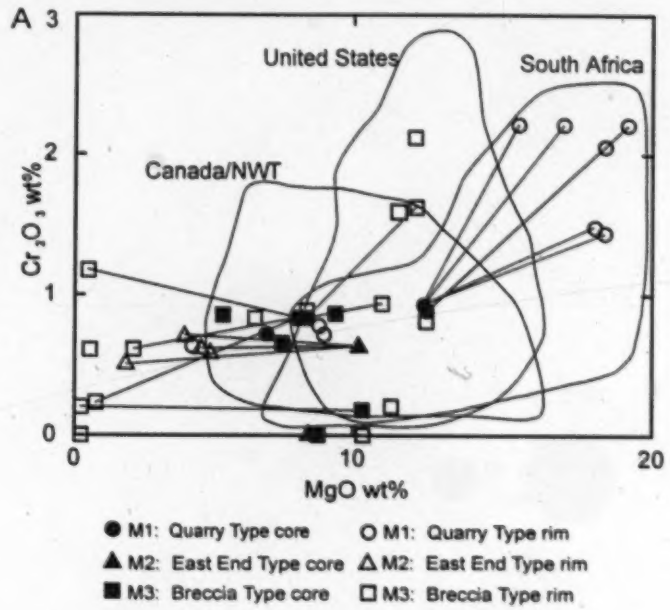

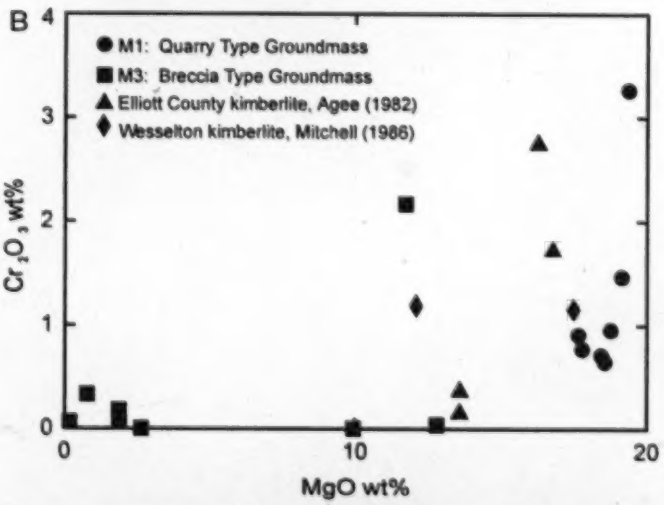

Figure 8 **A:** Cr_2O_3 vs MgO plot showing the relationship between core and rim ilmenite from M1, M2 and M3 from the Monastery kimberlite (this study). Ilmenite compositions from the North American kimberlites (Schulze et al., 1995) and South African kimberlite fields (Mitchell, 1973; Haggerty et al., 1979; and Pasteris, 1980) are outlined for comparison. **B:** Cr_2O_3 vs MgO plot of groundmass ilmenite from M1 and M3. Groundmass ilmenite compositions from the Elliott County kimberlite (United States) and the Wesselton kimberlite (South Africa) are shown for comparison.

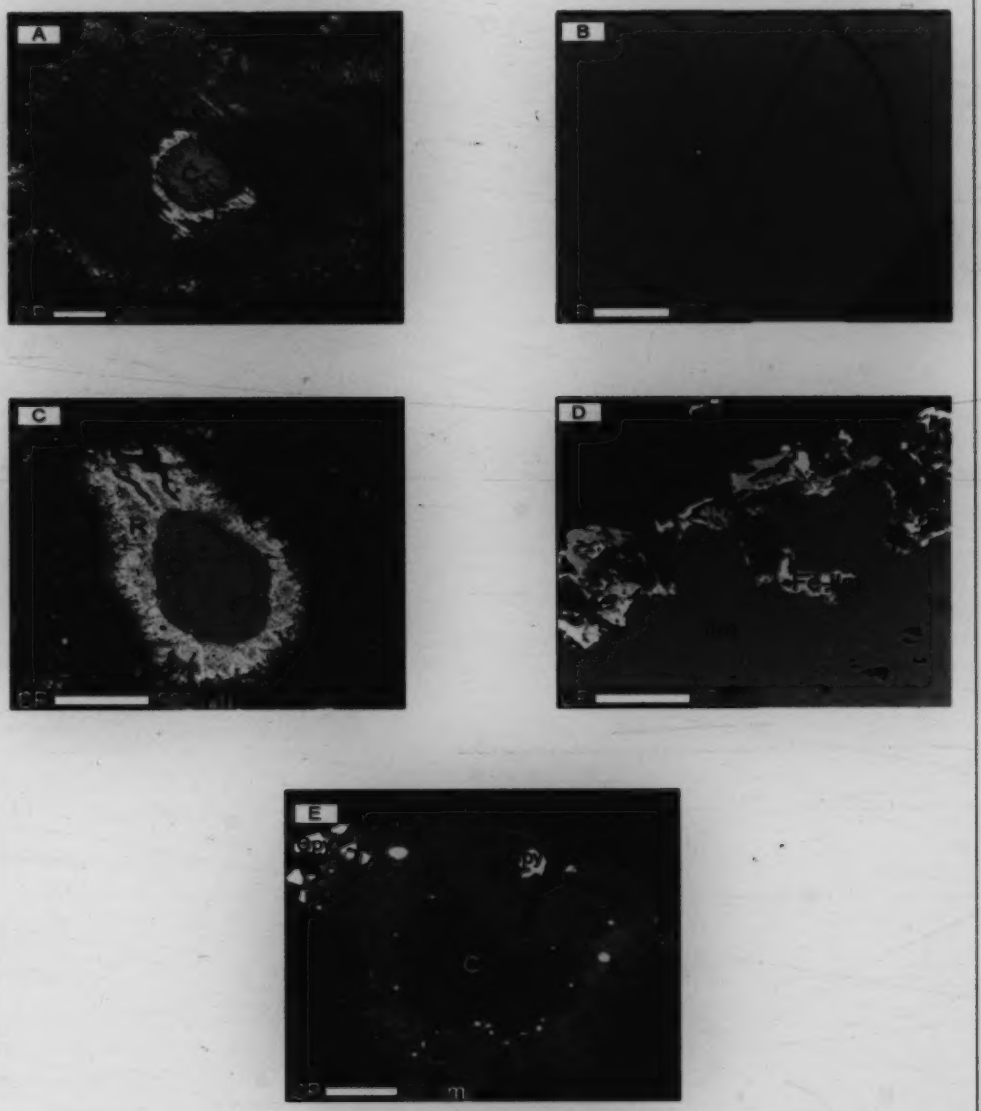

Plate 5 Back-scatter electron images of: **A:** Sample M2 - Deformed ilmenite macrocryst, **B** Sample M3 - Homogeneous ilmenite megacryst, **C:** Sample M1 - Homogeneous ilmenite core (C) with a reaction rim (R), **D:** Sample M3 - Ilmenite rim with Fe-ilmenite and perovskite (P) association, **E:** Sample M3 - Groundmass ilmenite with chalcopyrite (Cpy) association.

Large homogeneous ilmenite macrocrysts are abundant within sample M3. In the one macrocryst that was analysed (M-3c-2 analyses; Table 4), there is a slight, step-like MgO-enrichment (8.2 to 11.0 wt%) and FeO-depletion (28.5 to 24.8 wt%) toward the rim. TiO_2 shows no significant change from core (48.4 wt%) to rim (50.0 wt%) in this macrocryst. There is a high ilmenite component (> 50 mol %) in this macrocryst as well, which is comparable to core analyses from M1 and M2.

Two individual megacrystic ilmenite nodules (>1 cm) were analysed for variations within a single nodule and between nodules (Plate 5B). Approximately 100 microprobe points were taken across the nodules and the data show only a slight variation, within error, throughout the grains with similar compositions as the cores of the ilmenite macrocrysts. The averaged analyses for each megacryst nodule (M-1a and M-1b) are found in Appendix A (M-1b also found in Table 4). Megacryst material with a similar composition to these macrocrysts was used for isotopic analyses.

Compositional differences (largest differences are denoted by: Δ) are seen in the rims of the ilmenite macrocrysts compared to the cores. The rims are typically enriched in MgO (Δ 6.7 wt%), Fe_2O_3 (Δ 54.7 wt%), Cr_2O_3 (Δ 2.1 wt%) and Al_2O_3 (Δ 4.1 wt%) compositions and are depleted in TiO_2 (Δ 37 wt%) and FeO, relative to the cores (Table 4 cont'd and Appendix A). The MgO-enrichment towards the rim is coincident with the "Magmatic Reaction Trend" outlined by Haggerty et al. (1979). These variations translate to an enrichment in hematite/geikielite content and corresponding depletion in ilmenite content compared to core compositions. Figure 8A, illustrates the variations in MgO and Cr_2O_3 between core and rim compositions. This diagram does not distinguish between 'rim' and 'bright rim' analyses, however, they can be identified by their distinct chemical compositions. Bright rims are typically enriched in Fe_2O_3, depleted in MgO, but Cr_2O_3 compositions are generally similar to core compositions. The bright rims, therefore, are depleted in geikielite content and are enriched in either hematite or ilmenite compared to core compositions. Plate 5C is an example of a highly fragmented ilmenite macrocryst from the Quarry Type kimberlite (M1). This ilmenite macrocryst has a homogeneous core with a large reaction rim with the composition of a 'bright rim'; depleted MgO and TiO_2 and enriched Fe_2O_3 compositions.

Plate 5D is a close-up view of the rim of a homogeneous ilmenite macrocryst from the Breccia Type kimberlite (M-3a-1 analyses; Appendix A). There is a higher

hematite component (> 50 mol %) in the rim compared to the core and the lighter ilmenites are almost pure ilmenite (~ 99 mol %). The association of perovskite grains along with Fe-rich ilmenite around the rims of ilmenite macrocrysts, is common in the Monastery kimberlite.

Groundmass Ilmenite

Ilmenite grains ≤50 µm in diameter were categorized as groundmass ilmenite and were analysed from the Quarry Type kimberlite (M1) and the Breccia Type kimberlite (M3). M1 groundmass ilmenite is compositionally distinct from core ilmenite and M3 groundmass compositions. Groundmass ilmenite from sample M1 are enriched in MgO (17.7-19.4 wt%), Cr_2O_3 (0.6-3.2 wt%) and Al_2O_3 (3.6-4.5 wt%) but significantly depleted in TiO_2 (17.5-22.3 wt%) (Figure 8B). The more magnesian M1 groundmass ilmenite is similar to the Elliott County kimberlite (Agee et al., 1982), wherein the groundmass ilmenite are typically more magnesian than ilmenite macrocrysts. Agee et al. (1982) also note that groundmass ilmenite can be divided into two chemically distinct groups. The first containing high MgO but low Cr_2O_3 (<0.73 wt%) which resembles macrocryst rim compositions. The second group is characterized by both high MgO and high Cr_2O_3 (1.43-3.76 wt%). Based on chromium content, the groundmass ilmenite from samples M1 and M3 appear to overlap the two groups. The MgO contents of the M3 groundmass ilmenite are similar to core compositions of the ilmenite macrocrysts.

The percent ilmenite, hematite and geikielite contents in groundmass ilmenite analyses from the Monastery kimberlite are slightly different than those reported for the Elliott County kimberlite, Kentucky. Agee et al. (1982) report a narrow range for $MgTiO_3$ (46.8-57.3 mol%) and a wide range for Fe_2O_3 (1.9-13.9 mol%) for the Elliott County ilmenite, whereas, the $MgTiO_3$ and Fe_2O_3 contents for the Monastery ilmenite are 0.7-59.7 mol% and 0.0-57.7 mol%, respectively. Despite the compositional variation, however, the groundmass ilmenite from the Monastery kimberlite do have similar compositions as the ilmenite macrocryst rims commonly reported by Mitchell (1977), Pasteris (1980), Boctor and Boyd (1980) and Agee et al. (1982).

Figure 8C is a comparison of groundmass ilmenite with core and rim compositions of ilmenite macrocrysts on a ternary diagram. The rims of some discrete ilmenite from M1 and M3 have the same compositions as the groundmass ilmenite from M1 and M3 (Ilmenite 0 mol% and Hematite 0 mol%, respectively). The range in MgO

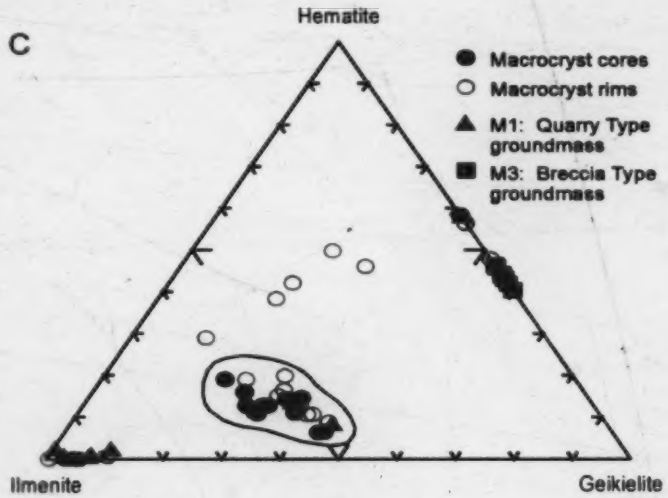

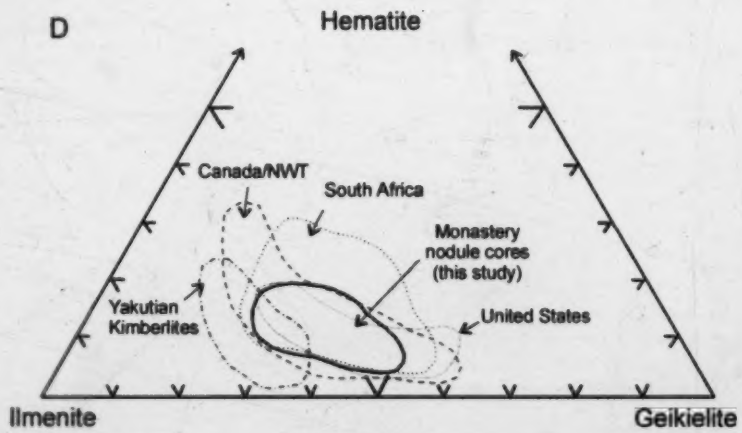

Figure 8 cont'd. **C:** Ternary plot showing the similarities between ilmenite macrocrysts and groundmass ilmenite from the Monastery kimberlite (this study). **D:** Ternary plot displaying kimberlite fields world wide. The Monastery nodule core data from this study is plotted as a comparison with the various fields. South Africa field based on data by Mitchell (1977); Haggerty et al. (1979); and Pasteris (1980), North American fields based on data compiled by Schulze et al. (1995), and Yakutian kimberlite field based on data by Garanin et al. (1979).

compositions for M1 and M3 macrocryst rims (8.9-19.2 and 0.2-12.5 wt%, respectively) is nearly identical to those found for groundmass ilmenite (17.7-19.4 and 0.2-12.8 wt%, respectively).

A few zoned groundmass ilmenite are depleted in MgO along the rims (largest decrease: Δ 12.0 wt%) and correspondingly are enriched in FeO (largest increase: Δ 20.3 wt%) (M-3a-3 analyses Appendix A; Plate 5E). Sample M3 groundmass rims have high ilmenite components (~ 88-97 mol %) compared to the core which is between ilmenite/geikielite compositions. Small grains of chalcopyrite are sometimes found as inclusions in the reaction rims of groundmass ilmenite (Plate 5E). Groundmass ilmenite are generally homogeneous and rarely display core/rim relationships (Mitchell, 1986). These features are consistent with homogeneous groundmass ilmenite resulting from a short crystallization period (Pasteris, 1980). Based on this logic, the zoned groundmass ilmenite found in the Monastery kimberlite in this study may result from a longer crystallization period.

Comparison with ilmenite from other kimberlite studies

The ternary plot of ilmenite, geikielite and hematite in Figure 6, shows the fields for discrete nodule ilmenites, polycrystalline nodules, ilmenite-pyroxene intergrowths along with the "Kimberlite Reaction Trend" and "Magmatic Reaction Trend" (Haggerty et al., 1979). This plot is based on 1040 mineral analyses compiled by Haggerty et al. (1979) from the Monastery kimberlite. Based on the chemical zonation in discrete ilmenite nodules, Haggerty et al. (1979) identified two separate enrichment trends. The first is a trend towards MgO-enrichment, termed the "Magmatic Trend" and the second involves FeO-enrichment, termed the "Kimberlite Reaction Trend". The majority of ilmenite megacryst and macrocryst core compositions analysed in this study plot within the "Kimberlite Reaction Trend" with some slight overlap with the "Magmatic Trend" (Figure 6).

The ilmenite megacryst and macrocryst cores analysed in this research have been compared to ilmenite from South Africa, Canada/NWT, the United States and the Yakutian kimberlites (Figure 8D). The South African field (Monastery, Kao, Frank Smith, Sekameng and the DeBeers kimberlite pipes) is based on data reported by Mitchell (1977), Haggerty et al. (1979) and Pasteris (1980). The Canada/NWT (Dry Bones Bay, Nord, Jos, Fort à la Corne, Attawapiskat, and Kirkland Lake kimberlites) and United

States (Sloan, Stockdale, Lake Ellen and Iron Mountain kimberlites) fields are a compilation of data collected by Schulze et al. (1995). The Yakutian kimberlite field is based on data published by Garanin et al. (1979). As shown in Figure 8D, the Monastery ilmenite core analyses from this study correlate well with the South African kimberlite field as well as other kimberlite fields. Ilmenite from kimberlite appear to have a strong ilmenite-geikielite component with <40 mol% hematite.

Phlogopite

The East End Type and Quarry Type contained only small amounts of highly-altered phlogopite. In contrast, phlogopite phenocrysts are very abundant and unaltered within sample M3 of the Monastery kimberlite. Many phlogopite phenocrysts possess homogeneous cores with alteration rims typically containing ilmenite inclusions (Plate 5F). Homogeneous phlogopite cores have 0.1-4.0 wt% TiO_2, 10.8-14.4 wt% Al_2O_3, and 2.4-7.2 wt% FeO, 0.1-0.6 wt% BaO, and 0-0.8 wt% Cr_2O_3 (Table 4). The alteration rims of phlogopite phenocrysts show an increase in BaO, TiO_2, Al_2O_3 and Cr_2O_3 with a very slight decrease in MgO and K_2O compared to the cores (Table 4). These chemical compositions are very similar to those reported for the Fayette County kimberlite, Pennsylvania (Hunter et al., 1984), Dutoitspan kimberlite (Jones and Smith, 1984) and the DeBeers kimberlite (Farmer and Boettcher, 1981).

Carswell (1975) characterized two different types of phlogopite found within garnet lherzolite xenoliths (Figure 8E). Phlogopites of xenocrystic origin are subdivided into *secondary* (found rimming garnets) and *primary* phlogopites from lherzolite xenoliths. Primary phlogopites are characterized by their lower TiO_2, Cr_2O_3, Al_2O_3, MgO and Na_2O but higher SiO_2 contents compared to the secondary phlogopites (Carswell, 1975). Dawson and Smith (1975) identified two distinct groups based on chromium and titanium content. The first group are Cr-rich and are considered to fall into the primary phlogopite field outlined by Carwsell (1975). The second group of phlogopite are megacrysts (crystallized from kimberlite magma) and are Cr-poor compared to primary phlogopite but are more Ti-rich. The numerical divisions of the groups are as follows: primary phlogopite are Cr_2O_3-rich (>0.5 wt%) with TiO_2 contents <0.6 wt% and FeO contents <3.7 wt%; secondary phlogopite have Cr_2O_3 contents >1.1 wt%; and megacrystic phlogopite are Cr_2O_3-poor (<0.5 wt%) with TiO_2 contents ranging 0.6-2.0 wt% and FeO contents >3.75 wt% (Dawson and Smith, 1975; Mitchell, 1986). Mitchell

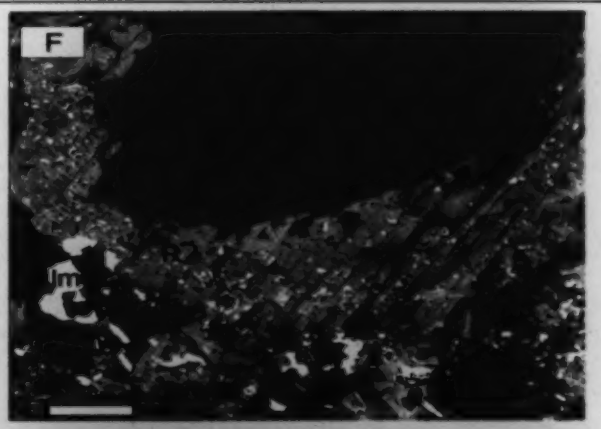

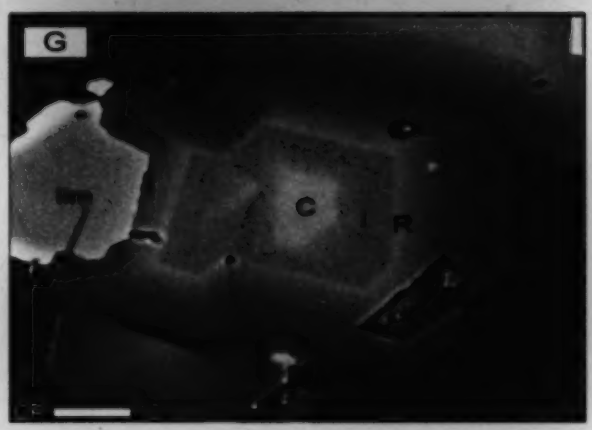

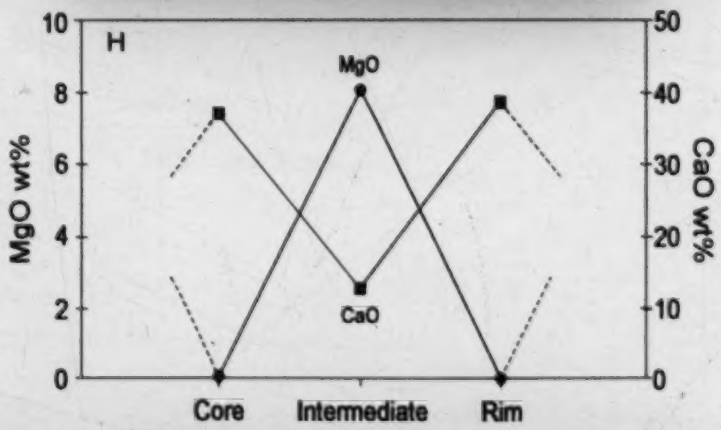

Plate 5 cont'd. **F:** Sample M3 - Phlogopite with ilmenite (Ilm) association on rim (R). **G:** Sample M1 - Zoned groundmass perovskite (C: core; I: Intermediate; R: rim). **H:** A variation diagram showing the changes in MgO and CaO content from core to rim for zoned perovskite shown in **G**.

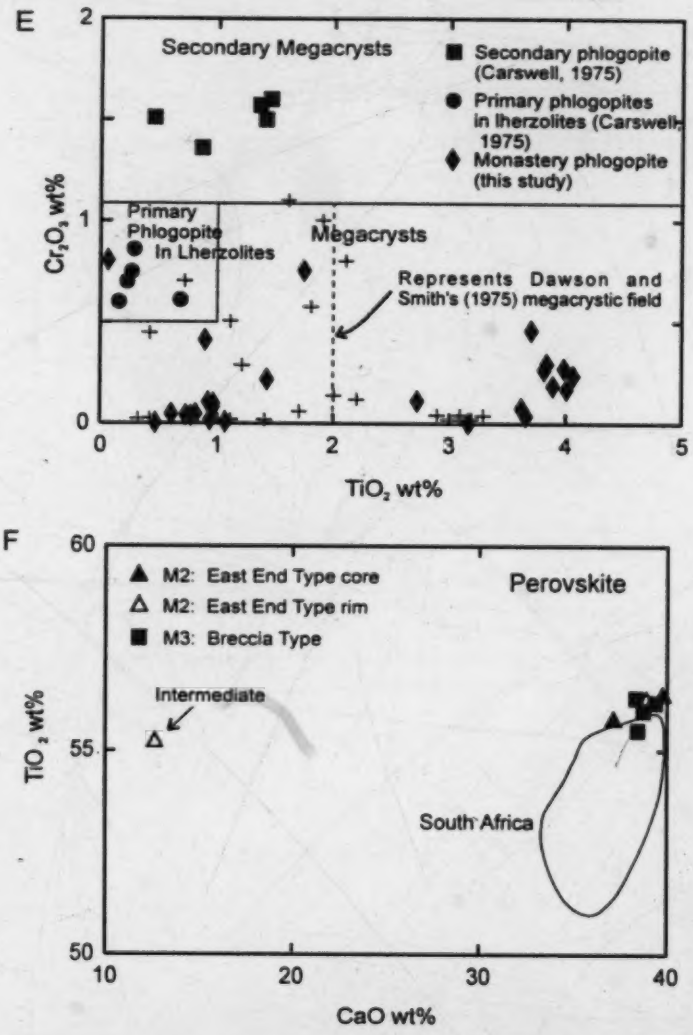

Figure 8 cont'd. **E:** Cr_2O_3 vs TiO_2 plot showing the classification for phlogopite. The cross symbols represent phlogopite analyses from micaceous kimberlites in South Africa after Smith and Dawson (1978). Mitchell (1986) suggests that the TiO_2 wt% field should be extended to 6 wt% from the 2 wt% outlined by Dawson and Smith (1975). **F:** TiO_2 vs CaO plot for perovskite. Perovskite data from South African kimberlites are shown for comparison (data from Mitchell, 1972; Boctor and Boyd, 1979, 1980; and Jones and Wyllie, 1984).

(1986) has suggested that the range outlined by Dawson and Smith (1975), is too limited for TiO_2 and should be extended to 6 wt%. Figure 8E is a plot of Cr_2O_3 vs TiO_2 showing the divisions of primary, secondary and phlogopite megacryst grains from Monastery as well as data collected by Carswell (1975). The phlogopite analyses in this study fall into the Cr-poor field for phlogopite megacrysts and are comparable with other phlogopite analyses from South African kimberlites by Dawson and Smith (1975).

Perovskite

A total of seven perovskite grains were analysed from samples M2 and M3. Homogeneous perovskite have the following compositions: CaO 37.2-39.8 wt%, MgO 0.05-0.08 wt%, TiO_2 55.2-56.3 wt%, and FeO 0.9-1.4 wt% (Table 4 and Appendix A). A core, intermediate and rim analysis was done on a zoned crystal (Plate 5G) where the core and rim have the same compositions as homogeneous perovskite. The intermediate portion however, is darker in colour and has higher MgO and FeO contents (8.1 wt% and 20.7 wt%, respectively) whereas, the CaO contents are significantly lower (12.7 wt%) (Figure 8F; Appendix A). TiO_2 contents do not vary throughout the zoned perovskite. There are few geochemical variations in perovskite that are comparable to those seen in ilmenite. Mitchell (1972) has noted that there is little chemical variation in perovskite within a kimberlite pipe or between perovskite populations from a variety of kimberlites. Perovskite is commonly found rimming ilmenite macrocrysts and these also do not show any significant major or minor element chemical differences from groundmass perovskite (Mitchell, 1972 and Agee et al., 1982). Perovskite was not identified as inclusions in any ilmenite megacrysts or macrocrysts.

Isotope Geochemistry

All chemical and isotopic analyses were conducted at the Radiogenic Isotope Facility in the Department of Earth and Atmospheric Sciences at the University of Alberta.

Analytical Techniques

Rb-Sr

The Breccia Type kimberlite was used for Rb-Sr phlogopite analyses because it contains large phlogopite books resulting in ease of mineral separation and minimizing the potential of accidental incorporation of xenocrystic material. Phlogopite megacrysts chosen for analysis in this study range in size from 0.7-2.5 cm in length and are similar to the one shown in Plate 6A. Plate 6B is a photograph of the phlogopite megacryst used for analyses AN3L and AN3NL. The margins of this megacryst are deformed and a thin light coloured reaction rim is present (Plate 6C). Phlogopite flakes were separated from six different megacrysts directly from the kimberlite matrix using a pair of tweezers. The first phlogopite cleavage layer from each 'book' was cleaved off and discarded to reduce the amount of surface-altered material in the fractions. Two megacrysts were randomly chosen for non-leached/leached paired analyses (AN1 and AN3) and the phlogopite flakes from the remaining megacrysts were leached (see below). A total of twelve fractions of phlogopite flakes were analysed and those denoted by '#2' represent duplicate analyses (see Table 5). Although most of the phlogopite fractions analysed here represent pure phlogopite aliquots, chlorite alteration was noted at the margins of some flakes (e.g. AN1 and AN3) and a small amount of host kimberlite was present in the fraction isolated from megacryst AN1.

Each of the twelve phlogopite fractions were weighed into acid-washed 15 ml PFA Teflon vessels. The leaching method of by Brown et al. (1989) was adopted to extract carbonate material in fractures and along cleavage planes of the phlogopite flakes for the nine fractions in Table 5. The phlogopite fractions were leached with 3 ml of 0.75N HCl and left in an ultrasonic bath for 30 minutes. The leachate was discarded and the phlogopite flakes were rinsed twice with millipore water to ensure complete removal of leachate. All phlogopite fractions were then completely spiked with a

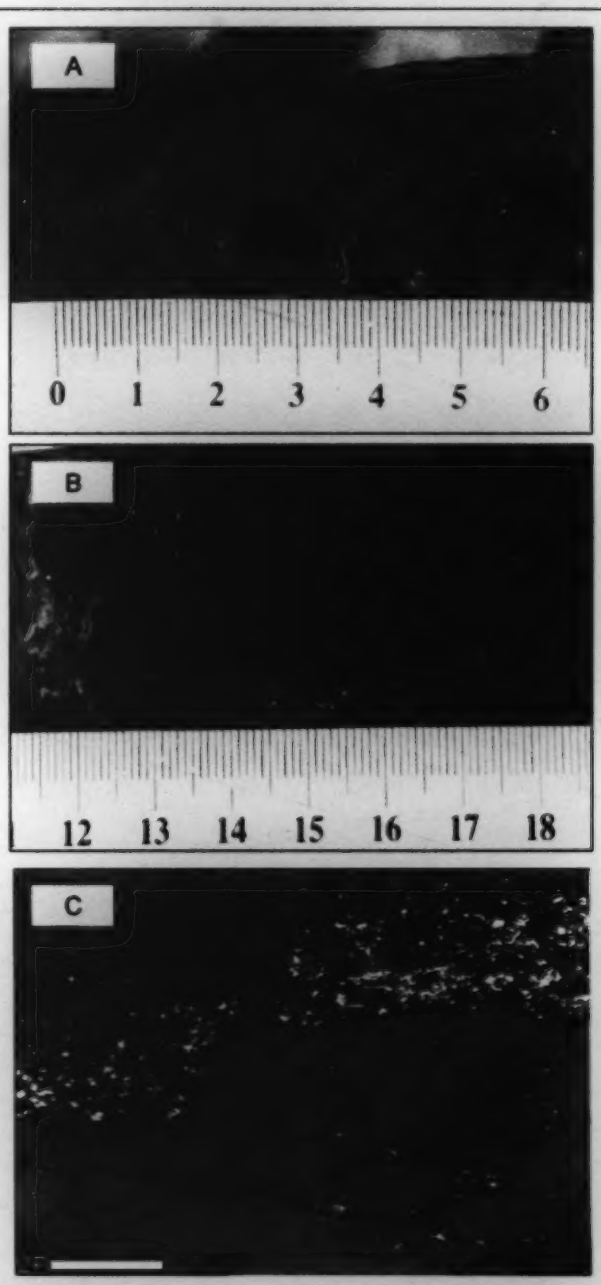

Plate 6 **A:** Phlogopite magacryst in Breccia Type kimberlite matrix. Similar to many of the phlogopite selected for Rb-Sr analyses. **B:** Photograph of the megacryst selected for analyses AN3L and AN3NL. **C:** Back-scatter electron image of phlogopite megacryst (AN3L and AN3NL analyses). Rims of phlogopite megacryst are deformed and fractures contains apatite and minor ilmenite. Phl=phlogopite.

Table 6 Rb-Sr results for phlogopite fractions from the Monastery kimberlite, South Africa.

Sample	Sample Weight (mg)	Spike Weight (mg)	Rb (ppm)	Sr (ppm)	$^{87}Rb/^{86}Sr$	$^{87}Sr/^{86}Sr$ ±2 sigma	Age (Ma) 0.705
AN1 NL	10.47	28.83	432.80	24.05	52.4203	0.774712 ± 0.00002	93.6
AN1 L	6.78	24.17	566.50	3.15	564.6916	1.579207 ± 0.00270	108.9
AN1NL#2	11.75	10.00	573.31	25.09	66.6845	0.796173 ± 0.00002	96.2
AN1L#2	41.27	30.00	540.48	3.29	506.6656	1.387294 ± 0.00002	94.8
AN2 L	12.60	32.97	562.57	2.83	647.7332	1.58687 ± 0.00012	95.8
AN2L#2	10.83	6.00	463.28	2.90	490.3625	1.327036 ± 0.00003	89.3
AN3 NL	16.53	49.36	1257.49	22.30	166.5418	0.918174 ± 0.00002	90.1
AN3 L	16.12	33.00	718.44	8.86	241.6914	1.017637 ± 0.00002	91.0
AN4 L	17.13	30.64	745.31	18.60	117.6702	0.856062 ± 0.00002	90.3
AN4L#2	16.43	30.00	595.27	4.74	381.2741	1.209475 ± 0.00004	93.1
AN6L	32.20	20.00	650.39	10.42	184.6522	0.93849 ± 0.00003	89.0
AN7L	28.93	17.00	599.77	3.64	506.7994	1.346278 ± 0.00004	89.1

Concentration data for both non-leached (NL) and leached (L) samples are based on sample weights prior to leaching.
Samples identified with "#2" represent a duplicate analysis.

measured amount of mixed ^{84}Sr-^{87}Rb tracer solution. The spiked leached and non-leached fractions were dissolved in 3 ml of 24N HF and 1 ml of 16N HNO_3 on a hot plate at 150°C for ~ 12 hours. The fractions were then evaporated to dryness. The fluoride precipitate was then converted to a chloride solution using 3 ml of 6N HCl at 80°C for 12 hours. In preparation for column chemistry, the samples were evaporated to dryness then re-dissolved in 3 ml of mixed oxalic and HCl acid. Rb and Sr were separated using conventional cation exchange chromatography (R.A. Creaser, pers. comm., 1999).

Purified Rb and Sr aliquots were re-dissolved in millipore water and loaded onto single rhenium filaments and coated with H_3PO_4 and tantalum gel. The Rb aliquots were analysed on the VG Micromass® 30 thermal ionization mass spectrometer in single collector mode and the Sr samples were analysed on the VG 354 thermal ionization mass spectrometer in multi-collector, dynamic mode. $^{86}Sr/^{88}Sr$ ratios were normalized to 0.1194 and replicate analyses of the NBS 987 standard during this study yielded an average $^{87}Sr/^{86}Sr$ ratio of 0.710271 ± 15 (n=20). Rb and Sr blanks are typically low (<400 pg Sr; <100 pg Rb), therefore, no blank corrections were applied to the data. The final $^{87}Rb/^{86}Sr$ ratio was calculated as a mean of 60 Rb analyses and 80 Sr analyses. The data were regressed using the method of York (1969). The ^{87}Rb decay constant used was 1.42×10^{-11} yr^{-1} (Davis et al., 1977), and age uncertainties are reported as 2 sigma. A blanket error of 1%, derived by replicate analyses of standards, is assumed as the uncertainty for $^{87}Rb/^{86}Sr$ ratios.

U-Pb (perovskite, zircon and ilmenite)

Perovskite was isolated from the East End Type kimberlite by standard crushing and mineral separation techniques (Heaman, 1989). The crushed kimberlite powder was then separated into 'heavy' and 'light' mineral fractions using a Wilfley table. The heavy material was passed through a 70 mesh nylon sieve and the < 70 mesh fraction was passed through the Frantz Isodynamic magnetic separator for an initial separation up to a current of 0.6 A. The 0.6 A non-magnetic material from the initial Frantz stage was further separated using the heavy liquid methylene iodide and the "heavy" (>3.2 g/cc^3) fraction was further separated using the Frantz at higher currents. Perovskite is usually magnetic between 0.6 and 1.4 amps. Each perovskite grain was hand-picked under a binocular microscope to ensure 100% purity of fractions. The grains are typically subhedral, however, some are cubic (Plate 6D). To test for possible age

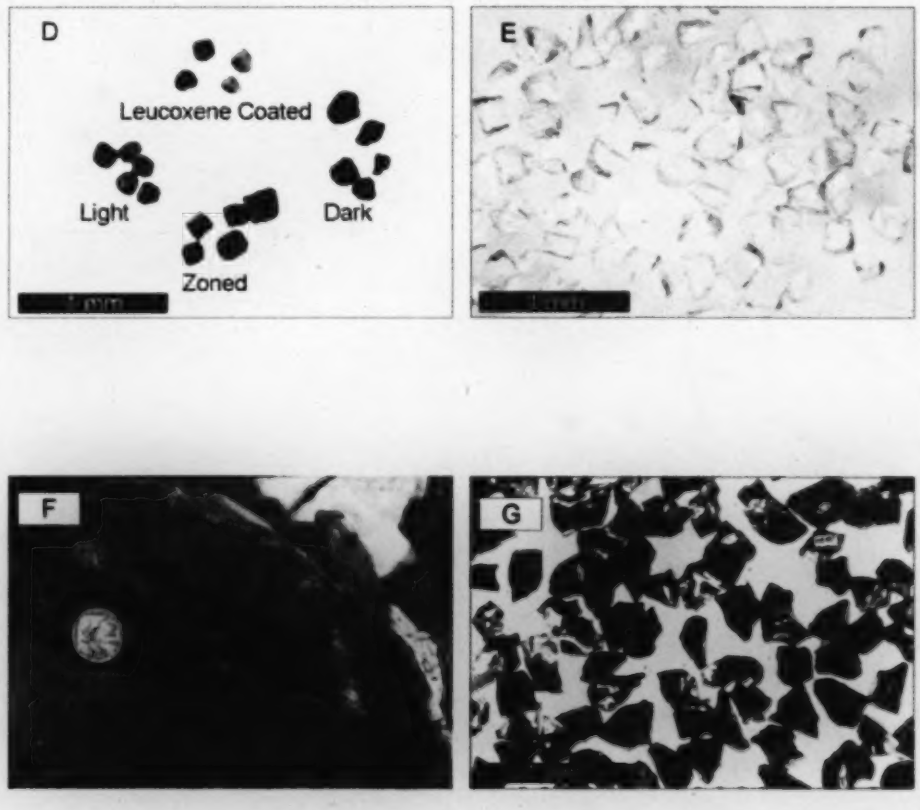

Plate 6 cont'd **D:** Variety of perovskite grains from the Monastery kimberlite. Field of view of photo is 1.1 mm. **E:** Picked fraction of mantle zircon fragments. Field of view of photo is approximately 3 mm. **F:** Ilmenite megacryst within East End Type kimberlite matrix. Similar to ilmenite crushed in this study. **G:** Picked ilmenite fractions. Field of view of photo is approximately 3 mm.

variations, four different types of perovskite grains were analysed (mixed light and dark, light coloured, dark coloured and grains with leucoxene coatings) (Plate 6D).

Mantle zircon grains or fragments were not identified in mineral separates from the East End Type kimberlite, therefore, a zircon xenocryst (~ 1 cm in diameter) collected from the heavy mineral concentrates at the Monastery mine, was selected for analysis. The crystal was crushed with a mortar and pestle and sieved through <70 mesh nylon sieve. The fragments were then hand-picked under a binocular microscope selecting only clear, inclusion-free pieces (Plate 6E). A total of eight, multi-fragment, mantle zircon fractions were analysed in this study.

Ilmenite selected for study include macrocrysts from crushed East End Type kimberlite (Plate 6F) and megacrysts that were collected at the Monastery mine dumps. For identification, the ilmenite from the East End Type kimberlite are labeled as M-2-2#*x* and the megacrysts are labeled as Mon-*x*. The ilmenite macrocrysts were hand-picked under a binocular microscope excluding fragments with leucoxene coatings or kimberlite matrix rinds (Plate 6G). The megacrysts were crushed with a mortar and pestle and were sieved with a < 70 mesh nylon sieve. These fragments were also hand-picked under a binocular microscope for the same reasons given above for zircon. A total of 13 ilmenite fractions were analysed; five isolated from crushed East End Type kimberlite and eight from megacrysts (three different megacrysts in total).

Prior to weighing, the perovskite, ilmenite and mantle zircon mineral fractions were washed twice with distilled acetone. The perovskite and ilmenite were washed in a solution of 2N HNO_3 and the zircon grains were washed in a solution of 4N HNO_3. All samples were left on a hot plate for 1 ½ hours to dissolve any impurities, such as apatite, in the samples. The grains were then thoroughly washed several times with millipore water and distilled acetone. The grains were weighed in an ultra-clean room using a UTM2 microbalance, and the perovskite and ilmenite fractions were then transferred to acid-washed 15 ml Savillex digestion vessels and mantle zircon fractions were transferred to Teflon pressure capsules. The mineral fractions were subsequently spiked with a mixed ^{205}Pb ^{-235}U tracer solution and dissolved in 20 drops HF and two drops 7N HNO_3 on a hot plate at 80°C. Perovskite required five days and ilmenite required 10 days at this temperature to dissolve completely. Mantle zircon fractions were placed in a metal carousel and left in an oven at 215°C for four days to dissolve. After the dissolution period, the samples were evaporated to dryness, 15 drops (five

drops in the zircon samples) of 3.1N HCl were added to the samples and then left on the hot plate (or in the oven in the case of mantle zircon) for 24 hours. This step converts the fluoride precipitate to a chloride solution in preparation for column chemistry.

Uranium and lead were separated from the perovskite and ilmenite fractions using large column HBr chemistry (Heaman and Machado, 1992). Minor changes to the procedure were necessary to enhance the extraction and elution of Fe^{2+}, Ti^{4+} and U^{4+} for the ilmenite samples. An extra column volume (~ 1 ml) of 7N HNO_3 was added to ensure complete extraction of Fe^{2+} and Ti^{4+} and during the final elution stage of U^{4+}, an extra column volume (~ 1 ml) of H_2O was added. For ilmenite fractions weighing > 5 mg, the procedure was performed twice as the fraction weights are larger than normal for this procedure. Uranium and lead from the zircon samples were separated using the HCl chemistry outlined by Krogh (1973) and micro-anion exchange columns.

The purified uranium and lead were loaded onto outgassed Re filaments with a mixture of silica gel and phosphoric acid (Cameron et al., 1969) and were analysed on a VG 354 Mass Spectrometer in single Daly photomultiplier detector mode. All isotopic data were corrected for Daly bias by a factor of 0.13%/amu for lead and 0.15%/amu for uranium and were also corrected for mass discrimination (0.09%/amu for lead and 0.16%/amu for uranium). For both perovskite and ilmenite analyses, total procedural blanks for lead and uranium are 8 pg (± 50%) and 2 pg (± 50%), respectively (blank corrections for ilmenite samples represented by "*", are 1 pg (± 50%) and 3 pg (± 59%), respectively. Corrected blank data for ilmenite are shown in Table 6. The total procedural blanks used for zircon were 6 pg (± 50%) Pb and 5 pg (± 20%) U. The ilmenite isotopic data resulted in large errors attributed to the blank corrections typically used for perovskite. Therefore, it was necessary to reduce the overall procedure blank during this study by continuously analysing the blank concentrations during these experiments as Monastery ilmenite and mantle zircon contain low concentrations of radiogenic lead.

The ^{238}U and ^{235}U decay constants used for age calculations are $1.55125 \times 10^{-10} y^{-1}$ and $9.8485 \times 10^{-10} y^{-1}$, respectively (Steiger and Jäger, 1977). Initial lead isotopic compositions were calculated using the Stacey and Kramers (1975) growth curve and all data calculations with respective errors were calculated using in-house software. All errors are reported at the 95% confidence level. Weighted mean and isochron age calculations were determined using Isoplot (Ludwig, 1998).

Table 6 U-Pb results for bomb and column blanks.

Blank	Common Pb (pg)	Spike	$^{207}Pb/^{206}Pb$	$^{204}Pb/^{206}Pb$	$^{206}Pb/^{204}Pb$	Pb Blank (pg)	U Blank (pg)
Column Blank 1	5.01	2.92	0.8213	2.0273	18.6797	5.0	1.5
Bomb Blank 1	2.45	2.92	0.8111	1.9032	18.5870	2.4	0.4
Bomb Blank 2	3.67	2.92	0.8442	1.9637	17.4331	3.4	0.3
Bomb Blank 3	0.85	2.92	0.7318	2.1120	24.8364	1.1	0.4
Bomb Blank 4	1.89	2.92	0.8437	2.0528	17.0424	1.8	0.3

Ratios corrected for fractionation and spike only.

Table 7 U-Pb results for perovskite fractions from the Monastery kimberlite, South Africa.

Sample	Description	Sample Weight (µg)	U (ppm)	Th (ppm)	Pb (ppm)	Th/U	Common Pb (pg)	$^{206}Pb/^{204}Pb$ ± abs	$^{238}U/^{204}Pb$ ± abs	$^{206}Pb/^{238}U$ ± abs	$^{207}Pb/^{204}Pb$ ± abs	$^{206}Pb/^{238}U$ Age (Ma)
M-2-2-A	270 mbed	87	119.8	857.3	12.3	7.155	634	34.102 ± 0.180	1036.6 ± 11.4	0.01406 ± 0.00036	16.380 ± 0.056	90.0 ± 2.4
M-2-2-B	140 light	43	76.8	341.6	9.5	4.445	306	29.030 ± 0.228	660.7 ± 14.2	0.01406 ± 0.00056	16.142 ± 0.056	90.0 ± 3.6
M-2-2-C	170 dark	50	114.7	850.1	10.9	7.414	299	36.461 ± 0.402	1214.4 ± 26.0	0.01402 ± 0.00034	16.494 ± 0.074	89.8 ± 2.2
M-2-2-D	205 leucoxene coating	89	112.5	871.3	10.6	7.743	496	37.322 ± 0.260	1267.9 ± 16.6	0.01406 ± 0.00032	16.517 ± 0.060	90.0 ± 2.0

Atomic ratios corrected for fractionation, blank (8 pgPb; 2 pgU), spike and common Pb. Uncertainties in atomic ratios are quoted at 2 sigma.

Results

Rb-Sr Phlogopite

The Rb-Sr phlogopite data from the Monastery kimberlite are summarized in Table 5 and an isochron plot displaying the data is shown in Figure 9. Fraction weights range from 6.8 mg to 32.2 mg. The Rb concentrations for the phlogopite range from 432.8-1257.5 ppm and the Sr concentrations range from 2.8-25.1 ppm. The Sr concentrations of phlogopite obtained in this study are lower than those reported by Allsopp and Barrett (1975) (36.1-402.7 ppm), but closer to those (12.2-29.9 ppm) reported by Smith and Barton (1996).

The calculated isochron age using eight (solid squares in Figure 9A) out of twelve phlogopite analyses is 89.9 ± 3.1 Ma with an initial $^{87}Sr/^{86}Sr$ value of 0.708 ± 0.011 (MSWD=21). Samples AN2L#2, AN1L#2, AN1L and AN2L were excluded from the isochron age calculation because they exhibit significant scatter however, they are included on the plot (open squares) for comparison. The scatter in samples AN1L, AN2L and AN4L is attributed to overspiking as all three have $^{84}Sr/^{86}Sr$ ratios >10 (Figure 9B). This problem is more likely to arise when spiking samples with low Sr and high Rb contents such as phlogopite when using a mixed Rb and Sr tracer solution that does not have comparable Rb/Sr ratios as the sample material. However, overspiking does not appear to explain the scatter for fraction AN1L#2.

Leaching phlogopite grains is a commonly practiced technique as it has been shown to improve the precision of Rb-Sr age determinations as well as reducing scatter about the regression line (Allsopp and Roddick, 1984; Smith et al., 1985). Brown et al. (1989) demonstrated this point by comparing non-leached, 10 minute leaching periods and 12 hour leaching periods with phlogopite from the Makganyene kimberlite. In comparing the non-leached and leached fractions in this study, an increase in precision is also obtained (Figure 9C&D). The isochron age obtained for the non-leached fractions is 88 ± 28 Ma and initial $^{87}Sr/^{86}Sr$ ratio of 0.711 ± 0.042 (MSWD=45), whereas, the isochron age determined for leached samples (excluding outliers) is 89.5 ± 5.1 Ma and initial $^{87}Sr/^{86}Sr$ ratio of 0.708 ± 0.025 (MSWD=16).

Considering that the leaching process removes carbonate contaminants from the phlogopite flakes, it has been suggested by Allsopp and Barrett (1975) and Brown et al. (1989), that the isochron diagram including only non-leached phlogopite actually represents a mixing relationship between phlogopite and carbonate (±apatite) end-

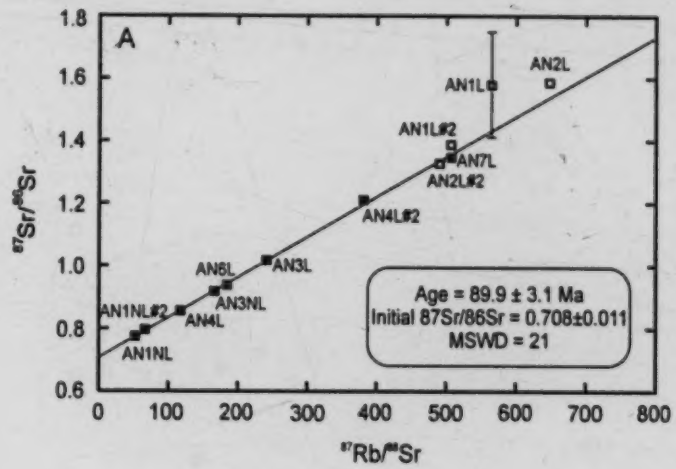

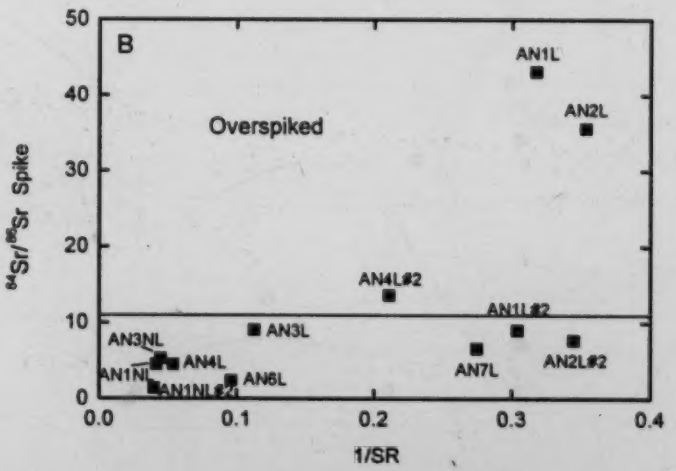

Figure 9 **A:** Isochron plot showing the distribution of all phlogopite samples analysed. **B:** $^{84}Sr/^{86}Sr$ vs 1/Sr diagram showing the distribution of the overspiked samples producing scatter on isochron diagram (A). All samples below the line are considered to be spiked correctly. Open symbols represent analyses not included in age calculation, L=leached and NL=non-leached samples.

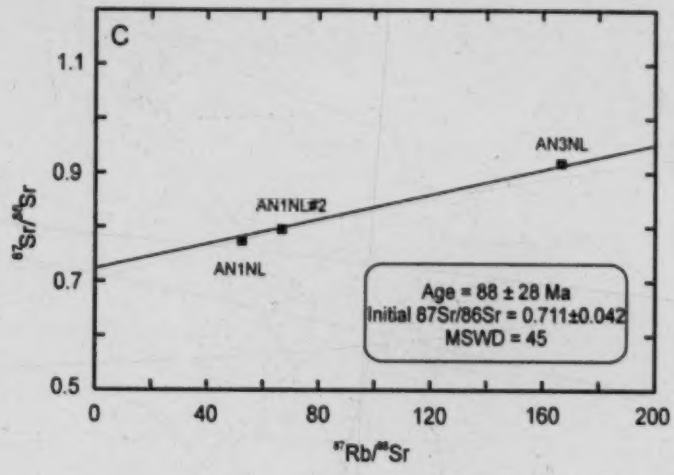

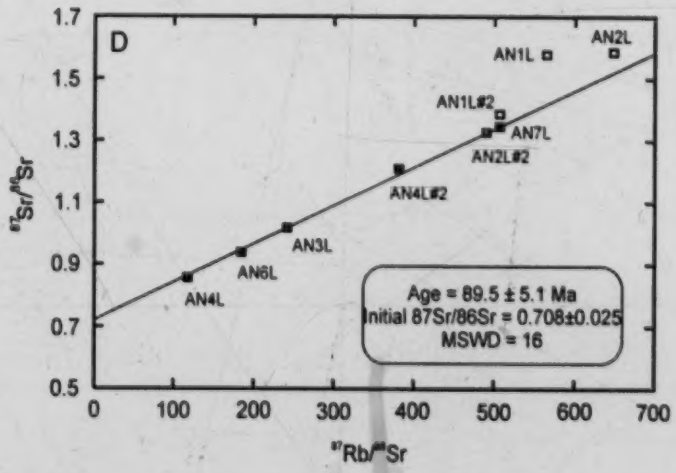

Figure 9 cont'd **C:** Isochron plot of non-leached samples yielding large errors. **D:** Isochron plot of leached samples with significantly reduced errors. Open symbols are not included in age calculations, L=leached and NL=non-leached samples.

members. Therefore, both end-members must be primary in order for the isochron age to represent the emplacement age of the kimberlite. For the majority of phlogopite analyses in this study there is no discernible difference between non-leached and leached phlogopite isochron ages (Figures 9C&D) or initial $^{87}Sr/^{86}Sr$ ratios within the quoted uncertainties.

U-Pb Perovskite

The U-Pb perovskite data from the Monastery kimberlite are summarized in Table 7. Four different multi-grain (140-270 grains) fractions were analysed: a mixed fraction comprised of light and dark perovskite grains, a light coloured fraction, a dark coloured fraction and a fraction comprised of perovskite grains possessing leucoxene ($CaFeTiO_5$) coatings (Plate 6D); their weights ranging between 43-89 µg. The range for $^{206}Pb/^{204}Pb$ and $^{238}U/^{204}Pb$ ratios (29.102 to 37.400 and 696.0 to 1273.5, respectively) are all very high and show a significant spread on the isochron diagram (Figure 10A).

The Monastery perovskite analysed in this study have variable U and Th concentrations (77-119 ppm and 342-871 ppm, respectively) and a smaller range in Pb concentrations (9.5-12.3 ppm). Common Pb contents are typically high, ranging from 299-634 pg which represents 35-43% of the total Pb present within the perovskite grains. These high common Pb contents require a significant correction in the age calculations (mostly the $^{207}Pb/^{235}U$ age) and the uncertainty in this correction is reflected in the magnitude of assigned uncertainties. The fraction of light coloured perovskite grains (M-2-2-B) contains the lowest U, Th and Pb contents and has a lower $^{238}U/^{204}Pb$ ratio compared to the other fractions suggesting that there is compositional variation, however, this seems to have no affect on the $^{206}Pb/^{238}U$ apparent age as the results for all analyses are within error (Table 7). The perovskite fraction picked specifically to have leucoxene coatings has slightly higher Th concentrations and $^{206}Pb/^{204}Pb$ and $^{238}U/^{204}Pb$ isotopic ratios, however, the $^{206}Pb/^{238}U$ apparent age remains within error with the other fractions. The leucoxene coating can contribute to the observed compositional variation however this does not appear to affect the apparent age calculation. This could be explained if alteration to form leucoxene occurred slightly later than but close in time to perovskite crystallization.

An isochron plot displaying the four perovskite fractions is shown in Figure 10A. These four fractions have a relatively large range in $^{238}U/^{204}Pb$ and a best-fit regression

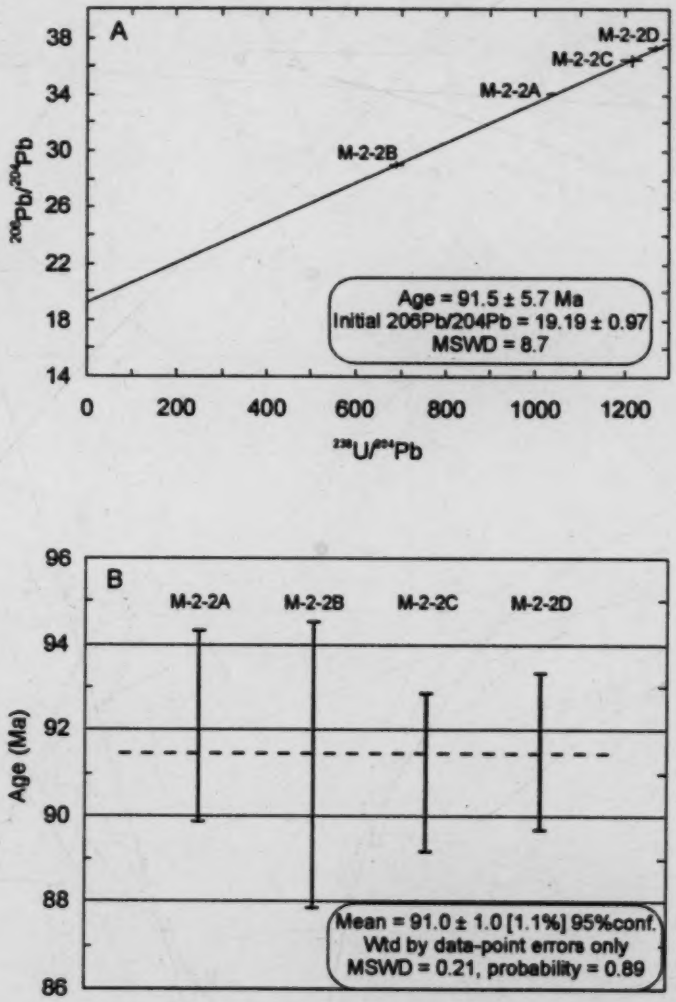

Figure 10 A: Isochron plot for Monastery perovskite showing the isotopic variation between fractions. **B:** Weighted Mean $^{206}Pb/^{238}U$ age using the initial $^{206}Pb/^{204}Pb$ ratio of 19.19 common Pb correction.

treatment yields an age of 91.5 ± 5.7 Ma with an initial $^{206}Pb/^{204}Pb$ ratio of 19.19 ± 0.97 (MSWD=8.7). The initial $^{206}Pb/^{204}Pb$ ratio of 19.19 is significantly higher than the average crustal model used for the common Pb correction (18.566) by Stacey and Kramers (1975). Therefore, the initial $^{206}Pb/^{204}Pb$ ratio of 19.19 was used to recalculate the $^{206}Pb/^{238}U$ apparent ages (Table 7) for the perovskite fractions yielding a weighted mean $^{206}Pb/^{238}U$ age of 91.0 ± 1.0 Ma (MSWD=0.21) (Figure 10A). This age is more precise and is interpreted to be the best estimate of the emplacement age for the Monastery kimberlite.

U-Pb Mantle Zircon

Eight fractions from the same mantle zircon xenocryst were analysed in this study. Mantle zircon data are presented in Table 8 and a weighted mean $^{206}Pb/^{238}U$ age calculation for the fractions is shown in Figure 11. Sample weights range from 327-772 µg and selected grains were free of inclusions and coatings (Plate 6E). Common Pb contents are typically quite low (2-20 pg) with one exception; Zir#6 which has 141 pg of common Pb. The common Pb content represents 10-48% of the total lead present.

The U (0.93-4.05 ppm), Pb (0.03-0.47 ppm) and Th (0.50-1.12 ppm) concentrations obtained in this study are some of the lowest reported for mantle zircons (Davis et al., 1976; Zartman et al., 1998). Figure 12 is a Th vs U plot illustrating the ranges of MARID (Mica - Amphibole - Rutile - Ilmenite - Diopside) zircons (Konzett et al., 1998) and kimberlitic zircons (Ahrens et al., 1967; Krasnobayev, 1980) in comparison with the Monastery zircon analysed in this study. The Th/U ratios for the zircon are < 1 and five analyses indicate a narrow range (0.195-0.209) which is typical for kimberlitic zircons (Ahrens et al., 1967). Such ratios are at the low Th/U end member for primary zircon that crystallized from felsic magmas.

Zartman et al. (1998) reported data for three colourless mantle zircon fractions from Monastery. For comparison, the data ranges are as follows: U (3.1-4.3 ppm), Th (0.72-0.86), Pb (0.04-0.06), Th/U (0.202-0.235) and $^{206}Pb/^{204}Pb$ (187-235) (Zartman et al., 1998). As stated earlier, the U concentrations for some Monastery mantle zircon fractions obtained in this study (e.g. Zir#5) are slightly lower than those reported by Davis et al. (1976) (6.1 ppm uranium) and by Zartman et al. (1998) (minimum 3.1 ppm uranium). As well, $^{208}Pb/^{204}Pb$ ratios from this study, exhibit a wide range, 27 - 22 832,

Table 8 U-Pb results for mantle zircon fractions from the Monastery kimberlite, South Africa. Uncertainties in atomic ratios are quoted at 2 sigma.

		Concentrations					Atomic Ratios				Apparent ages		
Sample	Sample Weight (µg)	U (ppm)	Th (ppm)	Pb (ppm)	ThU	Common Pb (pg)	$^{206}Pb/^{204}Pb$	$^{206}Pb/^{238}U$ ± abs	$^{207}Pb/^{235}U$ ± abs	$^{207}Pb/^{206}Pb$ ± abs	$^{206}Pb/^{238}U$ (Ma)	$^{207}Pb/^{235}U$ (Ma)	$^{207}Pb/^{206}Pb$ (Ma)
Zir#4	383	3.77	0.79	0.05	0.209	2	548	0.01420 ± 0.00006	0.0951 ± 0.0034	0.04856 ± 0.00164	90.9	92.2	126.5
Zir#5	692	0.93	0.70	0.05	0.732	7	1531	0.05178 ± 0.01950	0.3426 ± 0.1304	0.04799 ± 0.00256	325.4	299.2	99.0
Zir#6	327	4.05	< 0.10	0.47	0.008	141	27	0.01378 ± 0.00066	0.0893 ± 0.0462	0.03644 ± 0.02392	88.2	68.0	-
Zir#7	357	3.39	0.67	0.04	0.196	3	329	0.01367 ± 0.00022	0.0852 ± 0.0058	0.04517 ± 0.00300	87.5	83.0	-
Zir#8	597	3.87	1.12	0.05	0.289	8	1159	0.01574 ±0.00010	0.0997 ± 0.0052	0.04454 ± 0.00232	100.7	93.7	-
Zir#9	772	2.53	0.50	0.03	0.199	6	22832	0.01394 ± 0.00005	0.0852 ± 0.0061	0.04432 ± 0.00308	89.2	83.0	-
Zir#10	753	3.50	0.68	0.05	0.195	20	181	0.01351 ± 0.00008	0.0844 ± 0.0050	0.04531 ± 0.00260	86.5	82.3	-
Zir#11	719	3.85	0.75	0.05	0.196	10	595	0.03181 ± 0.00005	0.0864 ± 0.0043	0.04538 ± 0.00218	88.4	84.2	-

Atomic ratios corrected for fractionation, blank (6 pgPb; 5 pgU), spike and common Pb

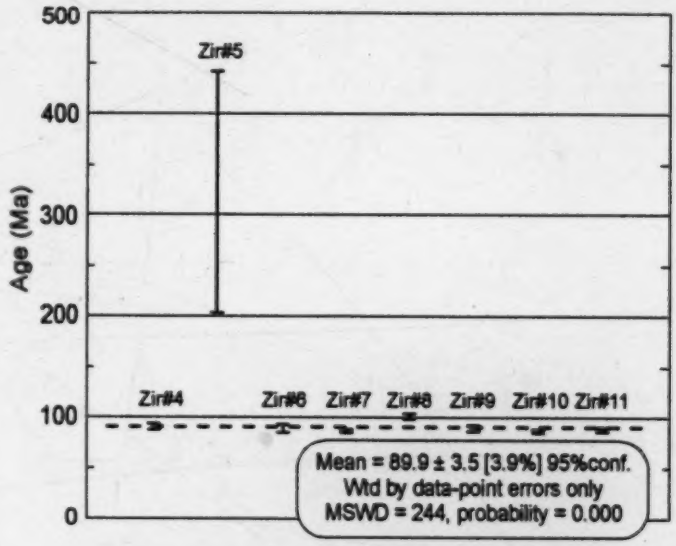

Figure 11 Weighted Mean diagram showing the distributions of zircon ages about the calculated mean $^{206}Pb/^{238}U$ age line (using Stacey/Kramers (1975) common Pb correction.).

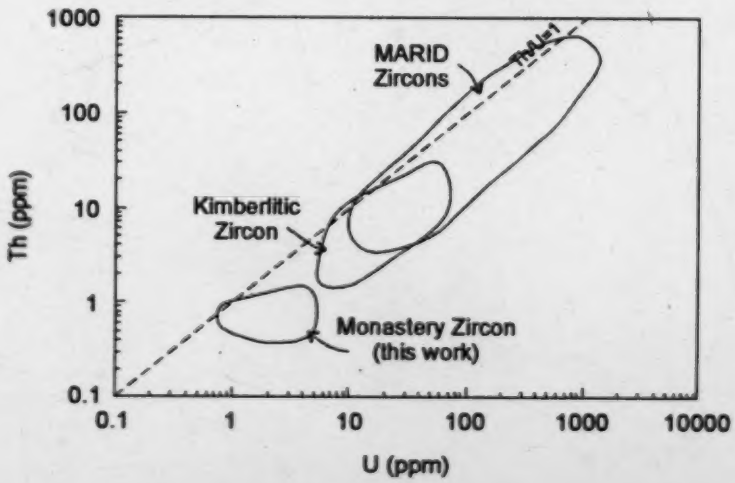

Figure 12 Th vs U plot showing the variation in zircon concentrations of MARID zircons (Konzett et al., 1998), kimberlitic zircons (Ahrens et al., 1967; Krasnobayev, 1980) and Monastery zircon (this work).

compared to the narrow range reported by Zartman et al. (1998). However, the Pb and Th concentrations and Th/U ratios from this study are quite similar to those reported by Zartman et al. (1998).

A weighted mean $^{206}Pb/^{238}U$ calculation yields an age of 89.9 ± 3.5 Ma (MSWD=244) using all eight fractions (Figure 11). Sample Zir#5 has an anomalously high $^{206}Pb/^{238}U$ apparent age (325.4 Ma), which may represent inheritance indicating either partial resetting of an old mantle zircon xenocryst or new zircon growth around an older core. Excluding fraction Zir#5 (325.4 Ma) does not significantly alter the precision of the calculated age. Uncertainty on $^{207}Pb/^{235}U$ ratios are high as a consequence of extremely low ^{207}Pb contents (<20 pg) and as a result, a concordia plot is not a useful diagram to display the zircon analyses.

U-Pb Ilmenite

This is the first comprehensive U-Pb study on kimberlitic ilmenite extending the early work of Kresten (1974) who analysed uranium concentrations in ilmenite nodules from a few South African kimberlites. In this study, both ilmenite megacrysts and macrocryst/groundmass (East End Type kimberlite) were analysed specifically for variations within and between megacrysts. In addition, the U-Pb results for megacrysts and macrocryst/groundmass ilmenite were compared. The U-Pb results for thirteen Monastery ilmenite fractions are presented in Table 9 and isochron plots for these data are shown in Figure 13.

Eight fractions from a total of three ilmenite megacrysts and five macrocryst/groundmass were isolated from a crushed sample of East End Type kimberlite; the fractions range in weight from 0.2-7.4 mg. For four fractions, a complete isotopic and age computation was not feasible because of errors in blank uncertainty. It was necessary to extrapolate the $^{206}Pb/^{204}Pb$ and $^{238}U/^{204}Pb$ ratios from a series of $^{207}Pb/^{204}Pb$ ratios, for fractions Mon-1#1, Mon-3#1 and M-2-2#1 in order to plot them on an isochron diagram. These fractions were not used in the isochron age calculation and are represented by open squares in Figure 13A.

The U, Th and Pb concentrations (ppm) in kimberlitic ilmenite are very low: 0.02-0.17, 0-0.14 and 0.01-1.32, respectively. Common Pb contents range from 52-943 pg representing 48-53% of the total lead present, similar to perovskite. The $^{238}U/^{204}Pb$ ratios are highly variable (1-311) and the $^{208}Pb/^{204}Pb$ ratios are fairly

Table 9 U-Pb results for ilmenite fractions from the Monastery kimberlite, South Africa. Uncertainties in atomic ratios are quoted at 2 sigma.

Sample	Description	Sample Weight (µg)	U (ppm)	Th (ppm)	Pb (ppm)	Th/U	Common Pb (pg)	$^{208}Pb/^{204}Pb$ ± abs	$^{238}U/^{204}Pb$ ± abs	$^{206}Pb/^{238}U$ ± abs	$^{207}Pb/^{204}Pb$ ± abs	$^{206}Pb/^{238}U$ Age (Ma)
Mon-1#1	10 grains	160	-	-	-	-	-	†18.700	†21.5	-	15.1512	-
Mon-1 #2	50 grains	1150	0.17	0.03	0.20	0.169	230	20.220 ± 0.120	56.4 ± 2.4	0.029 ± 0.007	15.753 ± 0.080	186.1 ± 42.1
Mon-1 #3	50 grains	1072	0.09	0.14	0.15	1.485	165	19.901 ± 0.144	39.8 ± 2.4	0.034 ± 0.010	15.663 ± 0.090	212.8 ± 60.4
*Mon-1#4	302 grains	7128	0.03	0.03	0.02	0.808	137	20.869 ± 0.092	115.5 ± 3.2	0.020 ± 0.003	15.659 ± 0.058	127.3 ± 20.4
*Mon-2#1	297 grains	5959	0.05	0.07	0.03	1.252	172	21.334 ± 0.090	115.2 ± 2.5	0.024 ± 0.003	15.717 ± 0.058	153.0 ± 20.4
*Mon-2#2	284 grains	5582	0.05	0.02	0.01	0.317	61	23.845 ± 0.390	311.4 ± 20.0	0.017 ± 0.001	15.803 ± 0.118	108.4 ± 8.0
Mon-3#1	278 grains	5218	-	-	-	-	-	†19.555	†71.5	-	14.8662	-
*Mon-3#2	299 grains	5662	0.04	0.00	0.01	0.027	53	23.174 ± 0.370	294.9 ± 21.8	0.016 ± 0.001	15.725 ± 0.080	99.9 ± 8.2
M-2-2#1	52 grains	1062	-	-	-	-	-	†18.545	†24.0	-	15.4099	-
M-2-2#2	50 grains	732	0.02	0.07	1.32	3.510	943	19.296 ± 0.044	1.0 ± 0.1	0.701 ± 0.072	15.722 ± 0.048	3424.8 ± 2469.4
M-2-2#3	53 grains	945	0.03	-	0.06	-	63	19.164	28.6	0.021	15.515	133.3
*M-2-2#4	339 grains	7413	0.02	-	0.01	-	53	21.330 ± 0.240	179.9 ± 13.4	0.015 ± 0.002	15.490 ± 0.078	98.3 ± 13.4
*M-2-2#5	383 grains	7010	0.02	-	0.01	-	52	21.517 ± 0.290	182.1 ± 13.9	0.016 ± 0.002	15.500 ± 0.122	103.6 ± 13.8

Atomic ratios corrected for fractionation, blank (8 pgPb; 2 pgU), spike and common Pb
*Atomic ratios corrected for fractionation, blank (3pgPb; 1pgU), spike and common Pb
† Extrapolated values

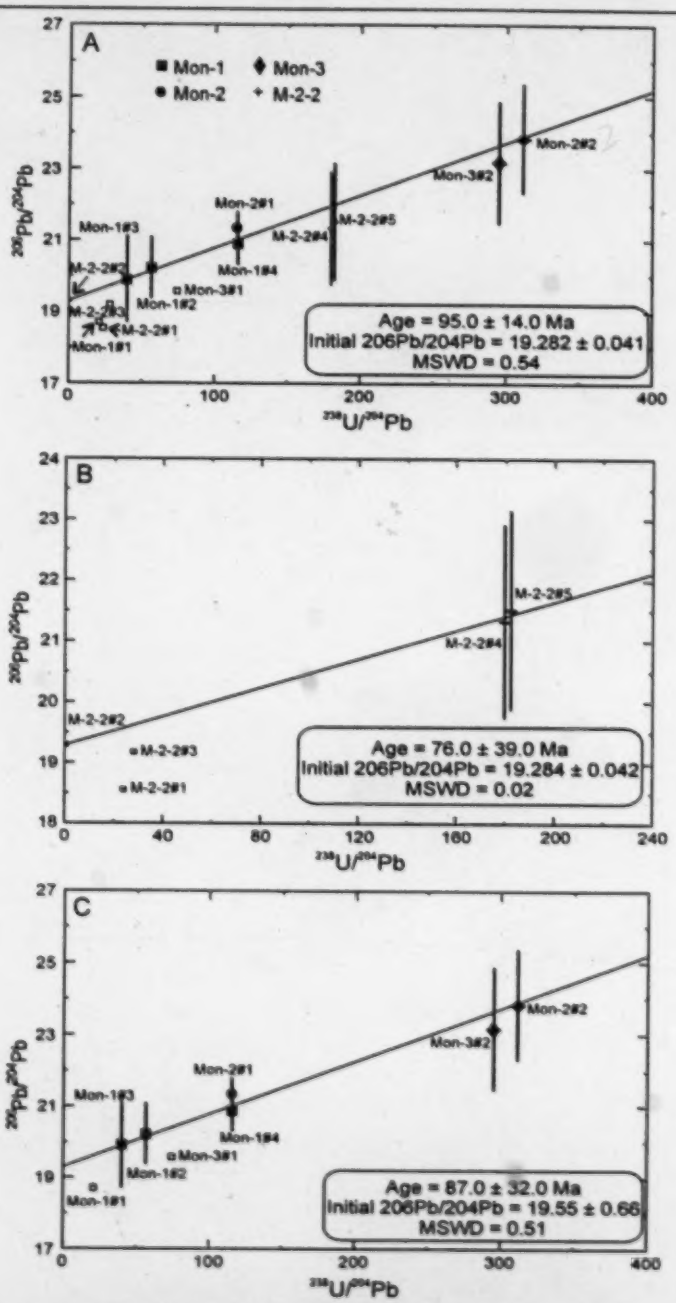

Figure 13 Isochron plots of ilmenite populations from the Monastery kimberlite (open symbols not included in age calculations). **A:** Includes all ilmenite analyses; **B:** includes ilmenite from the East End Type kimberlite; and **C:** inlcudes only ilmenite megacrysts.

consistent and highly radiogenic, 18.5-23.8. The ilmenite fractions (except for M-2-2#2) also have $^{238}U/^{204}Pb$ and $^{206}Pb/^{204}Pb$ ratios that are significantly high enough (> 10) indicating the feasibility of ilmenite geochronology. An age of 95.0 ± 14.0 Ma with an initial $^{206}Pb/^{204}Pb$ ratio of 19.282 ± 0.041 (MSWD=0.51) was obtained for the nine fractions. Blank uncertainties were evaluated in an attempt to reduce errors in the $^{206}Pb/^{204}Pb$ and $^{238}U/^{204}Pb$ ratios however, the errors associated with all $^{206}Pb/^{204}Pb$ ratios are large and primarily reflect the uncertainty in the common Pb correction (Figure 13A).

Separate isochron plots for macrocryst/groundmass ilmenite and ilmenite megacrysts are shown in Figures 13 B&C, respectively, to evaluate variations in age and initial $^{206}Pb/^{204}Pb$ ratios between different types of ilmenite. In Figure 13B, an isochron age of 76.0 ± 39.0 Ma and initial $^{206}Pb/^{204}Pb$ of 19.284 ± 0.042 was obtained for three macrocryst/groundmass ilmenite fractions. Two of the fractions (M-2-2#4 and M-2-2#5) have errors that are significantly high with a minimal spread in parent-daughter ratios decreasing the reliability of the isochron age. This isochron is essentially a two point reference line, hence the low MSWD value. In Figure 13C, an isochron age of 87.0 ± 32.0 Ma and an initial $^{206}Pb/^{204}Pb$ ratio of 19.55 ± 0.66 was obtained for ilmenite megacrysts. Within the quoted uncertainties, no difference can be discerned between the formation age of ilmenite megacrysts and macrocryst/groundmass ilmenite and the variations are not large as to identify isotopically distinct ilmenite populations.

Zircon and ilmenite commonly occur as intergrowths in the Monastery kimberlite (Whitelock, 1973), therefore, a comparative plot of Th versus U for ilmenite, MARID zircons (Konzett et al., 1998) and kimberlitic zircons (Ahrens et al., 1967; Krasnobayev, 1980) is shown in Figure 14. The ilmenite has significantly lower values than those found for zircon, suggesting that the partition coefficient (K_D) for U and Th are much lower for mantle ilmenite compared to mantle zircon:

$$K_{D_{Th,U}}^{Ilmenite} < K_{D_{Th,U}}^{Zircon}$$

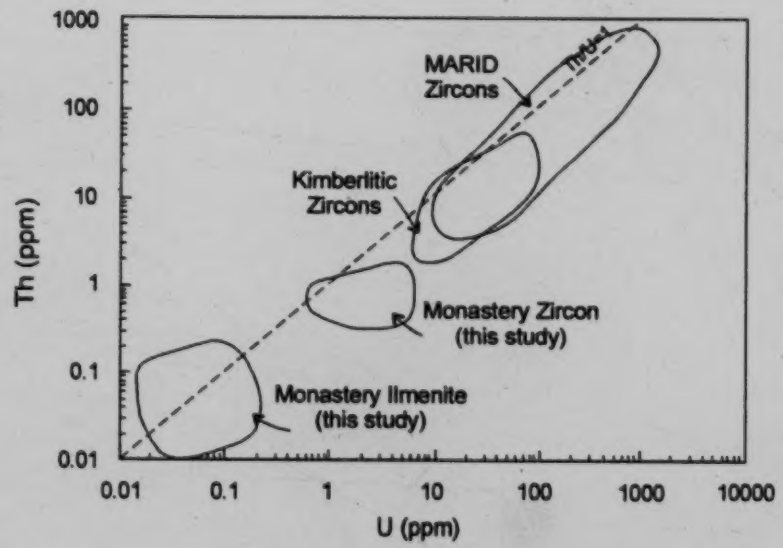

Figure 14 Th vs U plot showing the distribution of ilmenite versus MARID zircons (Konzett et al., 1998), kimberlitic zircons (Ahrens et al., 1967; Krasnobayev, 1980) and Monastery zircons (this study).

Discussion

Previously, dating kimberlite emplacement involved the use of Rb-Sr phlogopite, U-Pb perovskite or mantle zircon isotopic techniques. These minerals are present in some kimberlites, however, many kimberlites in North America are devoid of these minerals. Alternative isotopic techniques suitable for determining the emplacement ages of North American kimberlites are required to evaluate properly models of the origin of these mantle-derived magmas. Because, ilmenite is abundant in most kimberlites world-wide and contains low uranium concentrations, the feasibility of U-Pb ilmenite geochronology has been investigated in this study. The discussion initially focuses on the results of more traditional geochronometers (Rb-Sr phlogopite, U-Pb perovskite, U-Pb mantle zircon) to establish a temporal framework with which to compare the new U-Pb ilmenite results.

Geochronology of kimberlite - traditional techniques

Rb-Sr Phlogopite

The Rb-Sr phlogopite technique can yield accurate and precise emplacement ages for kimberlites. Phlogopite is typically abundant in most kimberlites, can occur as megacrysts and can be easily extracted from the kimberlite matrix. Alteration of phlogopite to chlorite, occurrence of calcite/apatite inclusions or the presence of xenocrystic mica could result in excessive scatter on an isochron diagram potentially producing kimberlite emplacement ages that are too old (Allsopp et al. 1986). Some of these problems can be minimized by selectively hand-picking the phlogopite grains under a binocular microscope and by using acid leaching techniques (Brown et al., 1989) to remove calcite/apatite along cleavage planes and grain fractures.

The trend of higher $^{87}Sr/^{86}Sr$ and $^{87}Rb/^{86}Sr$ ratios in phlogopite for leached fractions compared to non-leached fractions is interpreted by Brown et al. (1989) to be a result of removal of unradiogenic carbonate. A similar pattern exists for phlogopite analysed in this study as can be seen by comparing the non-leached/leached pairs in Figure 9A (AN1NL/AN1L, AN1NL#2/AN1L#2 and AN3NL/AN3L). A more significant increase in $^{87}Sr/^{86}Sr$ and $^{87}Rb/^{86}Sr$ ratios for phlogopite fractions AN1NL/AN1L and AN1NL#2/AN1L#2 compared to AN3NL/AN3L suggests that a large portion of unradiogenic Sr resided in carbonate or apatite that was dissolved during leaching

(Figure 9A). In the case of phlogopite megacryst AN3, numerous apatite inclusions are present and could be the primary source of unradiogenic Sr (Plate 6C). The removal of apatite and/or carbonate during leaching would also explain the significant reduction of total Sr in the leached fractions (see Table 5) with Rb concentrations remaining relatively constant.

Interestingly, the Rb concentration is higher in the leached fraction AN1L compared to fraction AN1NL. This could be related to either sample heterogeneity or to a decrease in sample weight during the leaching process due to the dissolution of soluble material as has been suggested by Brown et al. (1989). However, a similar pattern is not observed in the duplicate analysis of the leached fraction AN1L#2 compared to AN1NL#2. Therefore, a decrease in sample weight due to carbonate removal is ruled out and the Rb variability is most likely attributed to sample heterogeneity. The large range in $^{87}Rb/^{86}Sr$ ratios in the twelve phlogopite fractions analysed in this study (52.4-647.7) is significantly larger than the range obtained for a single megacryst (73.6-166.7) analysed by Smith and Barton (1996).

The Rb-Sr phlogopite age of 89.9 ± 3.1 Ma obtained here is in excellent agreement with the Rb-Sr phlogopite ages of 90.0 ± 4.0 Ma and 88.1 ± 0.6 Ma reported by Allsopp and Barrett (1975) and Smith and Barton (1996), respectively. The Rb-Sr phlogopite age determined by Smith and Barton (1996) is based on the analysis of six leached fractions from a single phlogopite megacryst from the Monastery kimberlite. The Rb-Sr phlogopite age (this study) also is in good agreement with the ages obtained by other radiometric techniques (U-Pb mantle zircon, Davis et al. 1976 and Zartman et al. 1998; and perovskite, Kramers and Smith 1983; Figure 7).

U-Pb Perovskite

U-Pb perovskite geochronology is highly advantageous because it is often a primary groundmass phase crystallizing directly from the kimberlitic magma, contains high concentrations of uranium (11-348 ppm; Heaman 1989), and groundmass perovskite is abundant within many kimberlites. U-Pb perovskite dating has been shown to yield precise kimberlite emplacement ages (e.g. Heaman and Kjarsgaard, 2000). The small grain size of perovskite (< 50 microns) is a disadvantage as selection of individual grains is time consuming which hinders widespread usage of this mineral.

The similar $^{206}Pb/^{238}U$ ages for the different perovskite fractions determined here (Table 7) indicates that there is no obvious age difference between the different coloured fractions. The fraction of darker perovskite grains has higher concentrations of U, Th and Pb than the lighter grains. This is consistent with the results from previous microprobe analyses that indicate the dark cores of zoned perovskite grains are typically enriched in U and Th (Heaman, 1989). The colour zonation observed in most Monastery perovskite (Plates 4F and 5G) with dark cores and light rims likely corresponds to a decrease in U and Th content of the magma during perovskite crystallization.

The initial $^{206}Pb/^{204}Pb$ ratio of Group I kimberlites is quite radiogenic (~19; Smith, 1983). Therefore, even the more radiogenic Stacey and Kramers (1975) average crustal Pb model used for the common Pb correction (18.566) may not be appropriate for these mantle-derived magmas. The initial $^{206}Pb/^{204}Pb$ ratio of 19.19 ± 0.97 calculated from the perovskite isochron regression (Figure 10A) was used for the common Pb correction to recalculate the $^{206}Pb/^{238}U$ apparent ages (Table 7). This resulted in a more precise weighted mean $^{206}Pb/^{238}U$ age of 91.0 ± 1.0 Ma using all four perovskite fractions.

Previous U-Pb perovskite geochronology of a Monastery kimberlite sample yielded an ^{238}U-^{206}Pb isochron age of 83 ± 3 Ma based on a leach/residue pair analysis (Kramers and Smith, 1973). This age is distinctly younger than the U-Pb perovskite age obtained in this study (91.0 ± 1.0 Ma) and is noticeably younger than many of the other radiometric ages obtained for the Monastery kimberlite (Figure 7). The possibility of multiple phases of intrusion varying in age (e.g. Kirkland Lake kimberlite field, Heaman and Kjarsgaard, 2000), may provide an explanation for this younger age.

U-Pb Mantle Zircon

The U-Pb mantle zircon dating technique is widely used to determine kimberlite emplacement ages (e.g. Davis, 1977; 1978) as zircon in general has a high closure temperature (~ 900°C) for Pb diffusion (e.g. Lee et al., 1997) and is a very robust and resistant mineral making it less susceptible to chemical and isotopic changes (LeCheminant et al., 1998). Also, information pertaining to timing and nature of mantle processes prior to kimberlite emplacement, can be preserved in mantle zircons. Mantle zircon is known to be xenocrystic, a rare accessory mineral in kimberlites, but is commonly recovered in heavy concentrates along with diamonds. Great care must be taken while selecting zircon grains for U-Pb geochronology; for example selecting

crystals devoid of inclusions, fractures and/or turbidity. Inherited zircons or zircon containing an older core can be encountered in determining kimberlite emplacement ages. In some instances the zircon xenocryst has not been completely isotopically reset during kimberlite emplacement, thus recording a history for the mantle zircon prior to entrainment in kimberlite magma (see below).

During the short period of mining in 1981-1982 at Monastery, hundreds of mantle zircon crystals were recovered providing new material for study. In addition to the single zircon megacryst investigated here, numerous other researchers have studied mantle zircon megacrysts that were recovered during diamond mining of the Monastery kimberlite.

The uranium content of Monastery mantle zircon analysed in this study (0.9-4.1 ppm) represents some of the lowest values ever reported. In two previous studies of mantle zircon chemistry, Ahrens et al. (1967) obtained a range of 7-28 ppm uranium and Kresten and Berggren (1975) report an even larger range of 6.7-66 ppm uranium. The data by Kresten and Berggren (1975) are based on fission track analyses and delayed neutron technique for 24 kimberlitic zircons. The majority of these mantle zircons typically contained < 30 ppm uranium (Kresten and Berggren, 1975) and these low values were considered to represent primary uranium contents within mantle zircon. The higher levels of uranium were interpreted to reflect possible contamination of either crustal zircon or zircon from other igneous sources (e.g. granitic zircon: 154-4116 ppm U; Ahrens et al., 1967; Kresten, 1974; Kresten and Berggren, 1975). Davis (1976) also reported a low U concentration of 6.1 ppm for a zircon crystal isolated from a peridotite nodule from the Monastery kimberlite which, at the time, was the lowest concentration obtained from any kimberlite-borne "mantle" zircon. The lowest published uranium concentration in a mantle zircon is 3 ppm (Zartman et al., 1998) for a zircon crystal from the Monastery kimberlite. In summary, some of the Monastery mantle zircons have some of the lowest uranium contents reported and, combined with its overall low trace element content (see Instrumental Neutron Activation Analyses for Monastery mantle zircon reported by Heaman et al., 1990), possibly represents the most chemically pure natural terrestrial zircon known.

There are two possibilities to explain the 'anomalous' old ages occasionally reported for mantle zircon (Kinny and Meyer, 1994; Schärer et al., 1997; Konzett, 1998; Klötzli, 1999). The first is the retention of older isotopic signatures with partial resetting

(Kinny and Meyer, 1994; Schärer et al., 1997). The second is a complex growth history for a mantle zircon crystal where new zircon growth occurs around an older core (Konzett, 1998; Klötzli, 1999). In both cases, the implication is that mantle zircons could have extremely high closure temperatures for Pb diffusion.

Mantle zircon and diamond are entrained in kimberlite magmas at great depths (> 100 km) (Davis, 1977; Kirkley et al., 1992). The isotopic systematics of zircon crystals residing in such deep mantle regions could be disturbed as the temperatures are too high for lead retention and therefore Pb (especially radiogenic Pb located in damaged lattice sites) can diffuse out of the crystal structure (Davis 1976; 1977). Lead is only retained within the crystal structure once the zircon has been entrained within a magma and brought to cooler temperatures (c.1000°C; zircon closure temperature estimated to be greater than 900°C, Lee et al., 1997), thus recording the time of entrainment and possibly the time of kimberlite emplacement.

Another process for lead diffusion in older zircon is outlined by Schärer et al. (1997) in an attempt to explain the older upper intercept age of 2.5 Ga for mantle zircon from the Mbuji-Mayi kimberlite (70 Ma). Schärer et al. (1997) proposed that the kimberlitic event at 70 Ma caused extensive lead-loss within old mantle zircon. However, considering that it would be necessary for a significant amount of radiogenic Pb to be lost from these old zircon grains (between 5 and 1000 ppm), the current chemical homogeneity of the zircon and the lack of inclusions, this mechanism was ruled out as an explanation for the Mbuji-Mayi zircon U-Pb results. Schärer et al. (1997) concluded that the age of 2.5 Ga represents the incorporation of common Pb that is quite radiogenic within the crystallizing zircon at time of kimberlite emplacement. The existence of an older Pb component in the source region for this kimberlite is supported by an older 528 Ma U-Pb age obtained by Kinny et al. (1989) for a mantle zircon inclusion in a diamond from the Mbuji-Mayi kimberlite.

Old mantle zircon ages have also been obtained through U-Pb SHRIMP (Sensitive High Resolution Ion MicroProbe) zircon analysis that do not represent the kimberlite emplacement age (e.g. Jwaneng kimberlite; Kinny and Meyer, 1994). However, Kinny and Meyer (1994) found that the anomalously old zircon age was not totally "reset" to the kimberlite emplacement age and therefore did not follow the assumptions outlined by Davis (1976 and 1977). Kinny and Meyer (1994) concluded that the retention of an older age may occur if the zircon was brought to cooler

temperatures where radiogenic lead would begin to accumulate within the zircon before being entrained within kimberlite magma

The possibility of multiple growth histories (e.g. Konzett et al., 1998; Klötzli, 1999) within a Monastery zircon xenocryst could also explain the anomalously old U-Pb ages. Konzett et al. (1998) identified a population of zircon from MARID xenoliths that have U-Pb ages older than the emplacement ages for the Kimberley kimberlite field (80-95 Ma). Cathodoluminescence imaging has revealed zonation patterns in these zircon crystals. The range of U-Pb SHRIMP ages obtained for the various zones (91-116 Ma) within a single megacryst were attributed to multiple growth events (Konzett et al., 1998).

These examples illustrate some of the possible explanations for anomalously old U-Pb mantle zircon ages, such as the 325.4 Ma age obtained for fraction Zir#5 in this study. Interestingly, this fraction also has the lowest uranium content (0.93 ppm) of the eight analyses. One possible interpretation is that the 325.4 Ma age represents a minimum estimate for the time of original xenocryst formation. However, it is impossible to be certain whether this particular zircon megacryst underwent multiple growth histories as proposed by Konzett et al. (1998) as it was not analysed by electron microprobe or cathodoluminescence to identify zonation patterns prior to analysis. If this zircon megacryst has a complex crystal structure then this would mean that the concentrations, isotopic ratios and U-Pb ages obtained in this study would represent an averaging effect that is related to the sample preparation techniques employed in this study (i.e. crushing of a single, large crystal).

The diamond stability field ranges in temperature from 900-1200°C (Kirkley et al., 1992) and it is likely that both diamond and zircon recovered from the Monastery kimberlite were extracted from a portion of the mantle at these temperature conditions. The preservation of old ages in the Monastery mantle zircon, whether the zircon was partially reset or possessed an older core, could be indirect evidence that the minimum closure temperature for Pb diffusion in zircon is at least as high as the lower temperature estimate for the diamond stability field of about 900°C. This estimate based on a natural example is similar to the minimum closure temperature for Pb diffusion of 900°C obtained by Lee et al. (1997) based on diffusion experiments using natural zircon.

Geochronology of kimberlite - New Technique

U-Pb Ilmenite

i) Geochemistry

The mineral chemistry for ilmenite obtained in this study (Figure 8C) has shown that the ilmenite megacrysts and macrocrysts used for U-Pb geochronology have compositions similar to those previously reported for Monastery "Magmatic" and "Kimberlite Reaction" trends shown on Figure 6 and as proposed by Haggerty et al. (1979). The *Magmatic Trend* reflects primary ilmenite (<1 wt% MnO) crystallization during a decrease in pressure, fO_2 and Fe_2O_3 of the kimberlite magma (Haggerty et al., 1979). The *Kimberlite Reaction Trend* (Haggerty et al., 1979) and the *Manganese Enrichment Trend* (Mitchell, 1986) reflect the control of carbonatitic fluids/melts or involvement of carbonatite/kimberlite immiscibility during ilmenite crystallization. Haggerty et al. (1979) report MnO-enrichment in Monastery ilmenite rims up to 5 wt.% and some macrocrysts in this study have "bright" rims with as much as 13 wt% MnO (Table 4). The ilmenite megacrysts and macrocrysts investigated here rarely contain inclusions and ilmenite cores are relatively homogeneous chemically. Occasionally perovskite occurs along the rims of ilmenite megacrysts and macrocrysts. Highly deformed and pitted ilmenite macrocrysts do occur in the Monastery kimberlite samples studied but likely do not possess significant chemical variations observed by Pasteris et al. (1979).

Compared to the whole-rock uranium concentration of 4.1 ppm for the Monastery kimberlite (Kresten, 1974), the uranium contents of ilmenite from the Kao, Lemphane and Sekameng/Kolo kimberlites, South Africa, also determined by Kresten (1974), are an order of magnitude lower (0.1-0.2 ppm). The range in uranium concentrations for Monastery ilmenite obtained here is also similar (0.02-0.17 ppm; Table 8). The Th/U ratios obtained for Monastery ilmenite are quite variable (0.03-3.51) but some fractions (Mon-1#3, Mon-2#1, M-2-2#2) have Th/U greater than one indicating that Th may be preferentially incorporated into ilmenite relative to uranium or that some perovskite is present. The ilmenite analyses with high Th/U do not have correspondingly high $^{238}U/^{204}Pb$ ratios, which would be expected if some perovskite is present so the variable Th/U ratios is considered a primary chemical feature of ilmenite.

It is interesting that even though perovskite and ilmenite have similar chemical formulae ($CaTiO_3$ and $(Mg,Fe)TiO_3$, respectively), the degree of uranium and thorium

partitioning is significantly higher in perovskite than in ilmenite. The reason for this is that the atomic radius for Ca^{2+} (1.12 Å) is very similar to the atomic radius of U^{4+} (1.05 Å), therefore, U^{4+} substitution for Ca^{2+} would be preferred over the Mg^{2+} (0.72 Å) and Fe^{2+} (0.78 Å) sites in ilmenite. Mitchell (1972) outlines one possible reaction for the formation of perovskite rims on ilmenite megacrysts:

$$Ca^{2+} + \text{'silica'} + \underset{\text{(ilmenite)}}{(Mg,Fe)TiO_3} = \underset{\text{(perovskite)}}{CaTiO_3} + \text{(Mg,Fe) silicates}$$

In order to explain the higher uranium and thorium content in perovskite, U^{4+} is concentrated in a vapour phase at time of ilmenite crystallization and is incorporated into the more suitable perovskite crystal lattice during reaction with kimberlite magma/fluid (Kresten, 1974).

An important factor to address for the interpretation of the U-Pb results (next section) is the large variation in $^{238}U/^{204}Pb$ ratios of ilmenite. Kresten (1974) has suggested that these variations could be the result of either the presence of perovskite or other high U/Pb mineral inclusions. Primary ilmenite nodules were found to contain approximately 0.1 ppm of uranium (slightly higher than most ilmenite analyses reported in this study, Table 9), however, it was found that calcite filled cracks contained 0.4 ppm of uranium (Kresten, 1974). Fission track analyses indicated that the majority of uranium is not located within the ilmenite or calcite grains but rather is concentrated at contact boundaries between calcite/ilmenite and perovskite/ilmenite grains. However, microprobe analyses of ilmenite megacrysts in this study revealed that they are chemically relatively homogeneous, the ilmenite grains were hand-picked avoiding perovskite and the grains were also washed in HNO_3 to remove such contaminants as carbonate along fractures, prior to dissolution. These precautions were employed to eliminate potential contaminants in the ilmenite fractions, therefore, the possibility of perovskite or carbonate contamination is considered unlikely for these samples.

ii) Geochronology

Encouraging results in this study enhance the potential of obtaining geologically meaningful U-Pb ilmenite ages. The isochron diagram for the six ilmenite megacryst fractions in Figure 13C, show significant variation in $^{238}U/^{204}Pb$ and $^{206}Pb/^{204}Pb$ ratios as well as significant variation for megacryst Mon-1. This is highly promising as such isotopic variations are essential for obtaining precise isochron ages. For example,

megacrysts Mon-1 and Mon-2 (square and circle symbols, respectively, Figure 13A&C) exhibit internal variations in the $^{206}Pb/^{204}Pb$ ratios (18.7-20.9 and 21.3-23.8, respectively) and an even larger variation in the $^{238}U/^{204}Pb$ ratios (21.5-115.5 and 115.2-311.4, respectively). The $^{206}Pb/^{204}Pb$ ratios and $^{238}U/^{204}Pb$ ratios (18.5-21.5 and 24.0-182.1, respectively) for macrocryst/groundmass ilmenite fractions (Figure 13B) are comparable to those of the megacryst variety falling within the range of Mon-1 and Mon-2. This is evidence for a primary internal geochemical variation within ilmenite and indicates the great potential to obtain U-Pb ages for a single ilmenite megacryst. These variations in ilmenite chemistry outlined above are considered here to be primary as every effort was made to eliminate the potential of perovskite and carbonate contamination.

Most important is the fact that the U-Pb ilmenite age (95.0 ± 14.0 Ma) obtained here is within error of previously published data (Figure 15) and is in agreement with Rb-Sr phlogopite, U-Pb perovskite and U-Pb mantle zircon ages obtained in this study demonstrating the feasibility of U-Pb ilmenite geochronology.

It is the precision of U-Pb ilmenite age determinations that requires refinement. It is apparent from the ages obtained for the Monastery kimberlite in this study, that the errors associated with the $^{206}Pb/^{204}Pb$ and $^{238}U/^{204}Pb$ ratios for ilmenite need to be reduced. The largest contribution to these errors is the uncertainty in the Pb blank correction. An attempt to reduce these errors by carefully evaluating the Pb blanks in this study (see Table 6) resulted in some improvement however, the errors are still significantly high enough to yield relatively imprecise ages. The uranium and lead concentrations are quite low as well however, this can be overcome by picking larger fractions of material. The requirement to analyse large ilmenite fractions does not pose a serious problem as ilmenite is quite abundant within most kimberlites. In the case where kimberlites do not possess abundant phlogopite, mantle zircon or perovskite, geologically meaningful emplacement ages with slightly larger errors can be established using U-Pb ilmenite geochronology.

Summary of Age Determinations

Figure 15 is a summary of the emplacement ages for the Monastery kimberlite obtained in this study and includes a region that outlines the range of previously published ages. The ages obtained by all three isotopic techniques, Rb-Sr phlogopite

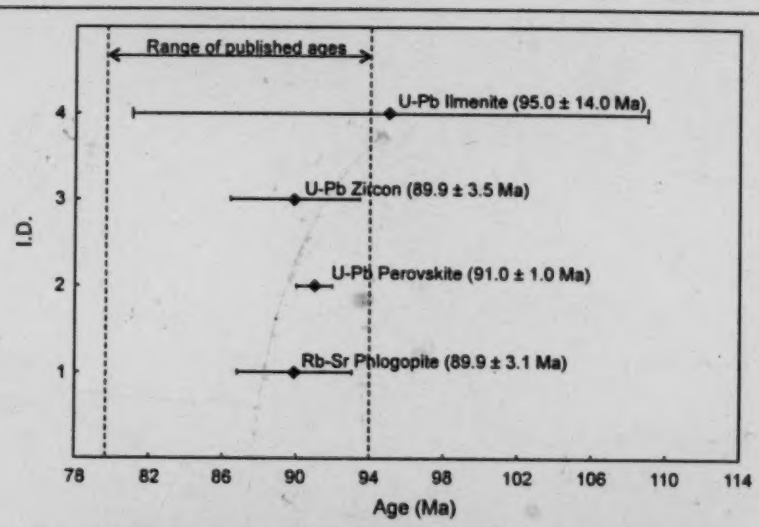

Figure 15 Summary of the ages for the Monastery kimberlite obtained in this study. The range of previously published ages is outlined as a comparison (from Figure 7).

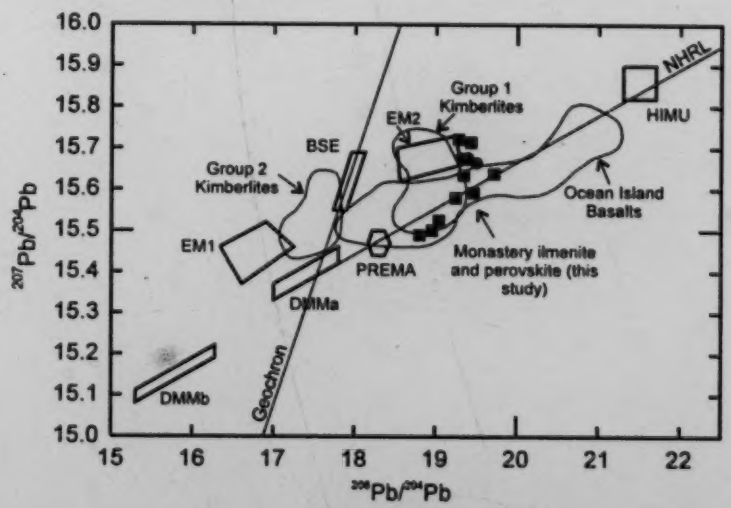

Figure 16 $^{207}Pb/^{204}Pb$ vs $^{208}Pb/^{204}Pb$ plot for mantle components. Monastery ilmenite (square symbols) and perovskite (circle symbols) (this study) (initial Pb compositions calculated at 90 Ma) are plotted for comparison with Group 1 & 2 kimberlites (Smith, 1983), and ocean island basalts (Hart, 1984). DMM = depleted MORB mantle, PREMA = prevalent mantle, EM1 = enriched mantle type 1, EM2 = enriched mantle type 2, BSE = bulk silicate earth, HIMU = high MU. The Northern Hemisphere Reference Line (NHRL) and the Geochron at 4.55 Ga are shown for reference. After Zindler and Hart (1986).

(89.9 ± 3.1 Ma), U-Pb perovskite (91.0 ± 1.0 Ma) and U-Pb mantle zircon (89.9 ± 3.5) agree remarkably well within the quoted uncertainties. This is the first study to attempt all three radiometric techniques on the same kimberlite and provides some confidence that geologically meaningful ages can be obtained. The age results obtained here are also in excellent agreement with previously published ages (Figure 7). The U-Pb ilmenite age of 95 ± 14 Ma obtained here for the Monastery kimberlite is the first attempt at determining an ilmenite crystallization age for any rock and also agrees very well with all other reported ages demonstrating the feasibility of U-Pb ilmenite geochronology.

Nature of kimberlite source regions

i) Lead

The initial $^{207}Pb/^{204}Pb$ and $^{206}Pb/^{204}Pb$ ratios for individual ilmenite and perovskite analyses calculated at 90 Ma are plotted in Figure 16 along with other mantle reservoirs and fields for South African kimberlites. The ilmenite and perovskite analyses plot adjacent to the enriched mantle type 2 (EM2) mantle component which also overlaps the isotopic signatures for ocean island basalts (Hart, 1984) and Group 1 South African kimberlites (Smith, 1983). In detail, the initial $^{206}Pb/^{204}Pb$ ratios for perovskite and ilmenite obtained from regression line calculations in this study (19.19 ± 0.97 and 19.28 ± 0.04, respectively) are quite radiogenic and most resemble ocean island basalt ratios (17.6-21.1) summarized by Hart (1984). The initial $^{206}Pb/^{204}Pb$ ratios obtained for the Monastery kimberlite (this study) fall within the range reported for Group 1 kimberlites (18.5-20.1) and are outside the range reported for Group 2 kimberlites (17.2-17.7; Smith, 1983). It is evident that Group 1 and Group 2 kimberlites are derived from two isotopically distinct mantle source regions. The mantle source for Group 1 kimberlites in Pb isotope space is slightly enriched and is characterized by high $^{238}U/^{204}Pb$ ratios, whereas, the mantle source for Group 2 kimberlites is slightly depleted relative to bulk earth and is characterized by lower $^{238}U/^{204}Pb$ ratios (Smith, 1983). The ilmenite and perovskite Pb isotopic data can be interpreted in two ways; either ilmenite and perovskite crystallized from a magma with a significant EM2 mantle signature or they crystallized from a magma with a mixed depleted MORB (DMM), EM2 and high Mu (HIMU) mantle signature. This latter interpretation is preferred by Hatton (1998) to explain the isotopic composition of Group 1 kimberlites in general. Hatton (1998) suggested that the HIMU mantle signature was incorporated in the Monastery kimberlitic

magma during emplacement and mixing with earlier DMM and EM2 melts. This interpretation can provide a possible explanation for the high $^{238}U/^{204}Pb$ ratios, as well as the large $^{238}U/^{204}Pb$ variations in ilmenite from the Monastery kimberlite. The enriched Pb isotopic nature of the Monastery source region may also apply to other kimberlites and may be an important consideration for selecting common Pb compositions to correct U-Pb perovskite analyses in other studies.

ii) Strontium

The Rb-Sr phlogopite age calculated for the Monastery kimberlite in this study (89.9 ± 3.1 Ma; Figure 15) and the initial $^{87}Sr/^{86}Sr$ ratio (0.708 ± 0.011), although less precise, is in agreement within error of results reported in previous studies. Smith (1983) obtained an initial $^{87}Sr/^{86}Sr$ ratio of 0.7033 ± 0.0011 for the Monastery kimberlite, whereas Mitchell and Crocket (1971) obtained a slightly more radiogenic initial $^{87}Sr/^{86}Sr$ ratio of 0.7067 ± 0.0006. Both initial Sr ratios by Smith (1983) and Mitchell and Crocket (1971) were based on one Monastery kimberlite whole rock analysis. The initial $^{87}Sr/^{86}Sr$ ratios obtained by these authors are statistically different and could indicate variations caused by an unknown amount of crustal xenoliths. The initial strontium isotopic composition reported for a single phlogopite megacryst (Smith and Barton, 1996) including the kimberlite whole rock analysis of Smith (1983) yields the most precise ratio of 0.7034 ± 0.0002.

The Monastery kimberlite is considered to be a Group 1 kimberlite based on mineralogical and age emplacement criteria (Smith, 1983). Group 1 kimberlites contain little to no groundmass mica and have emplacement ages ranging from 80 to 114 Ma, whereas, Group 2 kimberlites are micaceous and have emplacement ages ranging from 114 to 150 Ma (Smith, 1983). Smith (1983) has determined initial $^{87}Sr/^{86}Sr$ ratios for fresh Group 1 kimberlites to be typically 0.7033 to 0.7049 and for Group 2 kimberlites to be 0.708. These values were derived from whole rock analyses from South African kimberlites that are Jurassic and Cretaceous in age. The enrichment of $^{238}U/^{204}Pb$ and initial $^{206}Pb/^{204}Pb$ ratios (previous section) is not coupled with enrichment in $^{87}Rb/^{86}Sr$ (Zindler and Hart, 1986). Therefore, the low $^{87}Sr/^{86}Sr$ values of ~ 0.703 recorded in Group 1 kimberlites could be characteristic of a HIMU source (Zindler and Hart, 1986).

Conclusions

There are disadvantages and advantages for each isotopic method however, it has been demonstrated in this study that multiple techniques can yield consistent and reliable kimberlite emplacement ages. Rb-Sr phlogopite (89.9 ± 3.1 Ma), U-Pb mantle zircon (89.9 ± 3.5 Ma) and perovskite (91.0 ± 1.0 Ma) yield ages that are in excellent agreement with each other as well as with previous work. A few words of cautionary advice can be offered through the study of U-Pb mantle zircon for the Monastery kimberlite. The U-Pb mantle zircon analyses may reveal a more complex growth history or diffusion mechanism than has been previously reported. In instances where the zircon crystal is large enough, electron microprobe and cathodoluminescence studies would identify multiple growth bands or complex crystal structure.

The mineral chemistry for ilmenite obtained in this study have compositions similar to those previously reported for Monastery "Magmatic" and "Kimberlite Reaction" Trends shown on Figure 6 and as proposed by Haggerty et al. (1979). They are considered to have formed by primary crystallization in a kimberlitic magma and/or by late-stage interaction with a carbonatitic fluid (MnO-enrichment). A preliminary study of U-Pb ilmenite geochronology has yielded very promising results regarding determining kimberlite emplacement ages. The age of 95 ± 14 Ma is in agreement with the ages obtained by three different radiometric techniques in this study (see above) and in comparison to previously published age data for the Monastery kimberlite. This study has also demonstrated that the large variations in ilmenite $^{238}U/^{204}Pb$ ratios are primary and encourages the possibility of dating a single ilmenite megacryst. If these chemical variations observed for ilmenite megacrysts and macrocrysts are primary then they could be attributed to the mixing of a HIMU mantle component with DMM and EM2 mantle components during kimberlite emplacement.

It is obvious that more research on U-Pb ilmenite geochronology is necessary in order to reduce uncertainties related to blank corrections. Even at the current status, it is possible to potentially determine geologically meaningful U-Pb ilmenite ages for other kimberlites. Many questions have been generated as a result of this study. Are the uranium and lead concentrations of all kimberlitic ilmenite as low as the Monastery kimberlite ilmenite? Do all ilmenite megacrysts show primary variation in U/Pb? U-Pb ilmenite geochronology is still in its infancy, however, it is now possible to obtain kimberlite emplacement ages using U-Pb ilmenite with some confidence when phlogopite, perovskite or mantle zircon are rare or absent.

References

Agee, J.J., Garrison, J.R. and Taylor, L.A., 1982. Petrogenesis of oxide minerals in kimberlite, Elliott County, Kentucky. American Mineralogist, v. 67, p. 28-42.

Ahrens, L.H., Cherry, R.D. and Erlank, A.J., 1967. Observations on the Th-U relationship in zircons from granitic rocks and from kimberlites. Geochimica et Cosmochimica Acta, v. 31, p. 2379-2387.

Allsopp, H.L. and Barrett, D.R., 1975. Rb-Sr age determinations on South African kimberlite pipes. Physics and Chemistry of the Earth, v. 9, p. 605-617.

Allsopp, H.L. and Roddick, J.C., 1984. Rb-Sr and ^{40}Ar-^{39}Ar age determinations on phlogopite micas from the Pre-Lebombo Group Dokolwayo kimberlite pipe. Special Publication - Geological Society of South Africa, v.13, p.267-271.

Allsopp, H.L., Bristow, J.W., Smith, C.B., Brown, R., Gleadow, A.J.W., Kramers, J.D. and Garvie, O.G., 1986. A summary of radiometric dating methods applicable to kimberlites and related rocks. *In*: Kimberlites and related rocks: Their composition, occurrence, origin and emplacement, v.1, p. 343-357. Proceedings of the 4th International Kimberlite Conference, Perth, Australia.

Boctor, N.Z. and Boyd, F.R., 1979. Distribution of rare earth elements in perovskite from kimberlites. Yearbook - Carnegie Institute of Washington, v. 78, p. 572-574.

Boctor, N.Z. and Boyd, F.R., 1980. Oxide minerals in the Liqhobong kimberlite, Lesotho. American Mineralogist, v. 65, p. 631-638.

Boyd, F.R. and Nixon, P.H., 1973. Origin of the ilmenite-silicate nodules in kimberlites from Lesotho and South Africa. *In*: P.H. Nixon (Ed.) Lesotho Kimberlites, Lesotho National Development Corporation, Maseru, Lesotho, p. 254-268.

Boyd, F.R. and Nixon, P.H., 1975. Origins of the ultramafic nodules from some kimberlites of northern Lesotho and the Monastery Mine, South Africa. Physics and Chemistry of the Earth, v. 9, p. 431-454.

Brown, R.W., Allsopp, H.L., Bristow, J.W. and Smith, C.B., 1989. Improved precision of Rb-Sr dating of kimberlitic micas: an assessment of a leaching technique. Chemical Geology, v. 79, p. 125-136.

Cahen, L., Snelling, N.J., Delhal, J. and Vail, J.R., 1984. *The Geochronology and evolution of Africa*. Clarendon Press, Oxford, 512pp.

Cameron, A.E., Smith, D.H. and Walker, R.L., 1969. Mass Spectrometry of Nanogram-Size Samples of Lead. Analytical Chemistry, v. 41, no. 3, p. 525-526.

Carswell, D.A., 1975. Primary and secondary phlogopites and clinopyroxenes in garnet lherzolite xenoliths. Physics and Chemistry of the Earth, v. 9, p.417-430.

Clifford, T.N., 1970. The structural framework of Africa. *In*: African Magmatism and Tectonics, T.N. Clifford and I.G. Gass (Eds.). Hafner Publishing Company, Darien, Conn., p. 1-26.

Cox, K.G., 1970. Tectonics and vulcanism of the Karroo Period and their bearing on the postulated fragmentation of Gondwanaland. *In*: African Magmatism and Tectonics, T.N. Clifford and I.G. Gass (Eds.). Hafner Publishing Company, Darien, Conn., p. 211-235.

Dawson, J.B. and Reid, A.M., 1970. A pyroxene-ilmenite intergrowth from the Monastery Mine, South Africa. Contributions to Mineralogy and Petrology, v. 26, p. 296-301.

Dawson, J.B. and Smith, J.V., 1975. Chemistry and origin of phlogopite megacrysts in kimberlite. Nature, v. 253, p. 336-338.

Davis, G.L., Krogh, T.E. and Erlank, A.J., 1976. The ages of zircons from kimberlites from South Africa. Yearbook-Carnegie Institution of Washington, v. 75, p. 821-824.

Davis, G.L., 1977. The ages and uranium contents of zircons from kimberlites and associated rocks. Yearbook - Carnegie Institute of Washington, v. 76, p.631-635.

Davis, G.L., 1978. Zircons from the mantle. Yearbook-Carnegie Institution of Washington, v. 78, p. 86-88.

Davis, W.D., Gray, J., Cumming, G.L. and Baadsgaard, H., 1977. Determination of the (super 87) Rb decay constant. Geochimica et Cosmochimica Acta, v. 41, p. 1745-1749.

Droop, G.T.R., 1987. A general equation for estimating Fe^{3+} concentrations in ferromagnesian silicates and oxides from microprobe analyses, using stoichiometric criteria. Mineralogical Magazine, v. 51, p. 431-435.

Duncan, R.A., Hooper, P.R., Rehacek, J., Marsh, J.S. and Duncan, A.R., 1997. The timing and duration of the Karoo igneous event, southern Gondwana. Journal of Geophysical Research, v. 102, p. 18 127-18 138.

Farmer, G.L and Boettcher, A.L., 1981. Petrologic and crystal-chemical significance of some deep-seated phlogopites. American Mineralogist, v. 66, p.1154-1163.

Fitch, F.J. and Miller, J.A., 1971. Potassium-argon Radioages of Karroo Volcanic rocks from Lesotho. Bulletin Volcanologique, v. 35, p. 64-84.

Garanin, V.K., Kudryavtseva, G.P. and Lapin, A.V., 1979. Typical features of ilmenite from kimberlites, alkali-ultrabasic intrusions, and carbonatites. International Geology Review, v. 22, no. 9, p. 1025-1050.

Greenwood, J.C., Gibson, S.A., Thompson, R.N., Weska, R.K. and Dickin, A.P., 1998. Petrogenesis of Cretaceous kimberlites from the Paranatinga region, central Brazil. *In*: 7th International Kimberlite Conference, Extended Abstracts, p. 268-270.

Griffin, W.L., Moore, R.O., Ryan, C.G., Gurney, J.J. and Win, T.T., 1997. Geochemistry of magnesian ilmenite megacrysts from southern African kimberlites. Russian Geology and Geophysics, v. 38, n.2, p. 421-443. N.V. Sobolev and R.H. Mitchell (Eds.), Proceedings of the Sixth International Kimberlite Conference.

Gurney, J.J., Fesq, H.W. and Kable, E.J.D., 1973. Clinopyroxene-ilmenite intergrowths from kimberlite: a re-appraisal. *In*: P.H. Nixon (Ed.) Lesotho Kimberlites, Lesotho National Development Corporation, Maseru, Lesotho, p. 238-253.

Gurney, J.J., Jakob, W.R.O. and Dawson, J.B., 1979. Megacrysts from the Monastery kimberlite pipe, South Africa. *In*: The mantle sample; Inclusions in kimberlites and other volcanics. Proceedings of the 2nd International Kimberlite Conference, v. 2, p. 265-278.

Gurney, J.J., Moore, R.O. and Bell, D.R., 1998. Mineral associations and compositional evolution of Monastery kimberlite megacrysts. *In*: 7th International Kimberlite Conference, Extended Abstracts, p. 290-292.

Haggerty, S.E., Hardie III, R.B. and McMahon, B.M, 1979. The mineral chemistry of ilmenite nodule associations from the Monastery diatreme. *In*: The mantle sample; Inclusions in kinberlites and other volcanics. Proceedings of the 2nd International Kimberlite Conference, v. 2, p. 249-256.

Hart, S.R., 1984. A large-scale isotope anomaly in the Southern Hemisphere mantle. Nature, v. 309, p. 753-757.

Hatton, C.J., 1998. The kimberlite-megacryst link at Monastery Mine. *In*: 7th International Kimberlite Conference, Extended Abstract, p. 314-316.

Heaman, L.M., 1989. The nature of the subcontinental mantle from Sr-Nd-Pb isotopic studies on kimberlitic perovskite. Earth and Planetary Science Letters, v. 92, p. 323-334.

Heaman, L.M., Bowins, R. and Crocket, J., 1990. The chemical composition of igneous zircon suites: implications for geochemical tracer studies. Geochimica et Cosmochimica Acta, v.54, p. 1597-1607.

Heaman, L.M. and Machado, N., 1992. Timing and origin of midcontinent rift alkaline magmatism, Noth America: evidence from the Coldwell Complex. Contributions to Mineralogy and Petrology, v. 110, p. 289-303.

Heaman, L.M. and Kjarsgaard, B., 2000. Timing of eastern North American kimberlite magmatism: continental extension of the Great Meteor hotspot track? Earth and Planetary Science Letters, *in Press*.

Helmstaedt, H. and Gurney, J.J., 1984. Kimberlites of southern Africa - are they related to subduction processes? *In*: Kimberlites and Related Rocks, v.1, p. 425-434. Proceedings of the Third International Kimberlite Conference, France.

Hunter, R.H., Kissling, R.D. and Taylor, L.A., 1984. Mid- to late-stage kimberlitic melt evolution: phlogopites and oxides from the Fayette County kimberlite, Pennsylvania. American Mineralogist, v. 69, p. 30-40.

Jones, A.P. and Smith, J.V., 1984. Ion probe analysis of H, Li, B, F and Ba in micas, with additional data for metamorphic amphibole, scapolite and pyroxene. Neues Jahrbuch fuer Mineralogie, Monatshefte, v. 5, p. 228-240.

Jones, A.P. and Wyllie, P.J., 1984. Minor elements in perovskite from kimberlites and distribution of the rare earth elements: an electron probe study. Earth and Planetary Science Letters, v. 69, p. 128-140.

Kinny, P.D., Compston, W., Greistow, J.W. and Williams, I.S., 1989. Archean mantle xenocrysts in a Permian kimberlite: two generations of kimberlitic zircon in Jwaneng DK2, southern Botswana. *In*: Ross. J. (Ed.), Kimberlites and Related Rocks. Geological Society of Australia, Special Publication, v. 14, p. 833-842.

Kinny, P.D. and Meyer, H.O.A., 1994. Zircon from the mantle: a new way to date old diamonds. The Journal of Geology, v. 102, p. 475-481.

Kirkley, M.B., Gurney, J.J., and Levinson, A.A., 1992. Age, origin and emplacement of diamonds: a review of scientific advances in the last decade. *In*: Diamond Mining; Industrial Minerals Division of CIM Bull., v. 84, No. 956, p. 48-57.

Klötzli, U.S., 1999. Th/U zonation in zircon derived from evaporation analysis: a model and its implications. Chemical Geology, v. 158, p. 325-333.

Konzett, J., Armstrong, R.A., Sweeney, R.J. and Compston, W., 1998. The timing of MARID metasomatism in the Kaapvaal mantle: an ion probe study of zircons from MARID xenoliths. Earth and Planetary Science Letters, v. 160, p. 133-145.

Kramers, J.D. and Smith, C.B., 1983. A feasibility study of U-Pb and Pb-Pb dating of kimberlites using groundmass mineral fractions and wholerock samples. Isotope Geoscience, v. 1, p. 23-38.

Krasnobayev, A.A., 1980. Mineralogical-geochemical features of zircons from kimberlites and problems of their origin. International Geology Review, v.22, no. 10, p. 1199-1209.

Kresten, P., 1974. Uranium in kimberlites and associated rocks, with special reference to Lesotho occurrences. Lithos, v. 7, p. 171-180.

Kresten, P. and Berggren, G., 1975. Kimberlitic zircons - a possible aid in prospecting for kimberlites. Mineralium Deposita, v. 10, p. 47-56.

Krogh, T.E., 1973. A low-contamination method for hydrothermal decomposition of zircon and extraction of U and Pb for isotopic age determinations. Geochimica et Cosmochimica Acta, v. 37, p. 485-494.

LeCheminant, A.N., Heaman, L.M., Kretschmar, U. and LeCouteur, P.C., 1998. Complex origins and multiple ages of mantle zircon megacrysts from Canadian and South African kimberlites. Extended Abstract Volume, 7th International Kimberlite Conference, Cape Town, p. 486-488.

Lee, J.K.W., Williams, I.S. and Ellis, D.J., 1997. Pb, U and Th diffusion in natural zircon. Nature, v. 390, p. 159-161.

Ludwig, K.R., 1998. On the treatment of concordant uranium-lead ages. Geochimica et Cosmochimica Acta, v. 62, p. 665-676.

McIntyre, R.M. and Dawson, J.B., 1976. Age and significance of some south African kimberlites. Fourth European Colloquium on Geochronology, Cosmochronology and Isotope Geology, Abstracts; Amsterdam, v. 66.

Mitchell, R.H. and Crocket, J.H., 1971. The Isotopic Composition of Strontium in Some South African Kimberlites. Contributions to Mineralogy and Petrology, v. 30, p. 277-290.

Mitchell, R.H., 1972. Composition of perovskite in kimberlite. American Mineralogist, v. 57, p. 1748-1753.

Mitchell, R.H., 1973. Magnesian Ilmenite and its role in kimberlite petrogenesis. Journal of Geology, v. 81, p. 301-311.

Mitchell, R.H. 1977. Geochemistry of magnesian ilmenites from kimberlites in South Africa and Lesotho. Lithos, v. 10, p. 29-37.

Mitchell, R.H., 1986. *Kimberlites: Mineralogy, Geochemistry, and Petrology*. Plenum Press, New York, 442 pp.

Moore, R.O., Griffin, W.L., Gurney, J.J., Ryan, C.G., Cousens, D.R., Sie, S.H. and Suter, G.F., 1992. Trace element geochemistry of ilmenite megacrysts from the Monastery kimberlite, South Africa. Lithos, v. 29, p. 1-18.

Nixon, P.H., 1987. Kimberlitic xenoliths and their cratonic setting. *In*: Mantle Xenoliths, P.H. Nixon (Ed.), John Wiley and Sons Ltd.

Nixon, P.H. and Boyd, F.R., 1973. Notes on the heavy mineral concentrates. *In*: P.H. Nixon (Ed.) Lesotho Kimberlites, Lesotho National Development Corporation, Maseru, Lesotho, p. 254-268.

Pasteris, J.D., Boyd, F.R. and Nixon, P.H., 1979. The ilmenite association at the Frank Smith mine, R.S.A. *In*: The mantle sample; Inclusions in kimberlites and other volcanics. Proceedings of the 2nd International Kimberlite Conference, v. 2, p. 265-278.

Pasteris, J.D., 1980. The Significance of Groundmass Ilmenite and Megacryst Ilmenite in Kimberlites. Contributions to Mineralogy and Petrology, v. 75, p. 315-325.

Schärer, U., Corfu, F. and Demaiffe, D., 1997. U-Pb and Lu-Hf isotopes in baddeleyite and zircon megacrysts from the Mbuji-Mayi kimberlite: constraints on the subcontinental mantle. Chemical Geology, v. 143, p. 1-16.

Schulze, D.J., Anderson, P.F.N., Hearn Jr., B.C. and Hetman, C.M., 1995. Origin and significance of ilmenite megacrysts and macrocrysts from kimberlite. International Geology Review, v. 37, p. 780-812.

Smith, C.B., 1983. Pb, Sr and Nd isotopic evidence for sources of southern African Cretaceous kimberlites. Nature, v. 304, p. 51-54.

Smith, C.B., Brennesholtz, R. and J.B. Dawson, 1978. Chemistry of micas from kimberlites and xenoliths-I. Micaceous kimberlites. Geochimica et Cosmochimica Acta, v. 42, p. 959-971.

Smith, C.B., Allsopp, H.L., Kramers, J.D., Hutchinson, G. and Roddick, J.C., 1985. Emplacement ages of Jurassic-Cretaceous South African kimberlites by the Rb-Sr method on phlogopite and whole-rock samples. Transactions of the Geological Society of South Africa, v. 88, p. 249-266.

Smith, C.B. and Barton, E.S., 1996. Rb-Sr mica age of the Monastery kimberlite phlogopite megacryst sample ROM98. AARL Internal Report, DeBeers.

Stacey, J.S. and Kramers, J.D., 1975. Approximation of terrestrial lead isotope evolution by a two-stage model. Earth and Planetary Science Letters, v. 26, p. 207-221.

Steiger, R.H. and Jäger, E., 1977. Subcommission on geochronology; convention on the use of decay constants in geo- and cosmogeochronology. Earth and Planetary Science Letters, v. 36, p. 359-362.

Truswell, J.F., 1977. *The Geological Evolution of South Africa*. Purnell and sons, Cape Town, 218 pp.

Williams, A.F., 1932. *The Genesis of the Diamond*. Ernest Benn Ltd., London, v. 1, 352pp.

Whitelock,T.K., 1973. The Monastery mine kimberlite pipe. *In*: P.H. Nixon (Ed.) Lesotho kimberlites, Lesotho National Development Corporation, Maseru, Lesotho, p. 214-219.

York, D., 1969. Least squares fitting of a straight line with correlated errors. Earth and Planetary Science Letters, v. 5, p. 320-324.

Zartman, R.E., Richardson, S.H., Gurney, J.J. and Moore, R.O., 1998. U-Th-Pb ages of megacrystic zircon from the Monastery kimberlite, Free State, South Africa. *In*: 7th International Kimberlite Conference, Extended Abstracts, p. 989-991.

Zindler, A. and Hart, S., 1986. Chemical Geodynamics. Annual Review of Earth and Planetary Sciences, v. 14, p. 493-571.

Appendix A

Electron Microprobe Data

Abbreviations

(C): core
(R): rim
(I): intermediate
(dC): dark core
(dR): dark rim
(bR): bright rim

Total Fe expressed as FeO
Fe_2O_3 calculated using Droop (1987)
Mg#=100Mg/(Mg+Fe)

Electron microprobe analyses of ilmenite macrocrysts, Monastery

	M-1-1 (C)	M-1-1 (dR)	M-1-1 (bR)	M-1-1 (R)	M-1-1 (R)	M-1-1 (R)	M-1-2 (C)	M-1-2 (R)	M-1-2 (R)	M-1-3 (C)	M-1-3 (R)	M-2-1 (C)
MgO	12.47	15.54	4.62	19.19	17.05	18.43	12.39	18.10	18.43	7.10	8.95	8.52
V2O3	0.13	0.17	0.00	0.07	0.20	0.02	0.19	0.12	0.03	0.11	0.16	0.12
CaO	0.06	0.11	3.08	0.12	0.19	0.13	0.00	0.36	0.32	0.02	0.00	0.00
MnO	0.30	1.16	2.64	0.77	0.72	0.74	0.29	0.75	0.81	0.21	0.25	0.20
Al2O3	0.36	1.47	0.19	3.73	3.75	3.73	0.29	4.35	3.45	0.29	0.33	0.48
ZnO	0.00	0.09	0.00	0.08	0.00	0.26	0.00	0.00	0.00	0.06	0.12	0.16
TiO2	52.27	22.62	34.31	20.91	15.32	20.21	53.24	17.61	19.41	45.73	46.52	48.23
FeO_T	31.07	50.83	47.84	49.06	55.88	51.48	31.93	53.92	52.12	44.01	41.09	40.56
SiO2	0.00	0.93	0.63	0.04	0.02	0.06	0.01	0.03	0.01	0.02	0.01	0.03
Cr2O3	0.89	2.22	0.64	2.21	2.21	1.44	0.93	1.48	2.06	0.72	0.75	0.00
Total	97.53	95.13	93.94	96.19	95.35	96.50	99.28	96.72	96.65	98.27	98.19	98.30
Recalculated Analyses												
FeO	24.39	0.00	16.76	0.00	0.00	0.00	25.52	0.00	0.00	28.20	25.52	27.88
Fe2O3	7.42	56.49	34.53	54.52	62.10	57.22	7.13	59.92	57.92	17.56	17.31	14.09
New Total	98.28	100.79	97.39	101.64	101.57	102.23	99.99	102.73	102.45	100.02	99.93	99.71
Mg	0.44	0.52	0.17	0.62	0.56	0.60	0.43	0.58	0.59	0.25	0.32	0.30
V	0.00	0.00	0.00	0.00	0.00	0.00	0.00	0.00	0.00	0.00	0.00	0.00
Ca	0.00	0.00	0.08	0.00	0.00	0.00	0.00	0.01	0.01	0.00	0.00	0.00
Mn	0.01	0.02	0.06	0.01	0.01	0.01	0.01	0.01	0.01	0.00	0.01	0.00
Al	0.01	0.04	0.01	0.10	0.10	0.10	0.01	0.11	0.09	0.01	0.01	0.01
Zn	0.00	0.00	0.00	0.00	0.00	0.00	0.00	0.00	0.00	0.00	0.00	0.00
Ti	0.92	0.38	0.65	0.34	0.25	0.33	0.92	0.29	0.32	0.83	0.83	0.86
Fe2+	0.00	0.00	0.00	0.00	0.00	0.00	0.00	0.00	0.00	0.00	0.00	0.00
Si	0.00	0.02	0.02	0.00	0.00	0.00	0.00	0.00	0.00	0.00	0.00	0.00
Cr	0.02	0.04	0.01	0.04	0.04	0.02	0.02	0.03	0.04	0.01	0.01	0.00
Fe 2+	0.48	0.00	0.35	0.00	0.00	0.00	0.49	0.00	0.00	0.57	0.51	0.56
Fe 3+	0.13	0.96	0.65	0.89	1.03	0.93	0.12	0.97	0.94	0.32	0.31	0.25
Total	2.00	2.00	2.00	2.00	2.00	2.00	2.00	2.00	2.00	2.00	2.00	2.00
%ILM	49.16%	0.00%	41.36%	0.00%	0.00%	0.00%	50.23%	0.00%	0.00%	57.84%	51.80%	56.43%
%HEM	6.48%	47.85%	38.34%	41.76%	47.90%	43.94%	6.31%	45.53%	44.24%	16.21%	15.81%	12.83%
%GEIK	44.35%	52.15%	20.30%	58.24%	52.10%	56.06%	43.45%	54.47%	55.76%	25.95%	32.39%	30.75%

Ilmenite macrocrysts cont'd

	M-2-2 (C)	M-2-2 (bR)	M-2-2 (bR)	M-2-2 (bR)	M-2-2 (eR)	M-3a-1 (C)	M-3a-1 (R)	M-3a-1 (R)	M-3a-1 (bR)	M-3a-2 (C)	M-3a-2 (bR)	M-3b-1 (C)	M-3b-2 (C)	M-3b-2 (R)
MgO	10.20	4.91	2.39	4.35	5.22	8.83	10.34	12.07	0.15	10.81	0.88	7.63	8.42	12.12
V2O3	0.18	0.00	0.00	0.03	0.00	0.03	0.04	0.09	0.00	0.12	0.00	0.13	0.14	0.07
CaO	0.02	0.17	0.70	0.68	12.41	0.01	0.05	0.10	0.46	0.02	0.24	0.00	0.00	0.11
MnO	0.30	11.70	12.99	10.29	1.58	0.19	0.28	0.75	1.27	0.22	1.13	0.29	0.32	0.79
Al2O3	0.15	0.18	0.11	0.19	0.21	0.63	0.82	4.00	0.02	0.86	0.01	0.11	0.14	3.68
ZnO	0.00	0.00	0.00	0.00	0.00	0.05	0.11	0.00	0.07	0.00	0.10	0.16	0.04	0.03
TiO2	47.74	33.39	41.16	35.88	37.07	48.55	48.61	21.78	53.01	49.59	52.41	47.73	48.84	21.82
FeO_T	39.06	45.42	37.96	44.23	33.63	40.50	37.91	55.61	43.34	35.94	43.40	41.27	39.31	56.38
SiO2	0.02	0.17	0.24	0.17	0.00	0.02	0.00	0.06	0.26	0.01	0.05	0.00	0.01	0.05
Cr2O3	0.63	0.62	0.51	0.70	0.58	0.00	0.00	2.12	0.00	0.19	0.20	0.66	0.84	1.62
Total	98.29	96.56	96.04	96.51	90.70	98.82	98.17	96.58	98.58	97.76	98.42	97.97	98.06	96.68
Recalculated Analyses														
FeO	24.44	9.40	18.99	13.42	6.54	27.70	24.85	0.00	43.34	25.10	43.40	28.89	28.57	0.00
Fe2O3	16.25	40.03	21.08	34.24	30.10	14.23	14.52	61.80	0.00	12.05	0.00	13.75	11.94	62.66
New Total	99.92	100.56	96.15	99.94	93.71	100.24	99.63	102.77	98.58	98.97	98.42	99.35	99.25	102.95
Mg	0.36	0.18	0.09	0.16	0.20	0.31	0.36	0.41	0.01	0.38	0.03	0.27	0.30	0.41
V	0.00	0.00	0.00	0.00	0.00	0.00	0.00	0.00	0.00	0.00	0.00	0.00	0.00	0.00
Ca	0.00	0.00	0.02	0.02	0.34	0.00	0.00	0.00	0.01	0.00	0.01	0.00	0.00	0.00
Mn	0.01	0.24	0.28	0.22	0.03	0.00	0.01	0.01	0.03	0.00	0.02	0.01	0.01	0.02
Al	0.00	0.01	0.00	0.01	0.01	0.02	0.02	0.11	0.00	0.02	0.00	0.00	0.00	0.10
Zn	0.00	0.00	0.00	0.00	0.00	0.00	0.00	0.00	0.00	0.00	0.00	0.00	0.00	0.00
Ti	0.85	0.62	0.79	0.67	0.70	0.86	0.86	0.37	1.02	0.88	1.00	0.87	0.88	0.37
Fe2+	0.00	0.00	0.00	0.00	0.00	0.00	0.00	0.00	0.00	0.00	0.00	0.00	0.00	0.00
Si	0.00	0.00	0.01	0.00	0.00	0.00	0.00	0.00	0.01	0.00	0.00	0.00	0.00	0.00
Cr	0.01	0.01	0.01	0.01	0.01	0.00	0.00	0.04	0.00	0.00	0.00	0.01	0.02	0.03
Fe 2+	0.48	0.19	0.40	0.28	0.14	0.55	0.49	0.00	0.93	0.49	0.92	0.58	0.57	0.00
Fe 3+	0.29	0.74	0.40	0.64	0.57	0.25	0.26	1.06	0.00	0.21	0.00	0.25	0.22	1.07
Total	2.00	2.00	2.00	2.00	2.00	2.00	2.00	2.00	2.00	2.00	2.00	2.00	2.00	2.00
%ILM	48.93%	26.00%	58.04%	36.69%	22.27%	55.57%	49.88%	0.00%	99.39%	50.42%	96.52%	59.36%	58.38%	0.00%
%HEM	14.65%	49.79%	28.98%	42.11%	48.09%	12.84%	13.12%	56.37%	0.00%	10.89%	0.00%	12.71%	10.97%	56.62%
%GEIK	36.42%	24.21%	12.99%	21.21%	31.64%	31.59%	37.00%	43.63%	0.61%	38.69%	3.48%	27.94%	30.65%	43.38%

Ilmenite macrocrysts cont'd

	M-3c-1 (C)	M-3c-1 (R)	M-3c-1 (R)	M-3c-1 (bR)	M-3c-1 (dC)	M-3c-1 (R)	M-3c-2 (C)	M-3c-2 (R)	M-3c-2 (bR)	M-3c-2 (bR)	M-3c-2 (bR)
MgO	6.17	8.45	11.53	1.18	9.41	12.46	8.23	10.98	1.12	2.63	1.37
V2O3	0.24	0.29	0.11	0.00	0.30	0.15	0.10	0.18	0.06	0.00	0.00
CaO	0.00	0.08	0.10	0.26	0.00	0.10	0.00	0.07	0.49	0.51	0.28
MnO	0.27	0.32	0.72	2.18	0.24	0.46	0.29	0.41	0.71	0.98	1.95
Al2O3	0.07	0.11	3.82	0.01	0.23	0.43	0.17	0.23	0.02	0.11	0.04
ZnO	0.03	0.00	0.13	0.15	0.00	0.00	0.06	0.07	0.14	0.00	0.00
TiO2	43.45	43.77	21.67	52.64	47.31	51.82	48.41	49.96	51.24	51.42	50.94
FeO_T	46.08	43.24	57.40	41.76	39.73	32.71	39.48	35.44	42.19	41.07	39.92
SiO2	0.01	0.00	0.06	0.08	0.02	0.00	0.00	0.00	0.21	0.47	1.58
Cr2O3	0.85	0.89	1.59	0.61	0.87	0.81	0.84	0.94	1.18	0.62	0.23
Total	97.16	97.14	97.14	98.86	98.12	98.93	97.58	98.28	97.34	97.81	96.31
Recalculated Analyses											
FeO	27.78	23.87	0.00	41.76	25.54	23.82	28.52	24.80	42.19	40.46	39.92
Fe2O3	20.34	21.53	63.79	0.00	15.77	9.88	12.19	11.82	0.00	0.68	0.00
New Total	99.20	99.30	103.52	98.86	99.69	99.92	98.80	99.46	97.34	97.88	96.31
Mg	0.23	0.30	0.39	0.04	0.33	0.43	0.30	0.38	0.04	0.10	0.05
V	0.00	0.01	0.00	0.00	0.01	0.00	0.00	0.00	0.00	0.00	0.00
Ca	0.00	0.00	0.00	0.01	0.00	0.00	0.00	0.00	0.01	0.01	0.01
Mn	0.01	0.01	0.01	0.05	0.00	0.01	0.01	0.01	0.02	0.02	0.04
Al	0.00	0.00	0.10	0.00	0.01	0.01	0.00	0.01	0.00	0.00	0.00
Zn	0.00	0.00	0.00	0.00	0.00	0.00	0.00	0.00	0.00	0.00	0.00
Ti	0.80	0.79	0.37	1.00	0.84	0.90	0.88	0.88	0.99	0.97	0.99
Fe2+	0.00	0.00	0.00	0.00	0.00	0.00	0.00	0.00	0.00	0.00	0.00
Si	0.00	0.00	0.00	0.00	0.00	0.00	0.00	0.00	0.01	0.01	0.04
Cr	0.02	0.02	0.03	0.01	0.02	0.01	0.02	0.02	0.02	0.01	0.00
Fe 2+	0.57	0.48	0.00	0.88	0.51	0.46	0.58	0.49	0.91	0.85	0.86
Fe 3+	0.38	0.39	1.09	0.00	0.28	0.17	0.22	0.21	0.00	0.01	0.00
Total	2.00	2.00	2.00	2.00	2.00	2.00	2.00	2.00	2.00	2.00	2.00
%ILM	57.97%	49.09%	0.00%	95.22%	51.69%	47.19%	58.59%	49.92%	95.50%	89.00%	94.22%
%HEM	19.09%	19.92%	58.26%	0.00%	14.36%	8.81%	11.27%	10.70%	0.00%	0.67%	0.00%
%GEIK	22.95%	30.99%	41.72%	4.78%	33.95%	44.00%	30.14%	39.38%	4.50%	10.33%	5.78%

Electron microprobe analyses of ilmenite megacryst, Monastery

	M-1a	M-1b
MgO	7.88	7.92
V2O3	0.13	0.12
CaO	0.00	0.01
MnO	0.20	0.21
Al2O3	0.60	0.60
ZnO	0.04	0.09
TiO2	46.82	47.32
FeO	41.79	41.80
SiO2	0.03	0.02
Cr2O3	0.02	0.02
Total	97.52	98.09
Recalculated Analyses		
FeO	27.96	28.16
Fe2O3	15.37	15.15
New Total	99.06	99.61
Mg	0.28	0.28
V	0.00	0.00
Ca	0.00	0.00
Mn	0.00	0.00
Al	0.02	0.02
Zn	0.00	0.00
Ti	0.85	0.85
Fe2+	0.00	0.00
Si	0.00	0.00
Cr	0.00	0.00
Fe 2+	0.56	0.56
Fe 3+	0.28	0.27
Total	2.00	2.00
%ILM	57.28%	57.36%
%HEM	14.17%	13.88%
%GEIK	28.55%	28.76%

Electron Microprobe analyses of Groundmass Ilmenite, Monastery

	M-1-1	M-1-2	M-1-3 (C)	M-1-3 (R)	M-1-4	M-1-5 (C)	M-1-5 (R)	M-1-6	M-3a-1	M-3a-2 (C)	M-3a-2 (R)	M-3a-3 (C)	M-3a-3 (R)	M-3c-1	M-3c-2	M-3c-3
MgO	18.21	18.56	19.36	18.44	19.14	18.78	17.79	17.66	0.17	9.94	2.64	12.81	0.77	11.73	1.88	1.88
V2O3	0.08	0.12	0.06	0.11	0.10	0.12	0.18	0.09	0.00	0.20	0.01	0.09	0.02	0.06	0.00	0.00
CaO	0.19	0.18	0.07	0.10	0.10	0.11	0.07	0.17	1.29	0.05	0.01	0.10	0.19	0.21	0.47	0.25
MnO	0.72	0.74	0.81	0.76	0.86	0.87	0.75	0.77	1.39	0.26	1.55	0.49	0.84	0.89	1.24	2.20
Al2O3	4.06	4.07	4.24	4.16	3.65	4.03	4.26	4.49	0.01	0.71	0.01	0.61	0.00	3.90	0.01	0.01
ZnO	0.05	0.03	0.00	0.06	0.00	0.15	0.01	0.01	0.00	0.00	0.00	0.00	0.00	0.00	0.10	0.18
TiO2	17.79	19.98	21.87	20.48	22.31	21.20	18.43	17.52	49.77	48.24	51.48	52.50	52.05	20.42	52.83	51.77
FeO_T	51.41	51.89	46.63	51.12	49.12	50.85	53.69	54.41	43.59	38.45	41.76	31.81	44.25	57.00	41.85	40.91
SiO2	0.05	0.05	0.04	0.05	0.05	0.04	0.07	0.06	0.41	0.02	0.06	0.00	0.08	0.07	0.06	0.11
Cr2O3	2.95	0.65	3.27	0.71	1.46	0.96	0.77	0.91	0.07	0.00	0.00	0.04	0.33	2.17	0.18	0.06
Total	95.54	96.25	96.34	96.00	96.78	96.88	96.02	96.08	96.69	97.87	97.52	98.44	98.53	96.46	98.63	97.36
Recalculated Analyses																
FeO	0.00	0.00	0.00	0.00	0.00	0.00	0.00	0.00	41.87	25.37	40.06	23.75	44.05	0.00	41.85	40.48
Fe2O3	57.13	57.66	51.82	56.81	54.58	56.29	59.66	60.46	1.91	14.53	1.89	8.95	0.22	63.34	0.00	0.47
New Total	101.26	102.03	101.53	101.69	102.25	102.52	101.99	102.14	96.89	99.32	97.71	99.34	98.55	102.81	98.63	97.41
Mg	0.59	0.60	0.62	0.60	0.61	0.60	0.58	0.57	0.01	0.35	0.10	0.44	0.03	0.40	0.07	0.07
V	0.00	0.00	0.00	0.00	0.00	0.00	0.00	0.00	0.00	0.00	0.00	5.00	0.00	0.00	0.00	0.00
Ca	0.00	0.00	0.00	0.00	0.00	0.00	0.00	0.00	0.04	0.00	0.00	0.00	0.01	0.01	0.01	0.01
Mn	0.01	0.01	0.01	0.01	0.02	0.02	0.01	0.01	0.03	0.01	0.03	0.01	0.02	0.02	0.03	0.05
Al	0.11	0.10	0.11	0.11	0.09	0.10	0.11	0.12	0.00	0.02	0.00	0.02	0.00	0.10	0.00	0.00
Zn	0.00	0.00	0.00	0.00	0.00	0.00	0.00	0.00	0.00	0.00	0.00	0.00	0.00	0.00	0.00	0.00
Ti	0.29	0.33	0.35	0.33	0.36	0.34	0.30	0.29	0.97	0.86	0.98	0.91	1.00	0.35	1.00	0.99
Fe2+	0.00	0.00	0.00	0.00	0.00	0.00	0.00	0.00	0.00	0.00	0.00	0.00	0.00	0.00	0.00	0.00
Si	0.00	0.00	0.00	0.00	0.00	0.00	0.00	0.00	0.01	0.00	0.00	0.00	0.00	0.00	0.00	0.00
Cr	0.05	0.01	0.06	0.01	0.02	0.02	0.01	0.02	0.00	0.00	0.00	0.00	0.01	0.04	0.00	0.00
Fe2+	0.00	0.00	0.00	0.00	0.00	0.00	0.00	0.00	0.91	0.50	0.85	0.46	0.94	0.00	0.88	0.87
Fe3+	0.94	0.94	0.84	0.93	0.89	0.91	0.96	0.99	0.04	0.26	0.04	0.16	0.00	1.08	0.00	0.01
Total	2.00	2.00	2.00	2.00	2.00	2.00	2.00	2.00	2.00	2.00	2.00	2.00	2.00	2.00	2.00	2.00
% ILM	0.00%	0.00%	0.00%	0.00%	0.00%	0.00%	0.00%	0.00%	97.29%	51.13%	87.63%	46.93%	96.76%	0.00%	92.61%	91.91%
% HEM	44.19%	43.96%	40.32%	43.74%	41.86%	43.10%	45.84%	46.36%	1.99%	13.18%	1.87%	7.96%	0.22%	57.68%	0.00%	0.50%
% GEIK	55.81%	56.04%	59.68%	56.26%	58.14%	56.90%	54.16%	53.64%	0.72%	35.69%	10.30%	45.11%	3.02%	42.32%	7.39%	7.59%

Electron microprobe analyses of phlogopite, Monastery

	M-3a-1	M-3a-2	M-3a-3	M-3a-3 (bR)	M-3a-4	M-3a-4	M-3a-5	M-3a-6	M-3b-1	M-3b-2	M-3b-2 (bR)	M-3b-3	M-3b-4	M-3b-5
F	0.34	0.22	0.35	0.18	0.11	0.32	0.22	0.37	0.25	0.41	0.21	0.23	0.38	0.16
Na2O	0.14	0.30	0.19	0.30	0.91	0.14	0.22	0.25	0.28	0.20	0.22	0.33	0.14	0.20
Cl	0.03	0.02	0.02	0.01	0.03	0.00	0.03	0.01	0.03	0.03	0.01	0.03	0.03	0.08
BaO	0.04	0.11	0.01	0.20	0.57	0.55	0.13	0.12	0.11	0.03	0.17	0.10	0.08	0.04
MgO	24.38	21.41	24.68	21.38	26.07	23.76	21.79	22.57	23.15	24.53	21.93	21.93	24.32	24.46
K2O	10.60	10.11	10.17	9.52	9.22	10.59	10.04	10.29	9.57	10.67	10.32	10.43	10.39	10.80
TiO2	0.97	4.01	1.43	4.08	0.06	1.75	3.84	3.62	2.73	0.92	3.82	3.17	0.94	0.90
Al2O3	11.54	14.30	11.82	13.93	14.39	14.41	13.71	12.79	12.73	11.58	14.12	14.05	11.62	11.66
CaO	0.01	0.01	0.03	0.02	0.03	0.05	0.06	0.05	0.06	0.02	0.02	0.01	0.07	0.01
MnO	0.03	0.02	0.02	0.05	0.01	0.06	0.02	0.03	0.02	0.02	0.02	0.03	0.03	0.04
SiO2	41.85	39.65	41.90	39.40	40.96	38.87	40.07	40.52	40.47	42.20	39.87	40.34	41.77	41.98
Cr2O3	0.08	0.17	0.22	0.24	0.81	0.76	0.30	0.07	0.11	0.10	0.27	0.00	0.02	0.41
FeO	6.67	6.18	5.48	6.17	2.40	5.13	6.49	6.38	6.50	6.68	6.25	6.42	6.62	5.88
Total	96.52	96.42	96.16	95.37	95.50	96.25	96.82	96.91	95.90	97.22	97.12	96.95	96.25	96.53
F	0.15	0.10	0.16	0.08	0.05	0.14	0.10	0.17	0.11	0.19	0.09	0.10	0.17	0.07
Na	0.04	0.08	0.05	0.08	0.25	0.04	0.06	0.07	0.08	0.05	0.06	0.09	0.04	0.05
Cl	0.01	0.01	0.00	0.00	0.01	0.00	0.01	0.00	0.01	0.01	0.00	0.01	0.01	0.02
Ba	0.00	0.01	0.00	0.01	0.03	0.03	0.01	0.01	0.01	0.00	0.01	0.01	0.00	0.00
Mg	5.17	4.54	5.22	4.57	5.47	5.07	4.60	4.77	4.93	5.17	4.62	4.63	5.17	5.18
K	1.93	1.83	1.84	1.74	1.66	1.93	1.82	1.86	1.74	1.93	1.86	1.88	1.89	1.96
Ti	0.10	0.43	0.15	0.44	0.01	0.19	0.41	0.39	0.29	0.10	0.41	0.34	0.10	0.10
Al	1.94	2.40	1.97	2.36	2.39	2.43	2.29	2.14	2.14	1.93	2.35	2.34	1.95	1.95
Ca	0.00	0.00	0.00	0.00	0.00	0.01	0.01	0.01	0.01	0.00	0.00	0.00	0.01	0.00
Mn	0.00	0.00	0.00	0.01	0.00	0.01	0.00	0.00	0.00	0.00	0.00	0.00	0.00	0.00
Si	5.96	5.64	5.94	5.65	5.77	5.56	5.68	5.75	5.78	5.97	5.64	5.71	5.96	5.96
Cr	0.01	0.02	0.02	0.03	0.09	0.09	0.03	0.01	0.01	0.01	0.03	0.00	0.00	0.05
Fe2+	0.79	0.74	0.65	0.74	0.28	0.61	0.77	0.76	0.78	0.79	0.74	0.76	0.79	0.70
Total	16.11	15.79	16.02	15.72	16.00	16.12	15.79	15.93	15.88	16.15	15.82	15.87	16.11	16.04
Mg#	86.70	86.06	86.92	86.07	95.09	89.20	85.67	86.32	86.39	86.74	86.21	85.90	86.76	88.12

Phlogopite cont'd

	M-3b-5 (bR)	M-3c-1	M-3c-1 (R)	M-3c-2 (C)	M-3c-2 (R)	M-3c-3	M-3c-4	M-3c-5	M-3c-6	M-3c-6 (R)	M-3c-7
F	0.26	0.46	0.31	0.49	0.34	0.47	0.44	0.42	0.44	0.82	0.31
Na2O	0.26	0.16	0.24	0.18	0.28	0.17	0.15	0.13	0.13	0.11	0.27
Cl	0.03	0.03	0.02	0.05	0.03	0.03	0.03	0.03	0.02	0.01	0.03
BaO	0.14	0.02	0.17	0.04	0.12	0.02	0.05	0.03	0.02	1.10	0.12
MgO	21.65	24.18	22.56	24.50	21.52	24.92	25.29	24.50	24.51	24.99	21.89
K2O	10.50	10.13	9.40	10.23	10.01	10.58	9.76	10.53	10.46	10.39	10.16
TiO2	3.70	0.47	3.89	0.97	3.99	0.61	0.81	0.73	0.77	1.07	3.66
Al2O3	13.99	10.69	13.55	11.46	14.35	10.99	10.84	11.21	10.99	14.07	13.28
CaO	0.00	0.04	0.06	0.22	0.01	0.02	0.03	0.01	0.02	0.03	0.04
MnO	0.04	0.03	0.02	0.01	0.01	0.03	0.03	0.03	0.02	0.07	0.02
SiO2	39.68	41.96	39.57	42.34	40.04	42.49	42.09	42.06	42.26	39.36	40.60
Cr2O3	0.46	0.00	0.19	0.10	0.27	0.04	0.05	0.04	0.04	0.01	0.04
FeO	6.03	8.00	6.16	6.50	6.30	7.20	6.91	7.03	6.85	5.28	6.65
Total	96.62	95.97	96.01	96.86	97.14	97.37	96.29	96.56	96.31	96.96	96.93
F	0.11	0.21	0.14	0.22	0.15	0.21	0.20	0.19	0.20	0.37	0.14
Na	0.07	0.04	0.07	0.05	0.08	0.05	0.04	0.04	0.03	0.03	0.07
Cl	0.01	0.01	0.01	0.01	0.01	0.01	0.01	0.01	0.01	0.00	0.01
Ba	0.01	0.00	0.01	0.00	0.01	0.00	0.00	0.00	0.00	0.06	0.01
Mg	4.59	5.18	4.79	5.17	4.53	5.26	5.37	5.20	5.21	5.32	4.62
K	1.91	1.86	1.71	1.85	1.80	1.91	1.77	1.91	1.90	1.89	1.84
Ti	0.40	0.05	0.42	0.10	0.42	0.06	0.09	0.08	0.08	0.12	0.39
Al	2.35	1.81	2.28	1.91	2.39	1.83	1.82	1.88	1.85	2.37	2.22
Ca	0.00	0.01	0.01	0.03	0.00	0.00	0.00	0.00	0.00	0.00	0.01
Mn	0.00	0.00	0.00	0.00	0.00	0.00	0.00	0.00	0.00	0.01	0.00
Si	5.65	6.03	5.64	5.99	5.65	6.01	5.99	5.99	6.03	5.62	5.75
Cr	0.05	0.00	0.02	0.01	0.03	0.00	0.01	0.00	0.00	0.00	0.00
Fe2+	0.72	0.96	0.73	0.77	0.74	0.85	0.82	0.84	0.82	0.63	0.79
Total	15.87	16.18	15.83	16.12	15.81	16.20	16.12	16.16	16.13	16.41	15.85
Mg#	86.49	84.34	86.71	87.05	85.89	86.06	86.71	86.13	86.45	89.40	85.43

Electron microprobe analyses of perovskite, Monastery

	M-2-1 (C)	M-2-1 (I)	M-2-1 (R)	M-2-2	M-2-3	M-3a-1	M-3a-2	M-3a-3	M-3b-1
MgO	0.08	8.11	0.06	0.05	0.07	0.05	0.07	0.06	0.05
V2O3	0.07	0.00	0.01	0.00	0.01	0.07	0.00	0.00	0.00
CaO	37.16	12.65	38.90	39.77	39.17	39.38	38.35	38.73	38.44
MnO	0.02	0.33	0.05	0.01	0.01	0.08	0.00	0.01	0.01
Al2O3	0.17	0.12	0.14	0.18	0.14	0.11	0.17	0.14	0.15
ZnO	0.00	0.05	0.19	0.18	0.01	0.02	0.04	0.00	0.00
TiO2	55.73	55.20	56.22	56.33	56.12	56.17	56.28	55.97	55.50
FeO_T	1.44	20.66	1.05	1.05	1.00	1.40	1.28	1.27	0.91
SiO2	0.00	0.00	0.00	0.00	0.00	0.00	0.00	0.00	0.00
Cr2O3	0.00	0.57	0.17	0.04	0.02	0.02	0.00	0.00	0.03
Total	94.67	97.69	96.80	97.61	96.54	97.29	96.19	96.18	95.08
Mg	0.01	0.57	0.00	0.00	0.00	0.00	0.00	0.00	0.00
V	0.00	0.00	0.00	0.00	0.00	0.00	0.00	0.00	0.00
Ca	1.91	0.64	1.96	1.99	1.97	1.97	1.94	1.96	1.96
Mn	0.00	0.01	0.00	0.00	0.00	0.00	0.00	0.00	0.00
Al	0.01	0.01	0.01	0.01	0.01	0.01	0.01	0.01	0.01
Zn	0.00	0.00	0.01	0.01	0.00	0.00	0.00	0.00	0.00
Ti	2.01	1.96	1.98	1.97	1.98	1.98	2.00	1.99	1.99
Fe2+	0.06	0.82	0.04	0.04	0.04	0.05	0.05	0.05	0.04
Si	0.00	0.00	0.00	0.00	0.00	0.00	0.00	0.00	0.00
Cr	0.00	0.02	0.01	0.00	0.00	0.00	0.00	0.00	0.00
Total	3.99	4.03	4.01	4.02	4.01	4.02	4.00	4.01	4.00